was more complicated. Here it started at the inner side of the brace or at the outer weldtoe between crown and saddle point.

In appendix 3-III the crack growth diagrams of the surface cracks are given. Appendix 3-IV gives a picture of some specimens at the end of test.

3.4.6.2 Strain redistribution

The change in strain range at the hot spot is given in data sheets. For T joints with $\beta = 0.5$ the most typical form is given in fig. 3.5.36. At the cracked side the strain range dropped rather early. This decrease in strain range went on and even the strain range reversed from an elongation to a shortening. At the lowest point in the curve the crack went through the wall. After that the line goes up a little. At the uncracked side the line is horizontal until a very large (and deep) crack has been developed. Then there was a quick drop in strain range.
This behaviour can be explained as follows: With a small crack the gauge at the cracked side comes in the shadow of the crack, so the strain range decreases. When the crack is large (but not through) the chord wall is loaded in bending with compression at the outside, so the strain range reversed. After a through crack the bending in the chord wall will decrease, while there is no connection between the chord wall and the 'plug' of the connection, so the negative strain range decreases.
At the uncracked side the strain range changed when the crack becomes large. This is due to the rotation of the chord.

3.4.7 Possible failure criteria

The determination of failure criteria is rather difficult, since no operational definition of failure is available at the moment.
Possible failure criteria are:

a) first visible crack

Taking this as failure criterion is a rather conservative assumption, because after the first crack is discovered a node can sustain a lot of additional load cycles and also the static load capacity is still very large.

The SCF is the ratio of the maximum (hot spot) stress range (determined from the bi-axial strain situation at the weld toe) to the nominal stress range in the brace. Therefore:

$$SCF = \sigma_{HS}/\sigma_{nominal}$$

in which

$$\sigma_{HS} = \frac{E}{1-\nu^2} (\varepsilon_{HS} + \nu\varepsilon''_{HS})$$

ε''_{HS} = extrapolated strain perpendicular to ε_{HS} direction (parallel to weld toe).

For the axial loaded T joints the correlation between measurements and calculations is rather good. For the T joints loaded with in plane bending the correlation is not so good. For the X-joints, only calculated values from Wordsworth/Smedley are available. The correlation is rather good.

3.4.6 Joint behaviour during fatigue test

3.4.6.1 Crack growth

In an early part of the fatigue test a visible crack can be discovered. The ratio of the number of cycles at the first visible crack to the number of cycles at the end of test varies with the joint size. For the small joint the average ratio is about 2/3, for the medium and large ones the ratio is respectively 1/3 and 1/4.
The ratio of the number of cylces at a through crack to the number of cycles at the end of test varies also somewhat with the joint size.
For the small, medium and large joints the average ratio is respectively 89, 79 and 77 %.
On T- and X-joints with β ratio of 0.5 and 0.25, the crack always started at the saddle point of the intersection in the chordwall at the weldtoe. The crack then propagated along the weld toe and in a later stage the crack branched away from the weldtoe into the chordwall.
On the X-joints with $\beta = 1.0$ and $\tau = 1.0$ the crack started also at the saddle point. The X-joints with $\beta = 1.0$ and $\tau = 0.55$ the crack growth

under the aegis of a MaTS (Marine Technological Research in the Netherlands) project.

Table 3.4.3 gives the dimensions of the joints with the corresponding joint number. Fig. 3.4.18 and 19 give the element mesh of the β=0.5 and β = 1.0 joint as used in the SATE program.

Fig. 3.4.20 gives the element mesh at the hot spot in the ASKA calculations. In fig. 3.4.21 the coordinates and lines used in the plots of the SNCF's are indicated. Fig. 3.4.22 and 23 give the location of the origin of the horizontal axis used in the diagrams. Fig. 3.4.24 gives the loading cases. Fig. 3.4.25 to 3.4.35 give the results of the calculations. The results of the strain measurements are also plotted in the same figures for an easy comparison.

In general there is a good agreement in the results. For the X-joint with β and τ = 0.5 the ASKA calculation gives somewhat better results in the weld toe region. This is probably due to the more sophisticated and expensive modelling of the weld.

3.4.5 Comparison of the measured SNCF (SCF) and the SCF calculated with parameter formulae

In 3.4.3 the procedure to determine the hot spot strain range of the SNCF from measurements on test specimens is given. For design purposes a number of parametric formulae for calculating the stress concentration factor (SCF) are available.

A reference review up to 1977 is given in |3.9|. In |3.10| the first results of the research are compared with the formulae mentioned in |3.9| and with some recently published formulae |3.11 and 3.12|. In this report the measurements are compared with the values obtained by the formulae of Kuang |3.13|, Teyler/Gibstein |3.9| and Wordsworth/Smedley |3.6|. See table 3.4.4.

This table gives the maximum strain concentration factor (SNCF) and the maximum stress concentration factor (SCF). The maximum SNCF is the ratio of the hot spot strain range to the nominal strain range in the brace. Thus,

$$SNCF = \varepsilon_{HS}/\varepsilon_{nominal}$$

3.4.3.3.2 X-joints with $\beta = 1.0$ and $\tau = 0.5$ (Testspecimens 30/33, 36/38)

It was found that in this type of joint the initiation of crack did not start at the intersection of the weld toe with line 4 (outside). Here the crack started along line 5 under $\theta = \pm 45^{o}$ and/or at the inside of the brace at the root of the weld near line 2.
So for these type of joints it is meaningless to plot the results in an S-N diagram with the hot spot strain range along line 4 or 2.
FE calculations already showed that the SNCF along line 4 would be significantly higher than at line 2 or 4.
From strain measurements carried out on this type of joint the max SNCF along line 5 appeared to be 2.7 (see fig. 3.4.17).

Strain measurements indicated that the SNCF is rather high at the inside of the brace wall on line 2.
FE-calculations will be carried out in future to investigate the value of the SNCF in this area.
For the present it is recommended to use the max. SNCF of 2.7 as found form the strain measurements along line 5, to plot the results in the S-N diagram.
It should be noted however that this SNCF is higher than that calculated with the parameter formula given in most publications |3-6|.
Therefore a design cannot be based on the results plotted in this way and using the existing parameter formula at the same time.

3.4.3.4 Concluding remark about the use of the hot spot strain range

Although, in our opinion, using the hot spot strain range concept is better than using nominal strain or stress, there is some doubt about the validity of this concept as a governing parameter for fatigue. One of the problems is that a sharp notch at the toe of the weld will cause a theoretically infinite elastic strain or stress. A fracture mecahnics approach will probably give a better solution in future.

3.4.4 Comparison of the measured strain distribution and the finite element calculations

Three types of X-joints from this programme were calculated with a finite element program by Bovendeur |3.7| (Shell program 'SATE'). A finite element calculation with the program ASKA of one X-joint was made by Janssen |3.8|

If the measurements of the last strain gauge had been used (according to the approach in Marshall's paper), the strain ranges would have been significantly lower than with the approach adopted by the WG III which means that the fatigue results would have been plotted lower and so more unfavourable in comparison with the AWS-X curve.

3.4.3.3 Determination of the 'hot spot strain range' for X-joints with $\beta = 1.0$

3.4.3.3.1 X-joints $\beta = 1$ and $\tau = 1$ (Testspecimens 27, 28, 29)

In general the discussions about the extrapolation method of the strain measurements to the weld toe, held in the Working Group III, have been based on joints with $\beta = 0.5$.
For these type of joints the strain distribution near the weld toe along line 4 up to $0.2 \sqrt{rt}$ from the weld toe is approximately linear as can be seen in fig. 3.4.15.
Near the weld toe the linear strain distribution will be disturbed by the weld geometry. Because it is the intention to exclude the influence of the condition of the weld toe from the SNCF, the working group III has accepted the extrapolation method as described in 3.4.3.2.

However for joints with $\beta = 1$ it appears that there was not a linear strain distribution along line 4 (see fig. 3.4.16).
The extrapolation according to the method recommended by the Working Group III gives a SNCF of 2.3 an as average value of four test specimens, but it can be seen that this is not a correct value in this case.
In a study |3.5| based on finite element calculations and photo elastic analysis, it was found that the influence of the weld geometry extends only up to 0.4 T from the weld toe.
In our test specimen with $\beta = 0.5$ and $\tau = 0.5$ the value of $0.2 \sqrt{rt}$ is approximately equal to 0.4T so there is no difference which of these values is used.
However for $\beta = 1.0$ and $\tau = 1.0$ the value of 0.4 T is much smaller than $0.2 \sqrt{rt}$. So for the extrapolation we have used the point of the strain distribution curve at a distance of 0.4 T from the weld toe.
Using this point and a second point at a distance of 5 degrees from the weld toe, gives a value of the SNCF of 3.0 as the average value from 4 specimens.
This value agrees reasonably well with the existing parameter formula for this type of joints |3-6|.

after shakedown in model or prototype connection or calculated with best available theory".
The corresponding design S-N curve is the above mentioned AWS-X curve.

In the Offshore Installations: Guidance on design and construction |3.3| the following definition is used: *"Relationship Q applies to the main members of T, Y and K connections. The stress range corresponds to the peak range on the outer surface adjacent to the toe of the attachement weld between brace and chord members".* The corresoponding S-N curve Q is quite similar to the AWS-X-MODIFIED curve (at $N = 10^4$ a factor of 1.5 shorter on lifetime and at $N = 10^8$ no difference).

Marshall |3-4| stated that the hot spot stress (σ_{HS}) corresponding to the AWS-X curve is:

$$\sigma_{HS} = E \cdot \varepsilon_{TR}$$

where ε_{TR} is the measured strain range in a strain gauge perpendicular to and adjacent to the weld toe at the worst hot spot (therefore without extrapolation to the weld toe).
The European Working Group III - 'Tubular joints' has also discussed this problem comprehensively. The current view of the Working Group is given in figure 3.4.14. A linear extrapolation to the weld toe through the measured strain range in the points A and B will give the value for the maximum hot spot strain range, which has to be used for plotting the results in an S-N curve. To avoid very local effects from the weld toe the distance $a = 0.2 \sqrt{rt}$ should not be taken smaller than 4 mm. For the X-joints with diameter ratio of 1.0 this method cannot be used. The method used there will be discussed in 3.4.3.3.
The above mentioned extrapolation procedure attemps to include the effects of a) the global geometry of the joint and b) the global geometry of theweld but to exclude the effect of c) the condition of the weld toe. This last effect should be incorporated in the corresponding S-N curve.
The plots of the strain measurements at the hot spot can be found in the TEST DATA SHEETS (appendix 3-II).

Due to the complexity of the tubular joints and the restricted knowledge of its fatigue behaviour it is not evident which value for the stress or strain should be used in the S-N diagram. Table 3.4.2 gives an idea of the various S-values used in the Structural Welding Code |3.2|.
In the first four types of joints with the corresponding curves (D', E', K and T) a kind of nominal stress is used for the values on the vertical axis. The use of these curves is restricted to a certain geometry and these curves are based on a limited number of tests. Using these curves it is not necessary to know the strain distribution in the joints.

The last curve (X) supposes some knowledge about the strain or stress distribution in the joints. Especially the stress or strain range at the weld toe (the so called 'hot spot strain or stress range') has to be known. This curve is more generally applicable to the design of tubular joints.

In the European Working Group III "Tubular Joints" it was thought that the best presentation of the results was obtained using the 'hot spot strain range' as the S-value on the vertical axis. The way to determine the 'hot spot strain range' is described in the following chapters.

3.4.3.2 General determination of the 'hot spot strain range' or SNCF

The hot spot strain range of a tubular joint is influenced by the parameters: a) global geometry of the joint (γ,β,τ etc.);
b) global geometry of the weld (leg length);
c) condition of the weld toe (undercut, notches, angle between weld and parent metal).

The influence of the condition of the weld toe (c) is hard to determine by measurements or calculations and differs along the weld toe. Isolating the influence of the various parameters is also a difficult problem.

Therefore, it can be seen that there is no unique definition for the hot spot strain range.

The Structural Welding code |3-2| gives the following definition:
"Total range of worst hot spot stress or strain on the outside surface of intersecting members at the toe of the weld joining them - measured

3.4 Test results and analysis

3.4.1 Test data sheets

The TEST DATA SHEETS (see appendix 3-II) give the most important test data and results from each specimen, such as:

- joint type and geometry
- material properties
- method of loading
- strain distribution in an uncracked situation at hot spot
- change in strain range during fatigue test at hot spot
- number of cycles for various failure criteria
- crack growth

3.4.2 Strain distribution in the uncracked joints

Strain distributions were measured before the fatigue tests (see 3.3.3). Some results are given in fig. 3.4.1 to 3.4.13. For an easy comparison the results are shown as strain concentration factors (SNCF). The SNCF is the ratio of the local strain somewhere in the joint and the nominal strain in the loaded brace (i.e.: SNCF = $\varepsilon_{local}/\varepsilon_{nominal}$). On the horizontal axis the parameter ℓ/rt or ℓ/RT is used when the distribution is given in the longitudinal direction of the tube (r and t are brace radius and wall thickness and R and T are chord radius and wall thickness), when the distribution is given in circumferential direction the circumferential angle ϕ is used on the horizontal axis.
By comparing the results of the different joints the influence of various parameters can be found. Table 3.4.1 gives a survey of possible comparisons. More information about the strain distribution can be found in |3.1|.

3.4.3 Governing strain (stress) value for fatigue (determination $\Delta\varepsilon_{HS}$)

3.4.3.1 Introduction

The results of fatigue tests are normally presented in an S-N diagram. This is a log-log diagram with the number of cycles (N) to a certain failure criterion on the horizontal axis (see 3.4.7) and a certain stress or strain (S) value on the vertical axis. In this chapter the choice of the stress or strain value is discussed.

seawater to maintain the amount of dissolved oxygen within the required specification. The tests were carried out at a temperature of 20°C ± 1°C. The free corrosion potential was found to be approximately -0.67 V with respect to an Ag/AgCl reference electrode. The test under cathodic protection (nr. 16) was done with a potential of -0.8 V. An impressed current system was used.

3.3.3 Strain measurements

Of each geometry one specimen was extensively strain gauged (up to 100 gauges) to determine the strain distribution in the joint. On the other specimens of the same geometry there were only gauges to check the load range and to discover the appearance of a crack early.
At the Stevin Laboratory the strain gauges were measured dynamically. At the IBBC-TNO the strain gauges were measured under a static load.

Before the start of the fatigue test the specimens were loaded up to a load lower than the subsequently applied fatigue load to determine the strain distribution and the strain concentration factor (SNCF) (see 3.4.3). The loading procedure was repeated a couple of times before measurement, in order to avoid the effect of strain redistribution which may occur during the first few cycles. During the fatigue test strain readings were made periodically. These strain readings gave indications about the start of a crack, crack growth and through crack.
At the IBBC-TNO the whole measurement procudure was controled by a mini computer. This minicomputer controls several tests at the same time during the fatigue test. It carried out strain measurements periodically. It compared the measured strain range with the strain range at the first cycle. When a difference between these two strain ranges was measured to be beyond a prespecified limit, the minicomputer stopped the test: otherwise the test was recommenced.

3.3.4 Crack growth

When a fatigue crack was discovered, it was monitored visually and the surface crack length was measured periodically.
As mentioned in 3.3.3 the change in strain range also gives an indication of crack growth.
A through crack was determined by means of a low air pressure in the chord.

A fabrication data-sheet for each specimen was made during fabrication. On these sheets all relevant particulars are noted, such as: geometry, weld details, place of tack welds, number and position of runs with number of electrodes used, current and special items such as description of repairs, etc. A fabrication data sheet of some specimens is given in Appendix 3-I.

One special test specimen (nr. 41) was made to classify the weld procedure (see fig. 3.2.1):
Charpy V tests were carried out at a temperature of - 20°C of test specimens taken from: - weld metal
- fusion line of 914 mm pipe
- heat effected zone of the 914 mm pipe.

Table 3.2.5 gives the results of these tests. The average values were above the required value of 27 Joule.
Hardness measurements were taken from two cross sections (see fig. 3.2.2) over the weld. Table 3.2.6 gives the results of these measurements. The maximum allowable hardness of 350 HV was never measured.

3.3 Test and measurement equipment

3.3.1 Rigs

To avoid secondary effects all supports in the test rigs are hinges.
The loads were applied by servohydraulic actuators.
Fig. 3.3.1 to fig. 3.3.7 give an impression of the lay-out of the various test rigs.
The number of cycles was given on the loading control unit.

3.3.2 Seawater installation

The seawater conditions used for the 4 tubular tests was the same as used for the flat specimens (see paragraph 2.2.5). This means artificial seawater according to ASTM specification number D 1141-52, but without the presence of the stock solution number 3 (containing heavy metal ions).
The tube to tube connection was surrounded by a plastic box (see fig. 3.3.8), through which the seawater was circulating from a container.
During the test clean air was pumped continually into the supply of

joints have one (T1 and X1) or two (T2) additional unloaded braces. Two joints are tested with a random load and all others with a constant amplitude load. Some tests were carried out with $R = F_{min}/F_{max} = 0$ and others with R = -1. Four joints have been tested in artifical seawater, one of them with cathodic protection.

The steel grade of the tubular joints is in accordance with the standards mentioned in table 3.2.2.b. The actual dimensions of the wall-thickness of the tubes is given in table 3.2.2.a.
The mechanical properties are given in table 3.2.3. and the chemical composition can be found in table 3.2.4.

The welding consumables used have a grade notation of 3 YHH and code classifications of AWS - E 7016
DIN - E 5144 B10
ISO - E 514 B 14 (H)

The welding procedure for the tube connection is as mentioned below:

Welding process	:	MMAW, current: AC
Base metal	:	Fe 510 - 3N or similar
Joint preparation	:	according to API RP2A, 5.3, fig. 5.1
Welding parameters	:	amp. - 75 - 160
		position - 5G
		cleaning - wire brush between runs
Heat treatment	:	not required
Pre-heat temperature	:	$t < 20$ mm 65°C
		$20 \leq t \leq 40$ mm 100°C
Interpass temperature	:	$t < 20$ mm 65°C
		$20 \leq t \leq 40$ mm 100°C
Electrode diameter	:	root run electrode - $2\frac{1}{2}$ mm
		first two fill runs - $3\frac{1}{4}$ mm }
		next fill c.q. capruns - 4 mm } as applicable
Weld surface finish	:	as welded
Storage of electrodes	:	to be dried in oven at 300°C and stored at 100°C
Inspection	:	NDT-utrasonic 100 %

The fabrication of the specimens was carried out by a firm which has experience in constructing offshore structures. The specimens were welded in a horizontal position with both chord and brace horizontal.

3. FATIGUE TESTING OF TUBULAR JOINTS

3.1 Introduction

In the previous part, entitled 'Basic tests' the results of the flat plate specimens were given. These flat plate tests give basic information about the fatigue properties of steel (influence of material, welding parameters, post weld heat treatment, weld toe profile, loading condition, etc.).

Offshore steel structures, especially jackets, are build up from tubulars, connected together by welding. Therefore we are interested in the fatigue properties of such tubular connections. Forty tests on tubular T- and X-joints were carried out in this part of the Dutch programme. As far as the dimensions of the specimens are concerned, they can be divided into three groups: small, medium and large, with respective chord diameters of 168, 457 and 914 mm. The medium size specimens were tested at the Stevin Laboratory of Delft University of Technology. The small and the large ones were tested at the Institute TNO for Building Materials and Building Structures (IBBC-TNO).

Fig. 3.1.1 gives an idea of the test procedures. The critical area's of a specimen are determined by literature investigations and/or calculations. With this information, a strain gauge pattern was chosen for that specimen. Then, with a static load the strain distribution and the strain concentration factor (SNCF) were measured. A fatigue load was determined from the measured SNCF and the existing knowledge of the fatigue behaviour of the joints in order to get the desired number of cycles. After the fatigue test the result was plotted on an S-N diagram with a strain or stress range on the vertical axis and the number of cycles to a certain failure criterion on the horizontal axis.

3.2 Test specimen

Table 3.2.1 gives a survey of the test programme. Three small T-joints were loaded with in plane bending. All other joints were axially loaded. One X-joint was tested with both chord and brace axially loaded. Some

- Institute TNO for Building Materials
  and Building Structures (IBBC-TNO)
- Delft University of Technology (DUT)
  Stevin Laboratory
  Department of Civil Engineering

3. FATIGUE TESTING OF TUBULAR JOINTS

Ir. O.D. Dijkstra - IBBC-TNO
Ir. C. Noordhoek - DUT

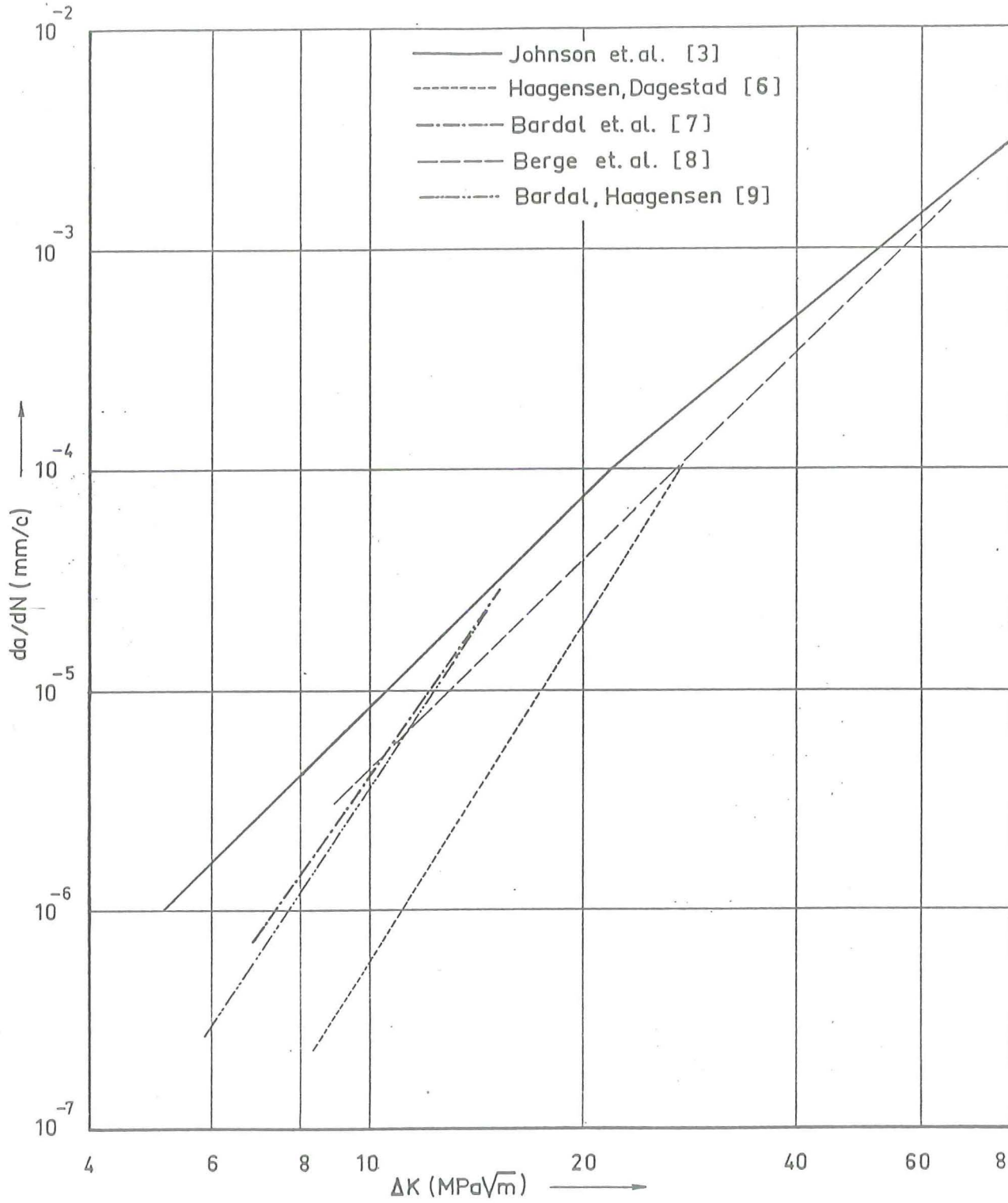

Figure 2.4.24 Crack growth data in air obtained by various investigators.

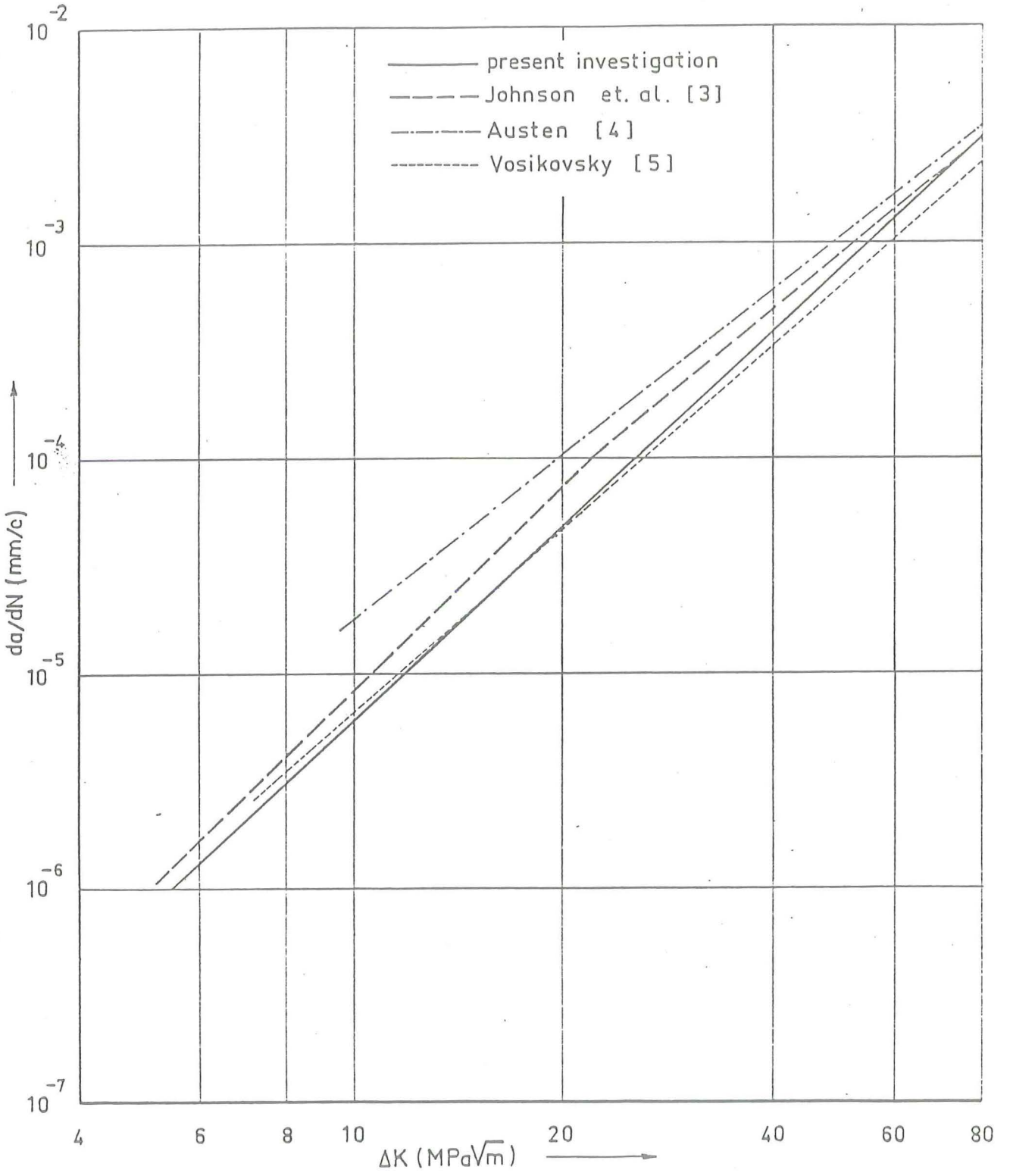

Figure 2.4.23 Comparison of the results of the present investigation (crack growth data in air) with the results of other investigations.

47 - 1

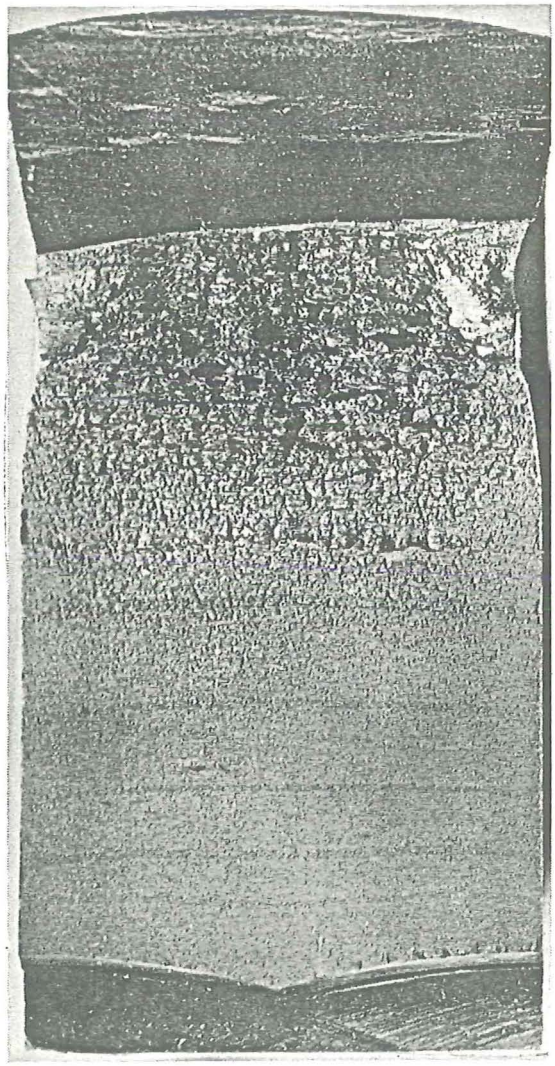

47 - 1

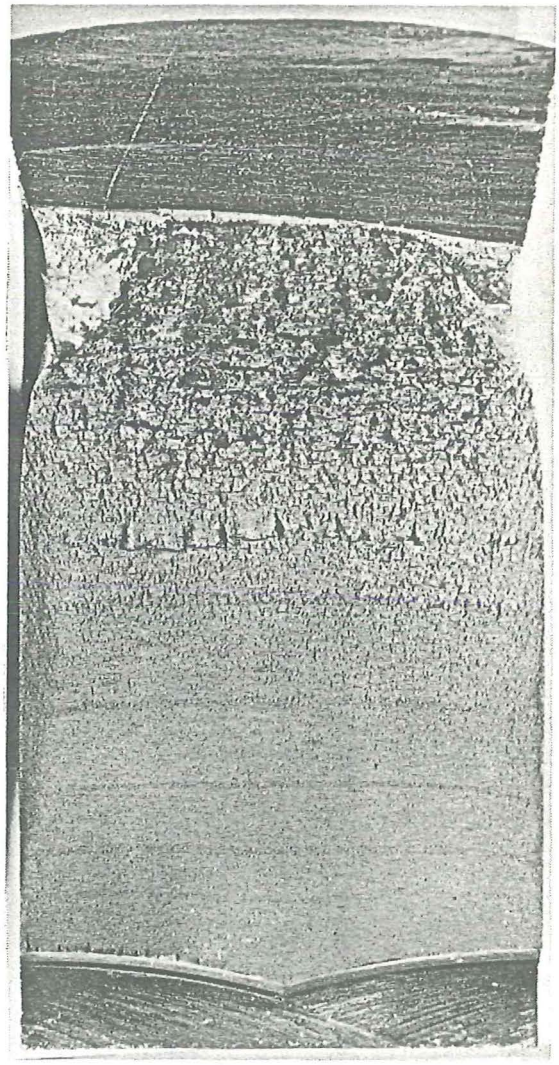

Figure 2.4.22 Crack surfaces of specimen 47-1.

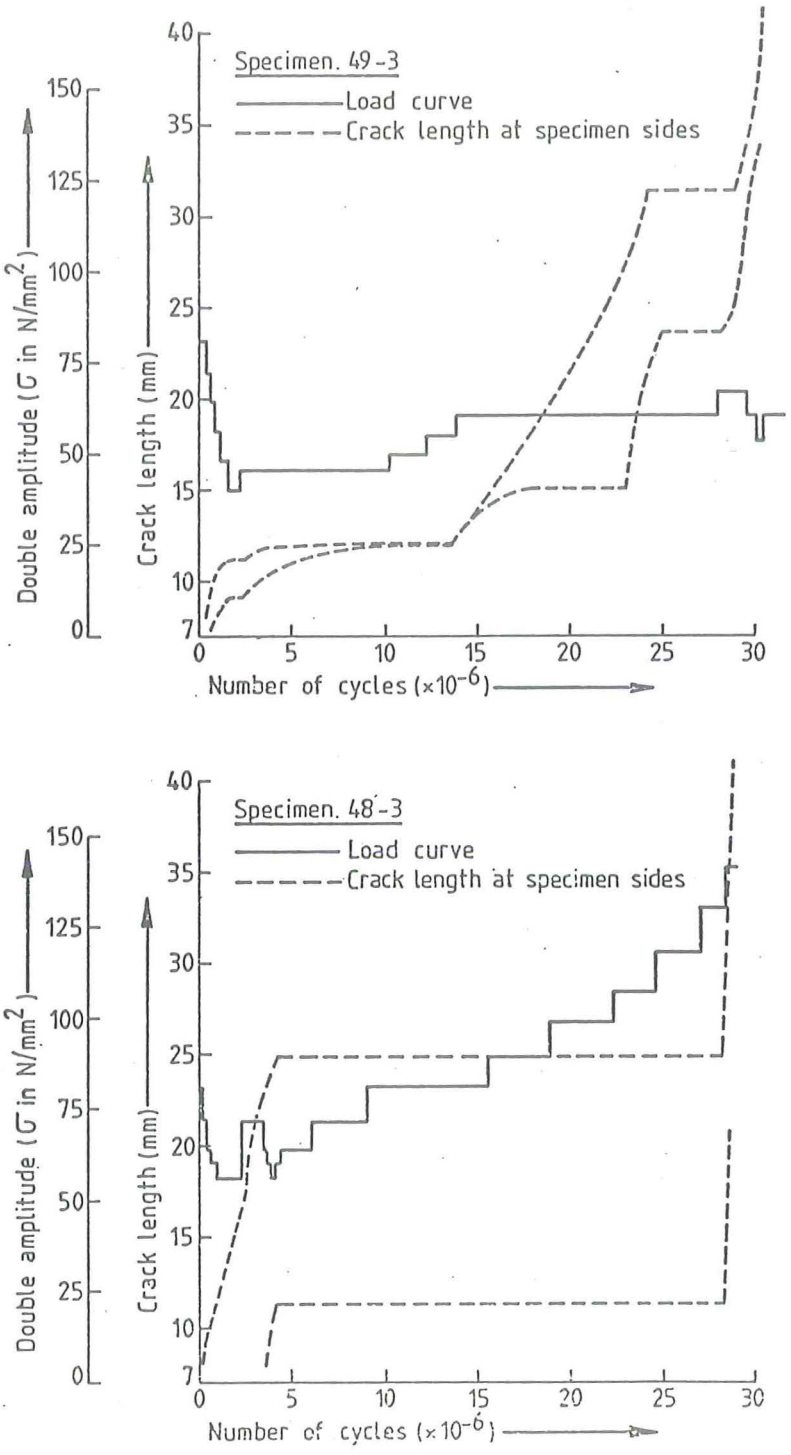

Figure 2.4.21 Loading history and crack growth development during testing of specimens 48-3 and 49-3.

48 - 3

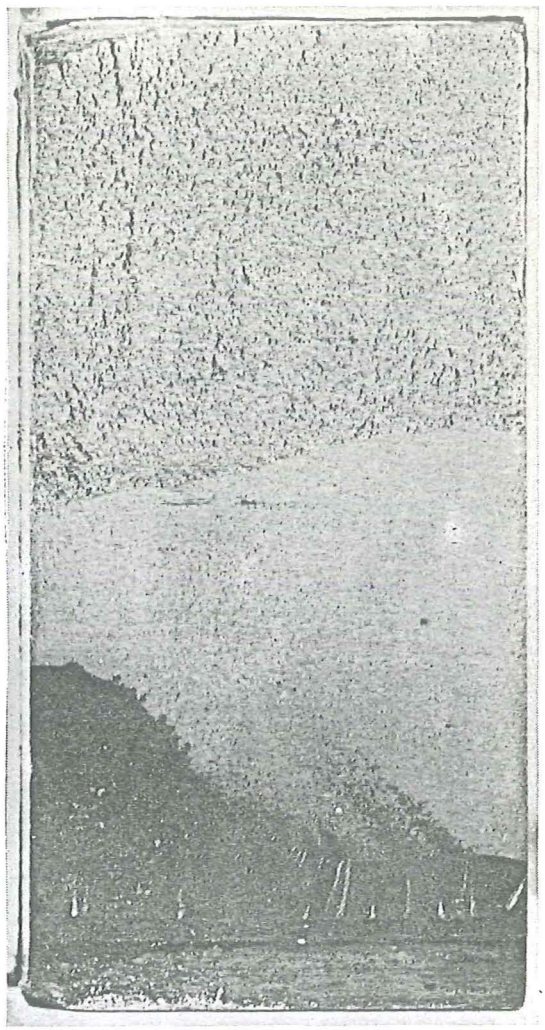

49 - 3

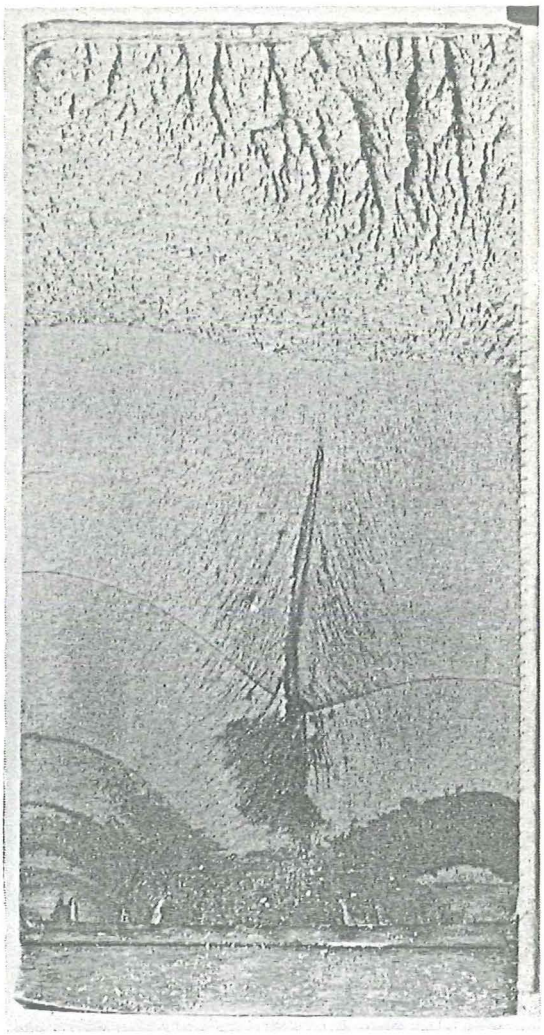

Figure 2.4.20 Crack surfaces of specimens 48-3 and 49-3.

49 - 1

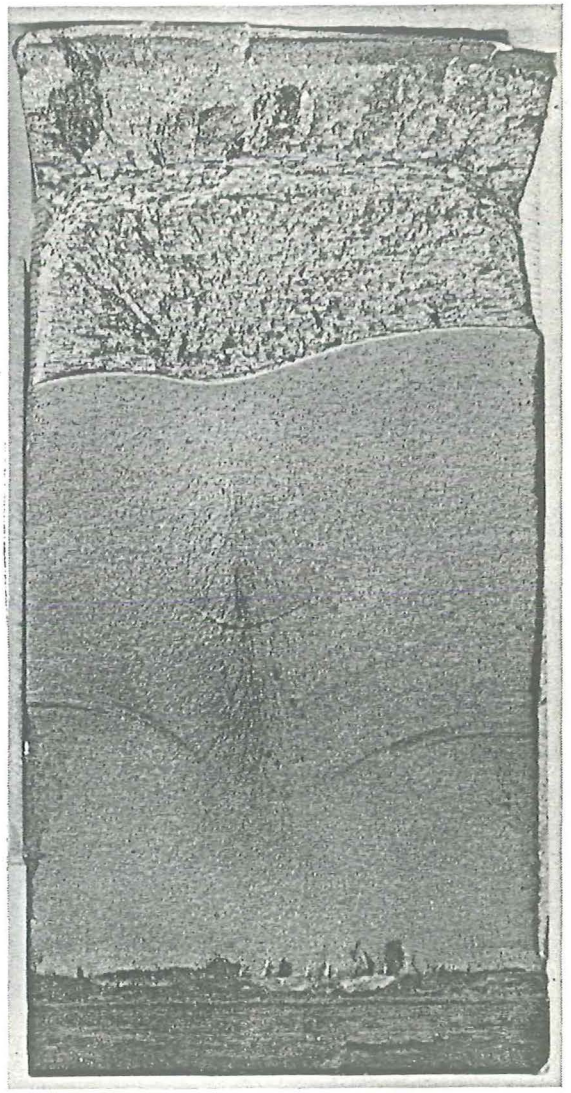

49 - 2

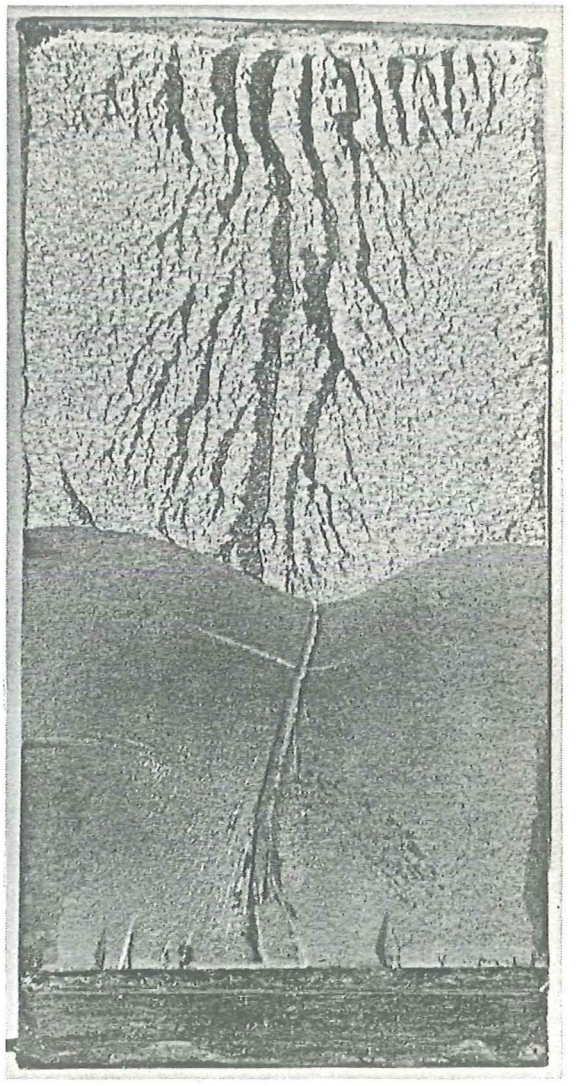

Figure 2.4.19 Crack surfaces of specimens 49-1 and 49-2.

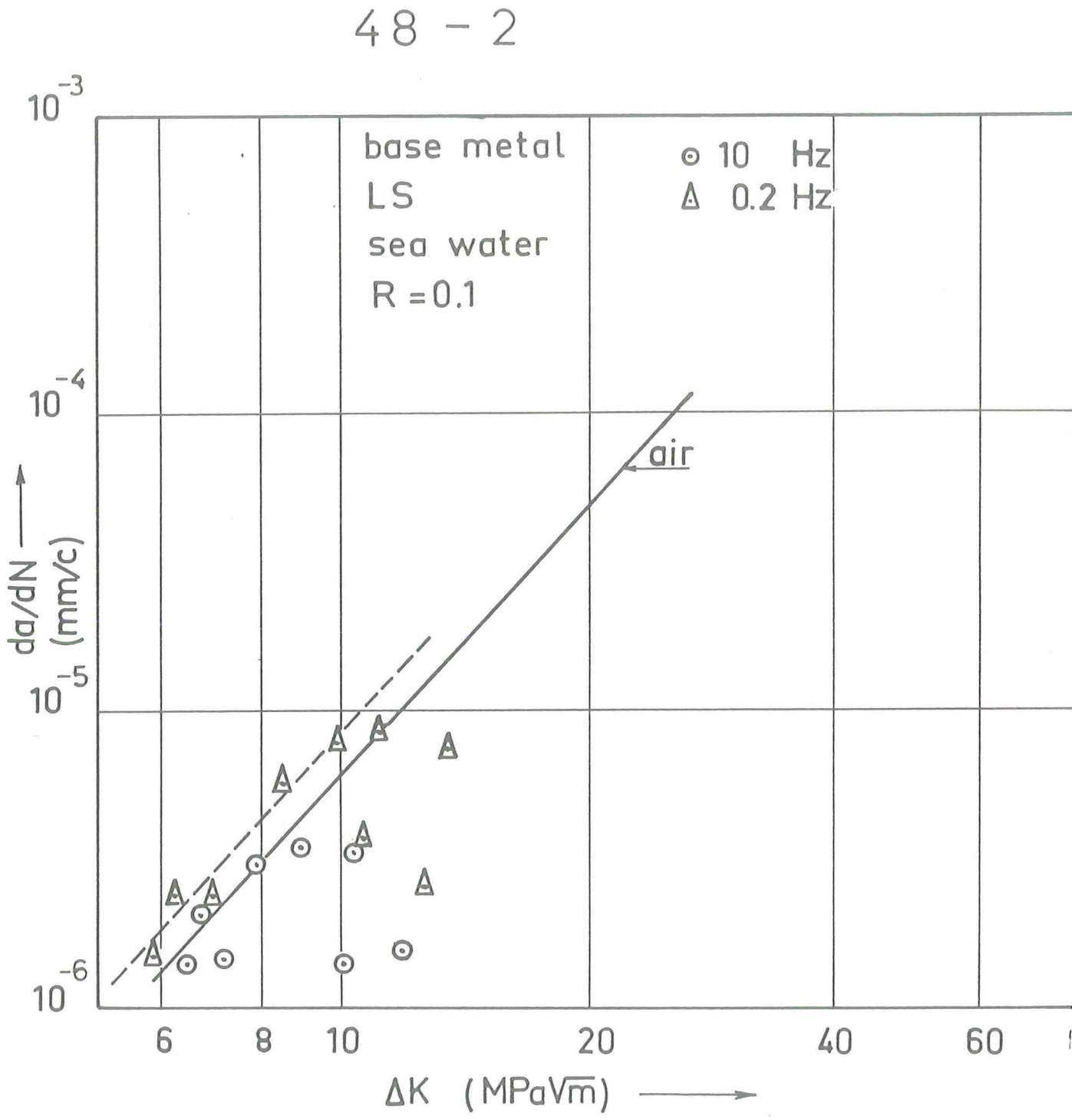

Figure 2.4.18. Results of testing of specimen 48-2.

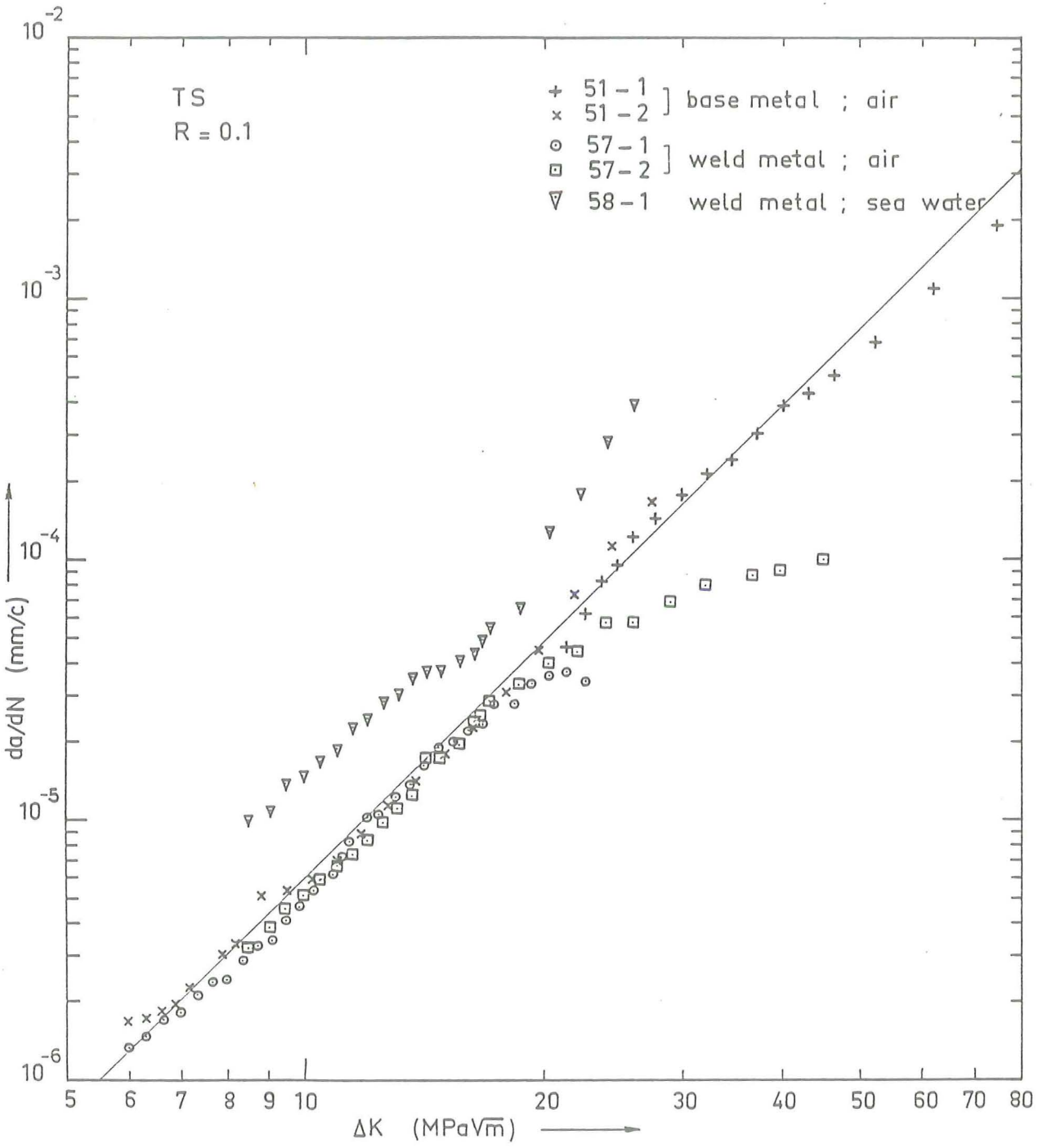

Figure 2.4.17 Comparison of fatigue crack propagation in base metal and weld metal (air and sea water).

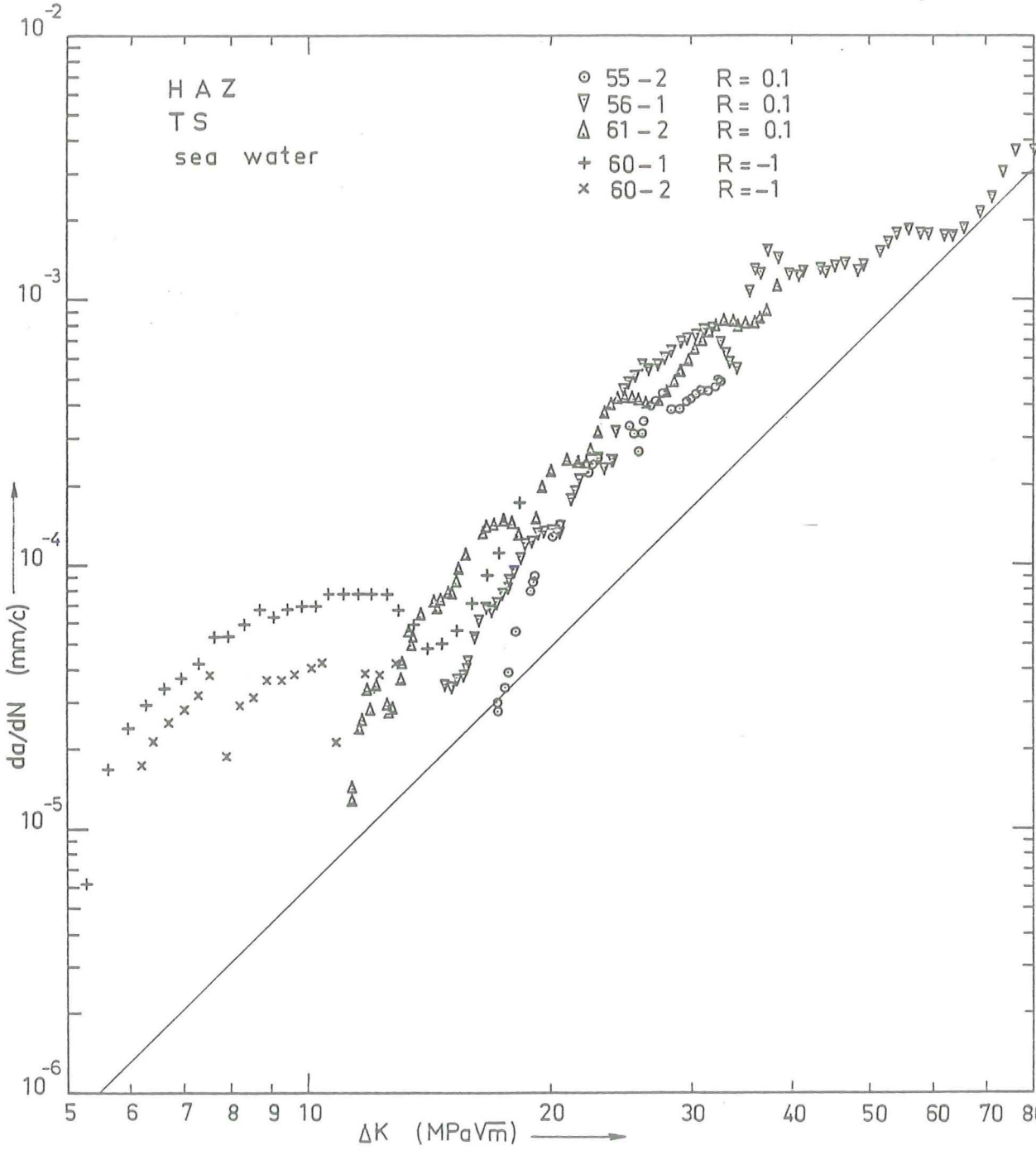

Figure 2.4.16 Influence of stress ratio (HAZ; sea water; R = 0.1 vs R = -1).

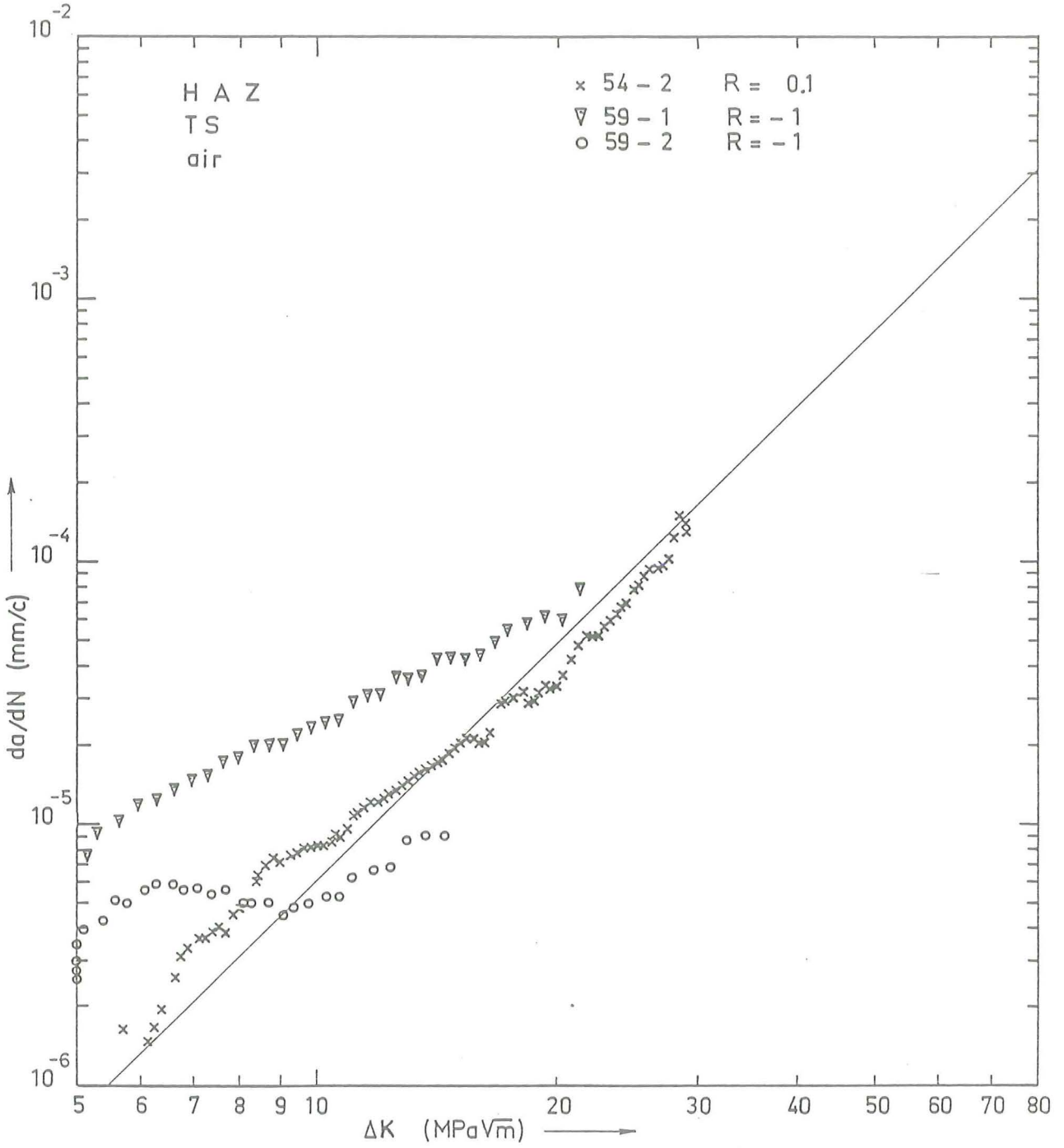

Figure 2.4.15 Influence of stress ratio (HAZ; air; R = 0.1 vs R = -1).

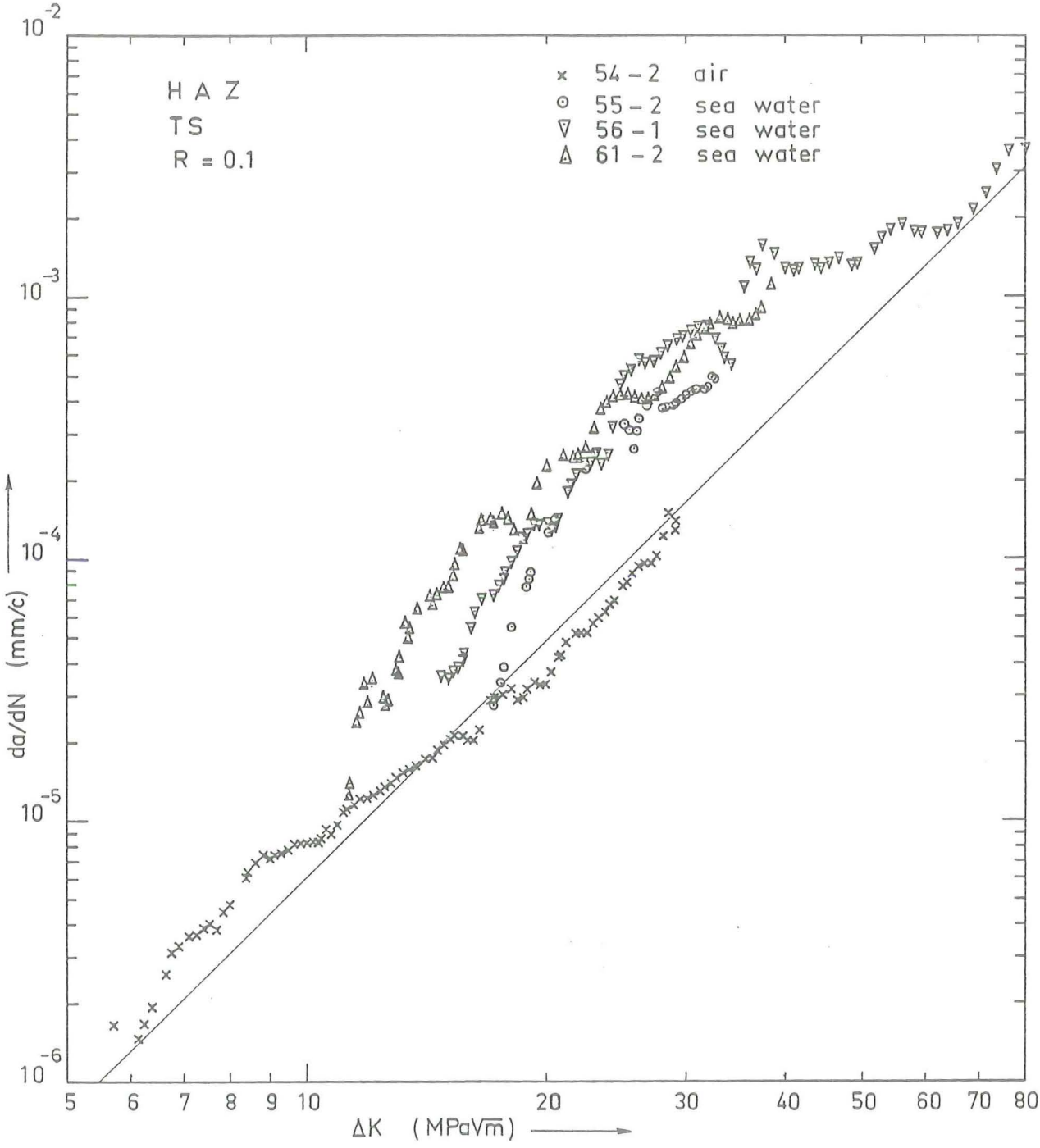

Figure 2.4.14 Influence of environment (HAZ; air vs sea water).

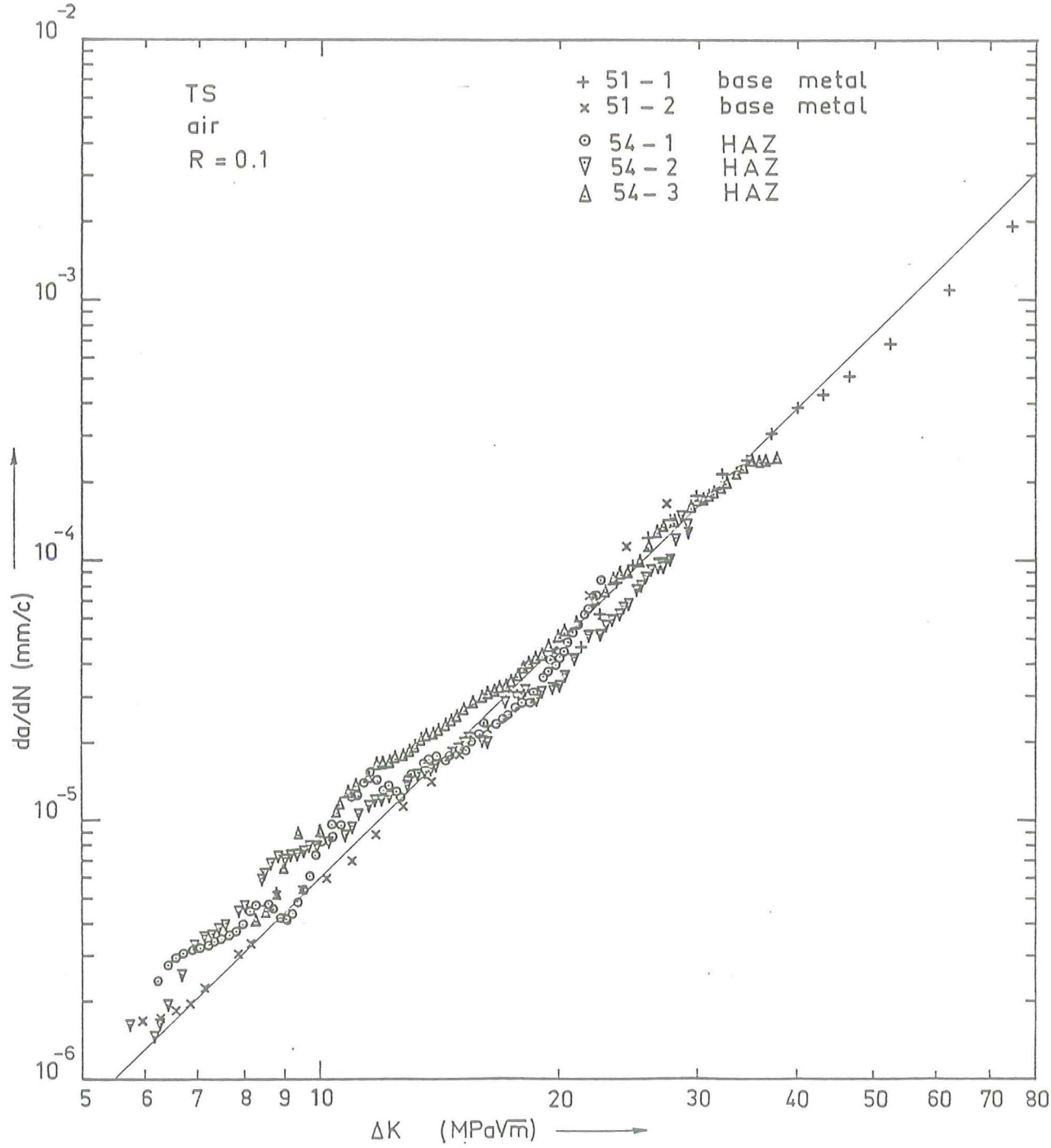

Figure 2.4.13 Comparison of fatigue crack propagation in base metal and HAZ (air; R = 0.1).

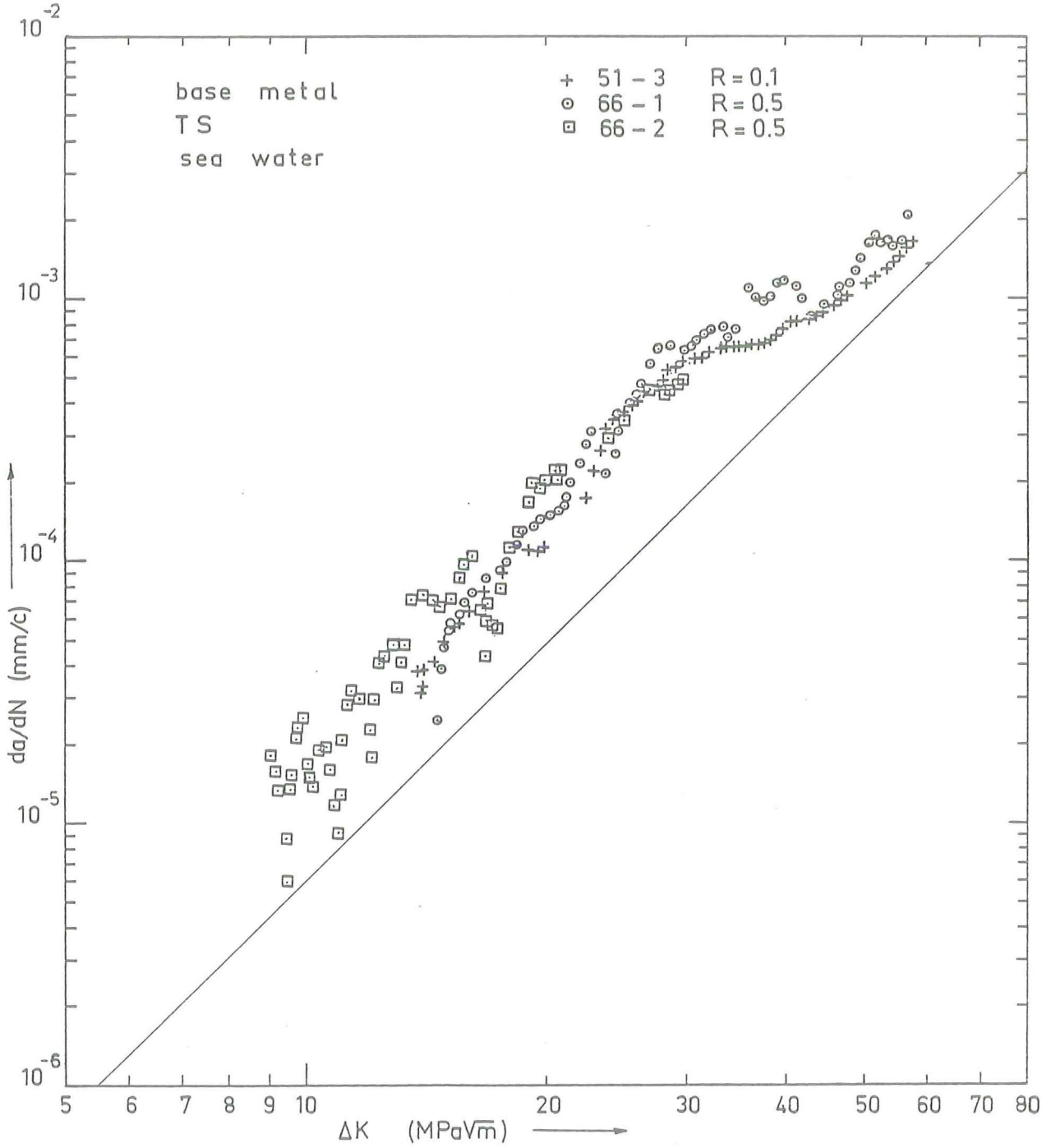

Figure 2.4.12 Influence of stress ratio (base metal; sea water; R = 0.1 vs R = 0.5).

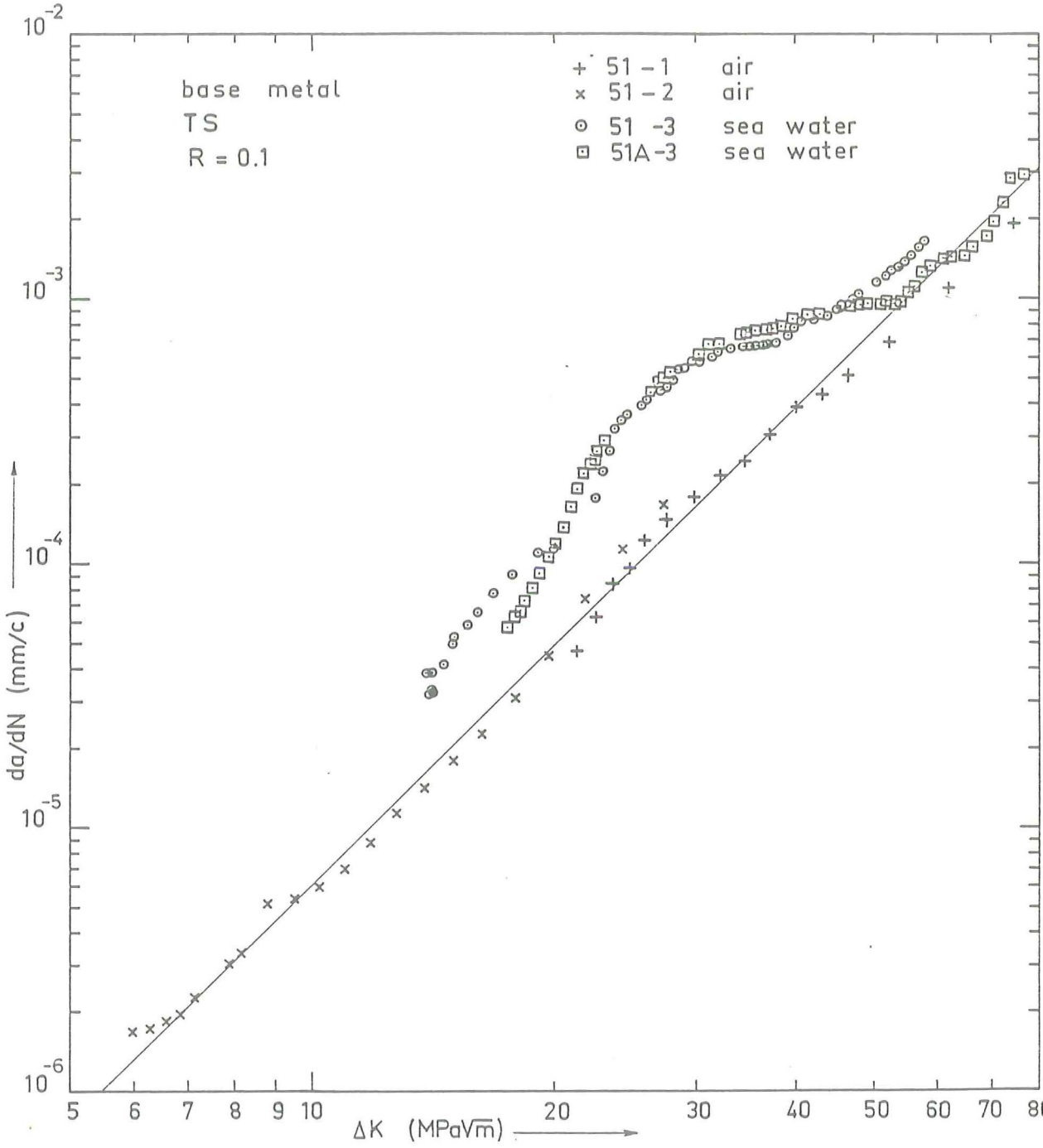

Figure 2.4.11 Influence of environment (base metal; air vs sea water)

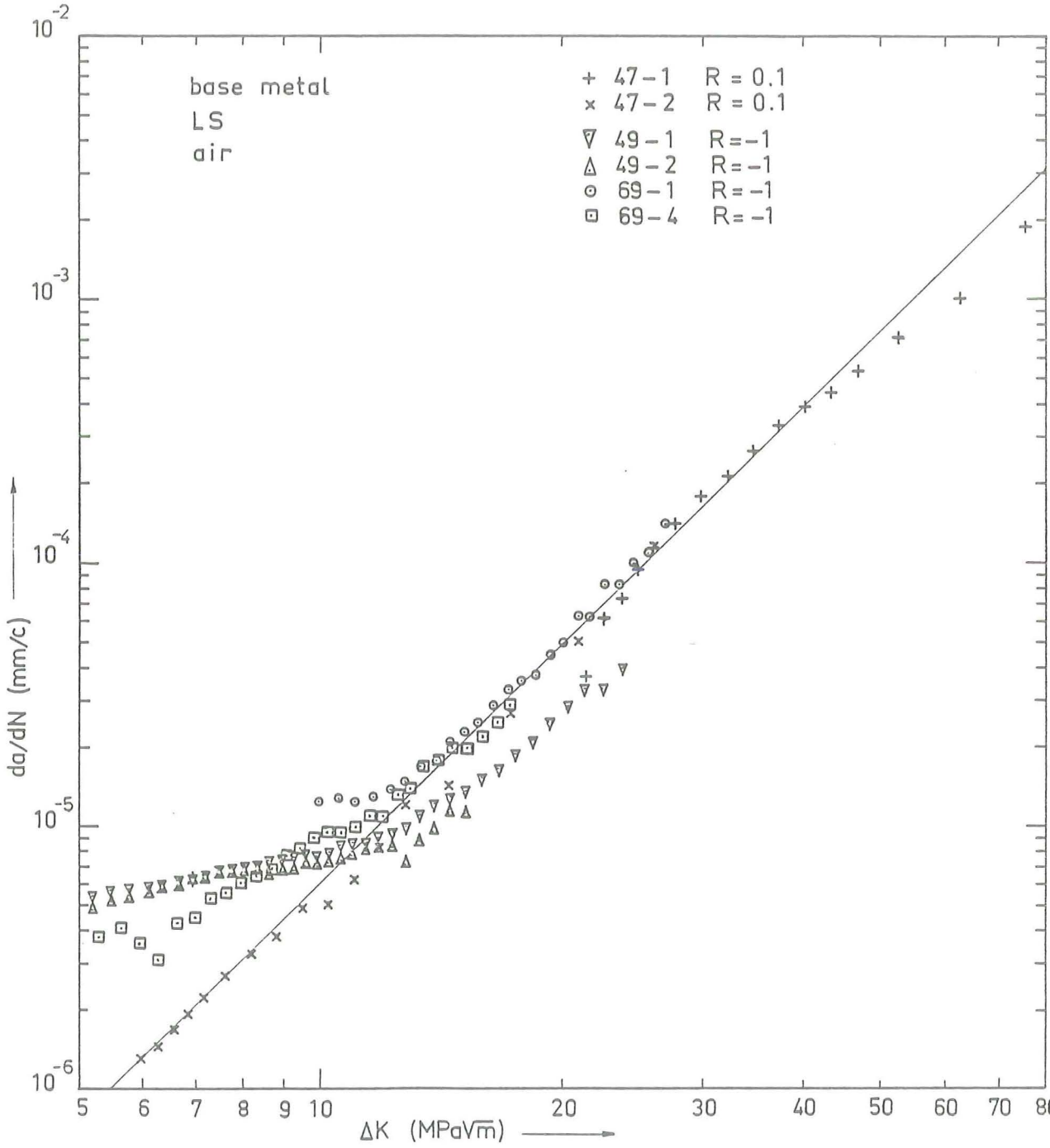

Figure 2.4.10 Influence of stress ratio (base metal; air; R = 0.1 vs R = -1).

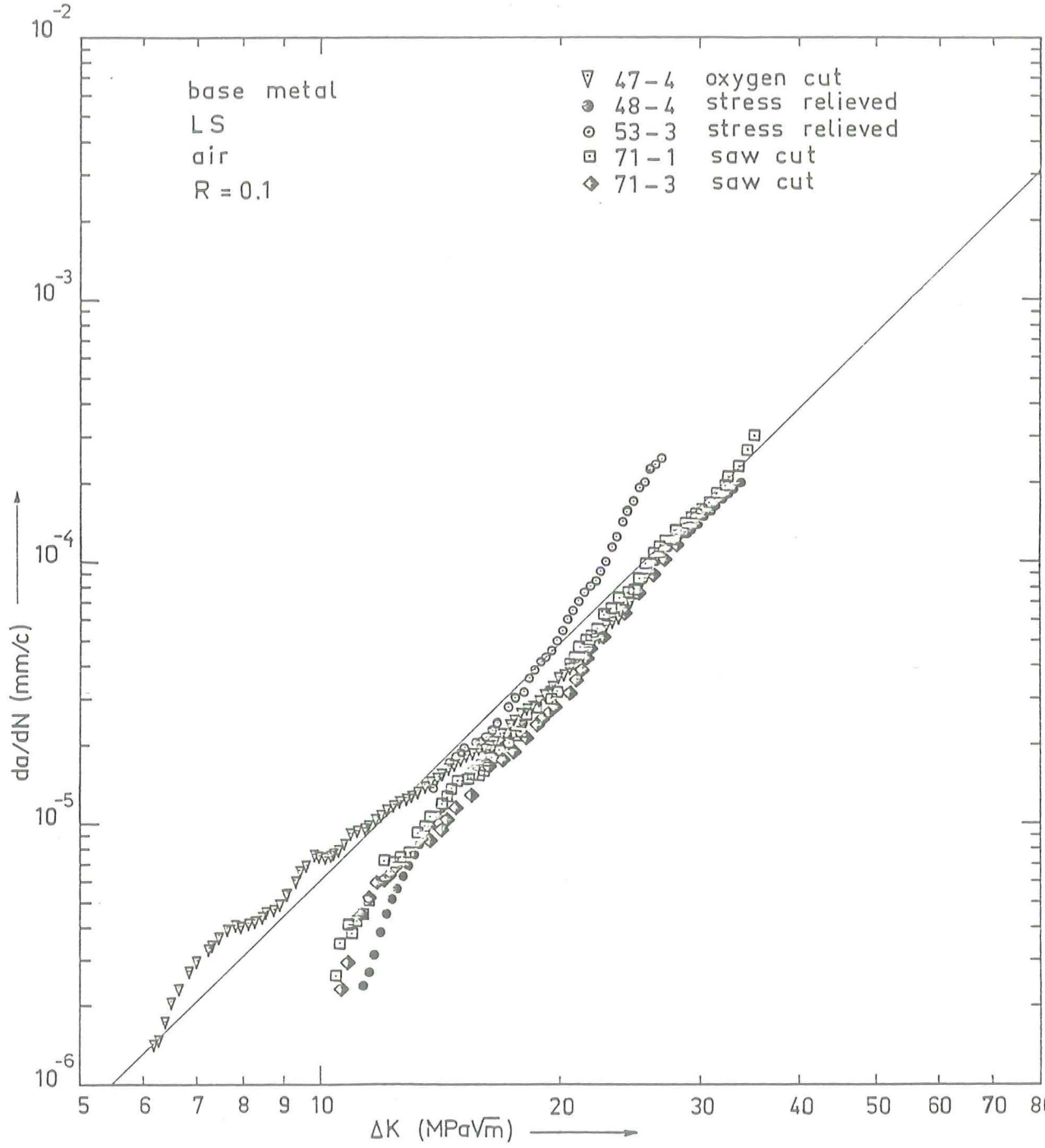

Figure 2.4.9 Influence of stress relieving and saw cutting (base metal; air).

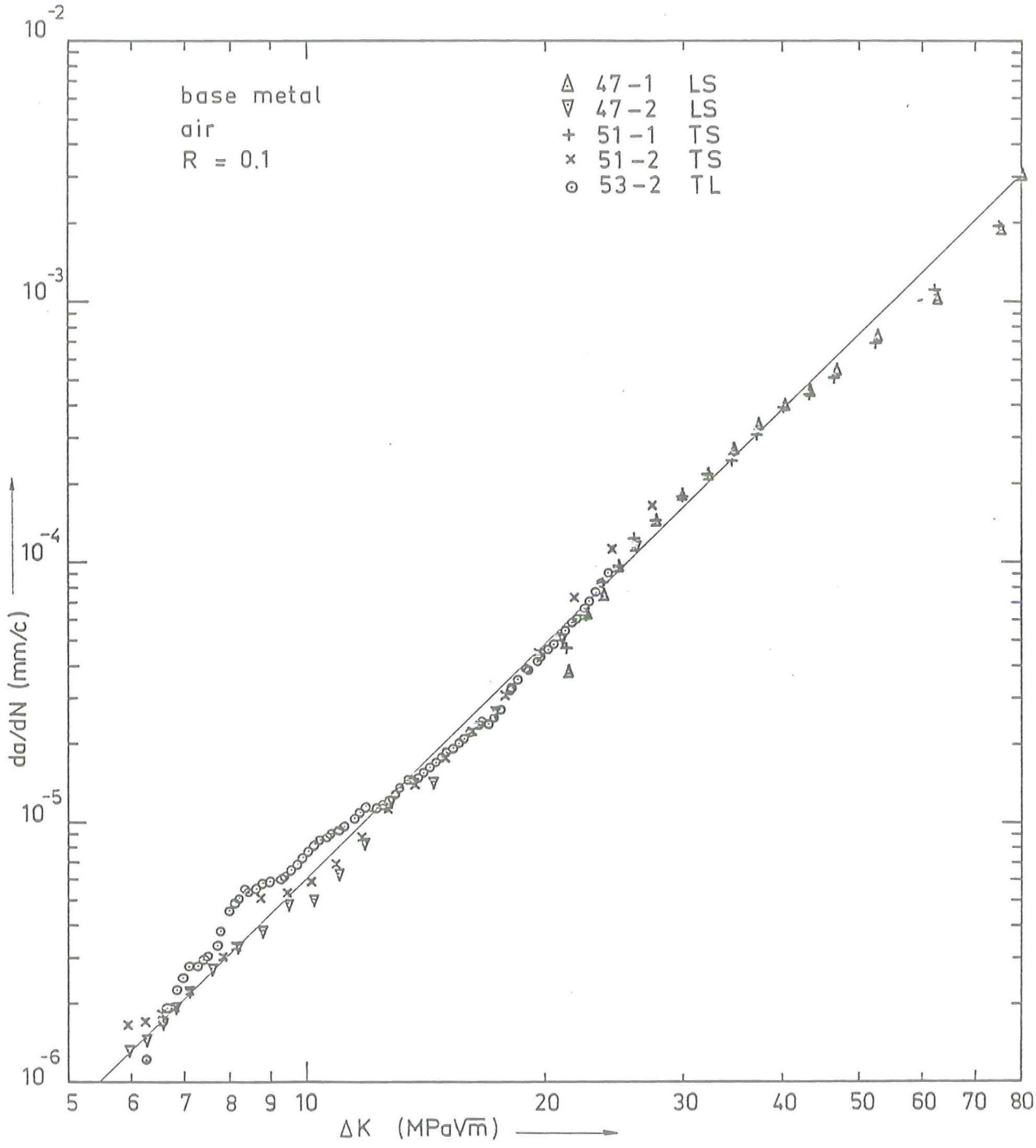

Figure 2.4.8 Influence of specimen orientation (base metal; air).

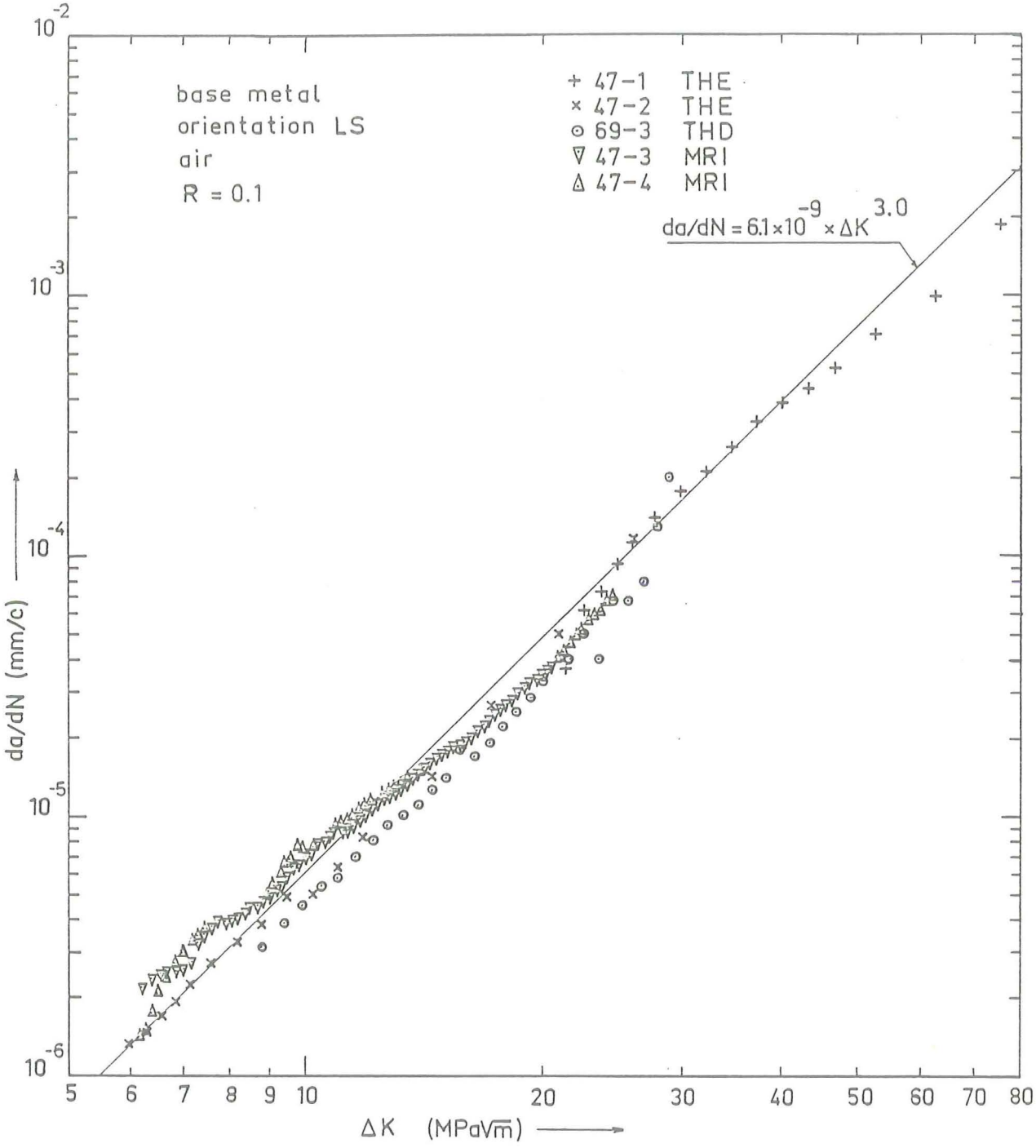

Figure 2.4.7 Results of experiments on fatigue crack propagation in base metal performed in the three participating laboratories.

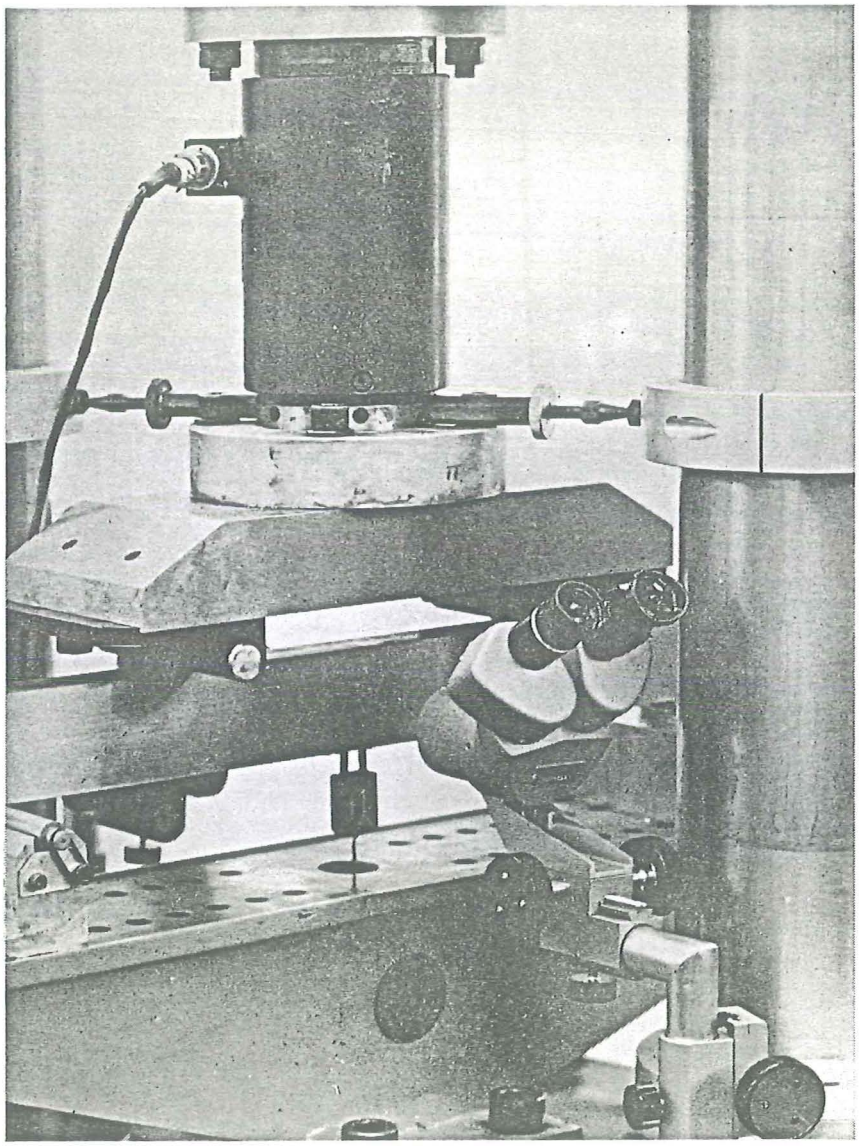

Fig. 2.4.6b Detail of 120 kN test equipment at the laboratory of structural fatigue, University of Technology, Eindhoven.

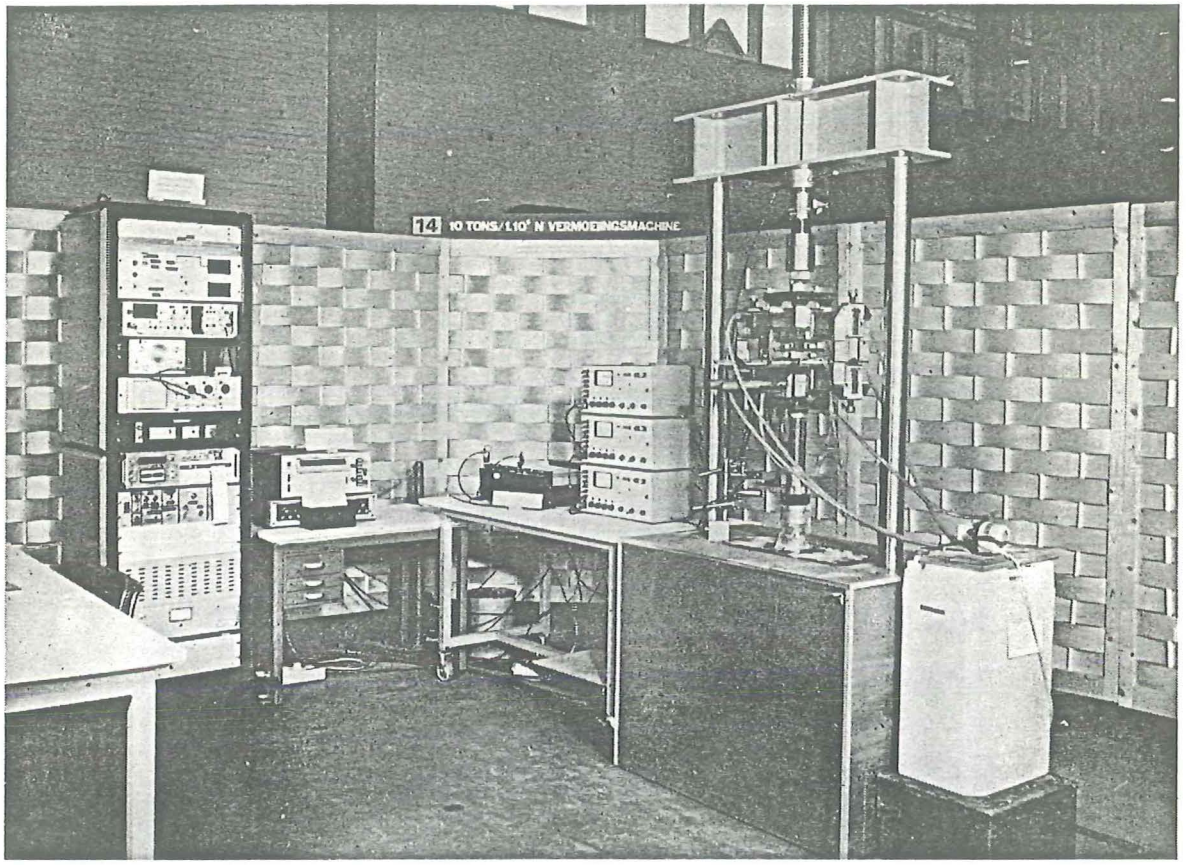

Figure 2.4.6a 100 kN test equipment at the ship structures laboratory University of Technology, Delft.

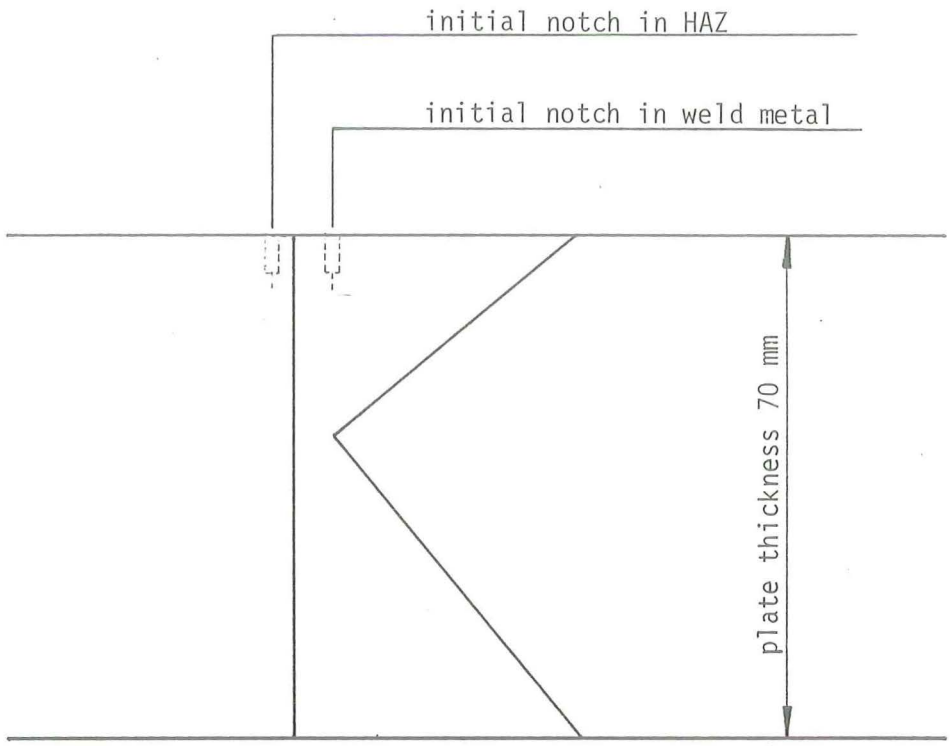

Fig. 2.4.5 Positioning of initial notch in specimens for experiments on crack growth in HAZ and weld metal

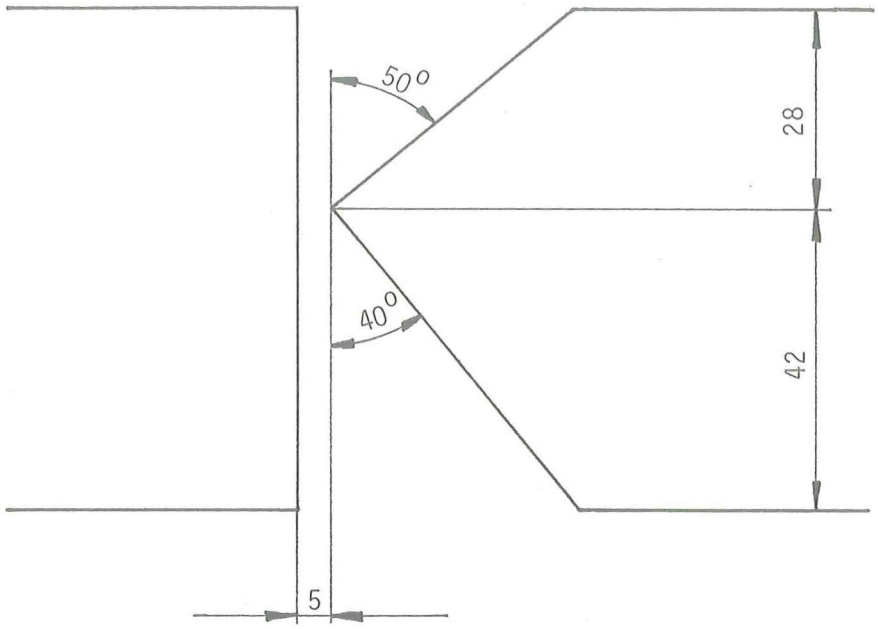

Fig. 2.4.4.a Joint preparation for K-weld

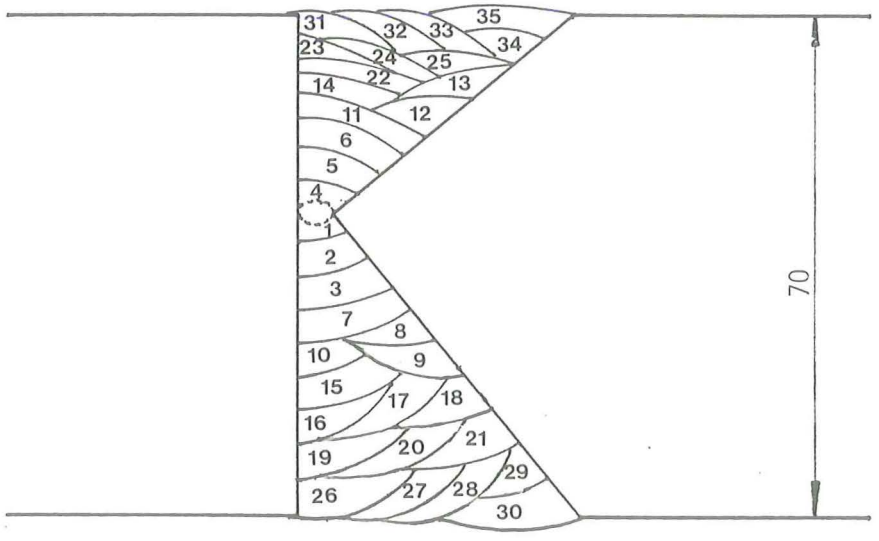

Fig. 2.4.4.b Build-up sequence of weld

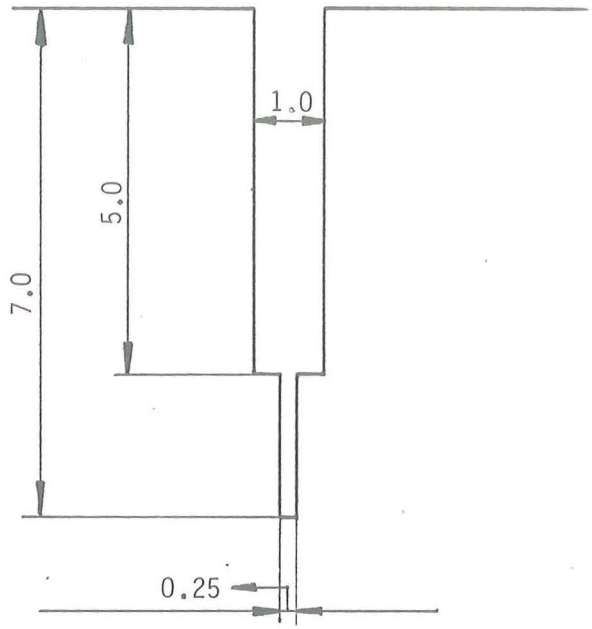

Fig. 2.4.3.a Initial notch with straight front

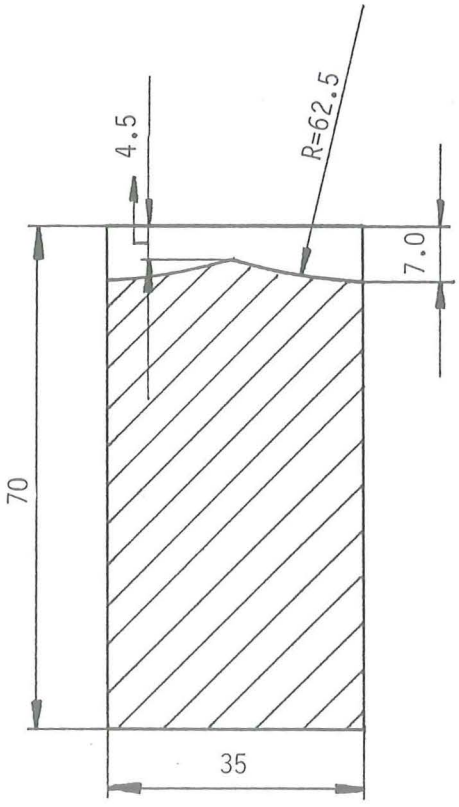

Fig. 2.4.3.b Chevron type initial notch

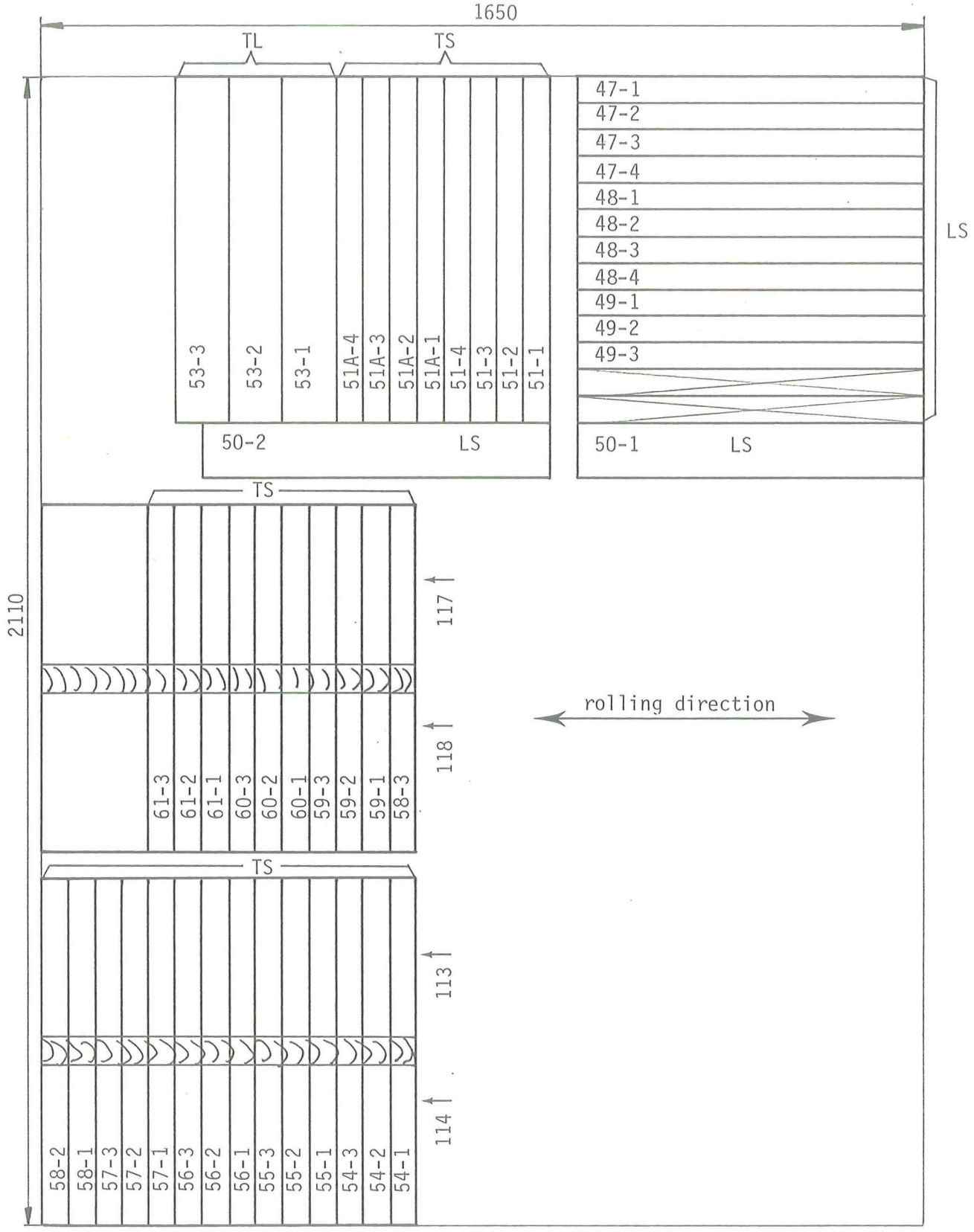

Fig. 2.4.2 Specimens for crack growth studies in base material, heat affected zone, and weld metal.
Original position in plate of specimens from series 47 through 61.

2.4.11. Figures

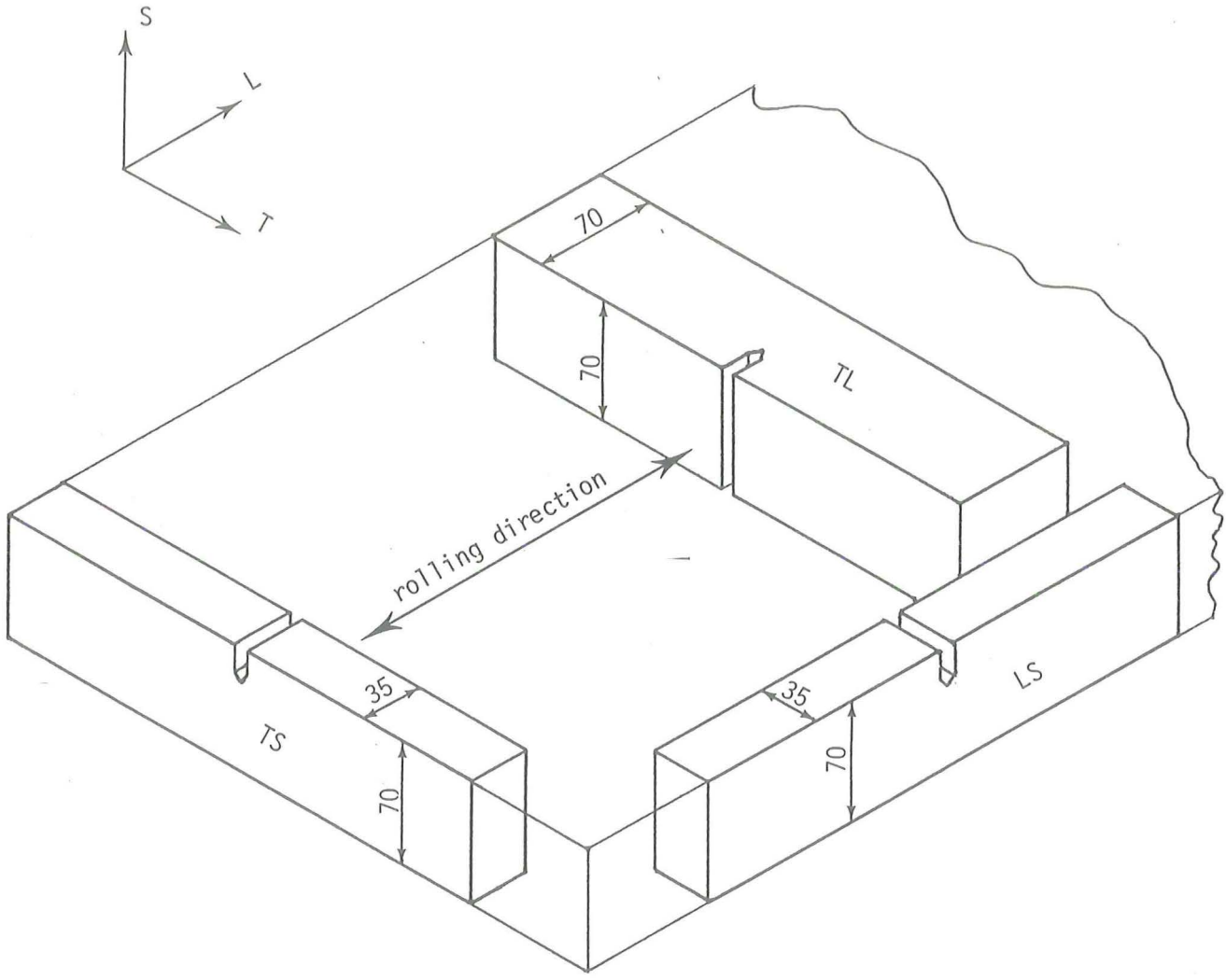

Fig. 2.4.1 Orientation of crack growth specimens and nominal dimensions of cross section.

Table 2.4.1 continued

Material	Orientation	Range Stress Ratio R	Environment	Nominal Stress (N/mm^2)	Comments	Laboratory *)	Specimen Designation
Weld Metal	TS	0.1	Air	30	Stress Relieved	THD	57-1
	TS	0.1	Air	45	"	THD	57-2
	TS	0.1	Sea-water	45	"	THD	58-1

*)
THD = University of Technology, Delft
THE = University of Technology, Eindhoven
MRI = Metal Research Institute TNO

**) evaluation of results cancelled
***) saw-cut specimens

2.4.10. Tables

Table 2.4.1. Summary of crack propagation tests

Material	Orientation	Stress Ratio R	Environment	Range Nominal Stress (N/mm^2)	Comments	Laboratory *)	Specimen Designation
Base Metal	LS	0.1	Air	126		THE	47-1
	LS	0.1	Air	33.3		THE	47-2
	LS	0.1	Air	37		MRI	47-3
	LS	0.1	Air	37		MRI	47-4
	LS	0.1	Air	50	Stress relieved	MRI	48-4
	LS	0.1	Air	50		MRI	50-1**)
	LS	0.1	Air	50		MRI	50-2**)
	LS	0.1	Air	50		THD	69-3
	LS	0.1	Air	50		MRI	71-1***)
	LS	0.1	Air	50		MRI	71-3***)
	LS	0.1	Sea-water	33.3		THE	48-2
	LS	-1	Air	45		THD	49-3
	LS	-1	Air	60		THD	49-1
	LS	-1	Air	60		THD	49-2
	LS	-1	Air	100		THD	69-1
	LS	-1	Air	60		THD	69-4
	LS	-1	Air/Sea-water	60		THD	48-3
	TS	0.1	Air	126		THE	51-1
	TS	0.1	Air	33.3		THE	51-2
	TS	0.1	Sea-water	72		MRI	51-3
	TS	0.1	Sea-water	90		MRI	51A-3
	TS	0.5	Sea-water	80		MRI	66-1
	TS	0.5	Sea-water	60		MRI	66-2
	TL	0.1	Air	37		MRI	53-2
	TL	0.1	Air	50	Stress Relieved	MRI	53-3
Heat Affected Zone	TS	0.1	Air	37	"	MRI	54-1
	TS	0.1	Air	37	"	MRI	54-2
	TS	0.1	Air	50	"	MRI	54-3
	TS	0.1	Sea-water	90	"	MRI	55-2
	TS	0.1	Sea-water	37	"	MRI	55-3**)
	TS	0.1	Sea-water	72	"	MRI	56-1
	TS	0.1	Sea-water	72	"	MRI	56-2**)
	TS	0.1	Sea-water	60	"	MRI	61-2
	TS	-1	Air	60	"	THD	59-1
	TS	-1	Air	36	"	THD	59-2
	TS	-1	Sea-water	60	"	THD	60-1
	TS	-1	Sea-water	48	"	THD	60-2

| 8| S. Berge, O.I. Eide, E.T. Moe
"Fatigue crack initiation in weldments of a C-Mn steel"
Ref |2|, paper 6

| 9| E. Bardal, P.J. Haagensen
"Corrosion fatigue crack propagation tests on steels for offshore structures"
OTC 2855, 9th Annual OTC, Houston, May 2-5, 1977

|10| P. Bristoll
Report on fatigue of offshore structures (crack propagation data)
KSLA 1975 (private circulation)

|11| O. Vosikovsky
"Effects of stress ratio on fatigue crack growth rates in X-70 pipeline steel in air and saltwater"
J. of Testing and Evaluation, vol 8, No. 2, March 1980, pp 68-73

|12| D. Benoit, H.P. Lieurade, M. Truchon
"Study of the propagation of fatigue cracks in the thermally affected zones of welded joints in E36 steel"
Ref |2|, paper 13

|13| P. Bristoll, J.A. Roeleveld
"Fatigue of offshore structures: effect of sea water on crack propagation in structural steel"
Ref |2|, paper 18

|14| J.L. van Leeuwen
"Endurance tests on plate specimens"
Chapter 2.2. of final report with respect to ECSC Convention 7210-KB/6/602 (J. 7.1 f/76):"Fatigue and corrosion fatigue behaviour of offshore steel structures".

2.4.9. References to chapter 2.4

|1 | H. Tada, P.C. Paris, G.R. Irwin
The stress analysis of cracks handbook
DEL-Research-Corporation, Hellertown, Pa, 1973

|2 | Select Seminar on European Offshore Steels Research
The Welding Institute, Abington Hall, Cambridge, U.K.
27-29 November 1978

|3 | R. Johnson, I. Bretherton, B. Tomkins, P.M. Scott,
D.R.V. Silvester
"The effect of sea water corrosion in fatigue crack
propagation in structural steel"
Ref |2|, paper 15

|4 | I.M. Austen
"Factors affecting corrosion fatigue crack growth in steels"
Ref |2|, paper 14

|5 | O. Vosikovsky
"Fatigue crack growth in an X-65 line-pipe steel at low
cyclic frequencies in aqueous environments"
Closed Loop, the Magazine of Mechanical Testing,
April 1976, pp 3-12

|6 | P.J. Haagensen, V. Dagestad
"Random load crack propagation in sea water in a medium
strength structural steel"
Ref |2|, paper 22

|7 | E. Bardal, J.M. Søndenfor, P.O. Gartland
"slow corrosion fatigue crack growth in a Structual Steel
in artificial sea-water at different potentials, crack depths,
and loading frequencies"
Ref |2|, paper 16

8. At R = -1 a higher crack propagation rate (in comparison with base metal) is observed in the HAZ in the region of low ΔK-values. This may be due to residual stresses. (fig. 2.4.15).

9. The results of the present investigation are in good quantitative accordance with the results obtained in other investigations. Nevertheless a mutual comparison of the results of the different investigations reveals that crack propagation data may show large differences, particularly in the region of low ΔK-values. In this region the results seem to be very sensitive to the presence of residual stresses, the load shedding procedure and the entire test procedure.

10. Although at low ΔK-values the sea water environment appears to have a minor influence on fatigue crack propagation the conclusion sometimes stated that sea water has no detrimental influence on the fatigue life of offshore structures seems to be premature.

2.4.8. Conclusions

1. The results of fatigue crack propagation tests at R = 0.1 in air performed in the three participating laboratories are in good agreement. They can be described by the relation $da/dN = 6.1 \times 10^{-9} \times \Delta K^{3.0}$ in the region $6 < \Delta K < 80$ MPa$\sqrt{m}$ (fig.2.4.7) (da/dN in mm/c; ΔK in MPa$\sqrt{m}$).

2. The orientation of the crack plane proves to have no significant influence on the fatigue crack propagation rate (fig. 2.4.8).

3. At R = -1 crack growth rate in air proves to be notably higher than at R = 0.1 in the initial stages of the tests. As crack growth proceeds the da/dN - ΔK curves for R = -1 and R = 0.1 tend to converge (fig. 2.4.10).

4. It is believed that the initial higher crack growth rate at R = -1 (when compared with R = 0.1) is due to the fact that the fatigue crack originated at the root of a mechanical notch. It is considered worthwhile to pay adequate attention to this phenomenon in future studies because the magnitude of the crack growth rate in the region of low ΔK-values has an important influence on fatigue life.

5. In sea-water the fatigue crack growth rate is about a factor 3 higher than in air. As crack growth rate increases the magnitude of the influence of the sea-water decreases and finally vanishes ($\frac{da}{dN} > 10^{-3}$mm/c) In the region of low crack growth rates ($<10^{-5}$mm/c) the influence of of the sea-water seems to be smaller as ΔK is lower (fig. 2.4.11).

6. The crack propagation rate in sea water at R = 0.5 appears to be only slightly higher than at R = 0.1. In the region of low ΔK-values which is the most interesting region from the viewpoint of fatigue life - this trend is obscured by scatter. Nevertheless this tendency is in accordance with the results of tests performed elsewhere.(fig. 2.4.12).

7. The crack propagation rate at R = 0.1 in air in the weld metal and the HAZ is not significantly different from the crack propagation rate in base material. (fig. 2.4.13; 2.4.17).

The initial relatively high crack growth rate at R = -1 (when compared with the results on base metal at R = -1) may be due to residual stresses, inspite of the postweld heat treatment.

Finally the minor influence of the sea water environment at low ΔK-values, as found by Johnson et al |3|, and by Bristoll |10, 13| is recalled. In |3| the sea water influence on crack propagation seems to have completely vanished below 20 MPa $\sqrt{m}$ and in |10| below 13 MPa$\sqrt{m}$. This might lead to the conclusion that with respect to offshore structures, where the value of the stress intensity factor of defects is assumed to be very low during the major part of its life time, the influence of the sea water environment on fatigue life will be negligible.

For the time being such a conclusion seems to be premature however.

In the present investigation (endurance tests on small scale T-joints |14|) a substantial influence of the sea water environment was apparent at nominal stress ranges above 100 N/mm^2 (the amount of experimental data at lower $\Delta\sigma_o$ values in air and sea water is too small to make a reliable comparison). Assuming a stress concentration factor (SCF) of 3 the stress range relevant to a weld toe defect and corresponding to $\Delta\sigma_o$ = 100 N/mm^2 would be 300 N/mm^2. Now it is generally agreed that initial defects with a depth of 0.4 mm may be present at the weld toe. The geometrical correction factor F for a long crack with this depth will have a value of about 1.122 |1| (free surface correction). This will lead to an initial ΔK-value of the defect of

$$\Delta K = F.SCF.\Delta\sigma_o \sqrt{\pi a} = 1.122 \times 3 \times 100 \sqrt{\pi} \times 0.4 \times 10^{-3} = 12 \text{ MPa } \sqrt{m}$$

In many cases ΔK will have been lower (shallower defects, semi elleptical defect shape, lower SCF).

According to the crack growth results from |3| and |10| no or only a very slight influence of the sea water environment would be expected at $\Delta\sigma_o$ = 100 N/mm^2. The present crack propagation tests reveal however that crack growth in sea water may already be a factor 2 faster than in air at ΔK-values below 12 MPa $\sqrt{m}$ (cf figure 2.4.17). This implies that at a stress range $\Delta\sigma_o$ = 100 N/mm^2 or even lower the fatigue life in sea-water environment may be substantially shorter than in air, as emerges from |14|.

A more thorough discussion of the investigations where these results have been taken from, viz |3|, |6-9|, is outside the scope of this report. Nevertheless it should be emphasized that in the region of low ΔK-values the results of crack propagation tests are very sensitive to the presence of residual or secondary stresses, to the load shedding procedure applied, and to the operating procedure during testing.
In sea-water the crack growth rate proved to be about a factor 3 higher than in air. This is in good agreement with the results obtained by Johnson |3| and with results obtained by Bristoll |10|. In both references the tendency is noticed that the influence of the sea-water environment is less severe at low ΔK-values. This tendency appears to emerge from the present investigation as well, although the region of low ΔK-values was not investigated extensively during the sea-water tests.

At a stress ratio $R = -1$ the results of the present investigation show a relatively high initial crack growth rate when compared with similar test results at $R = 0.1$. This is at variance with the results of Johnson |3| who did not observe this trend. On the other hand Bristoll |10| observed that the growth rate of cracks emanating from a notch was higher at $R = -1$ than at $R = 0.1$. When the notch was machined away this difference disappeared however. Clearly the compressive part of the load cycle yielded a contribution to fatigue crack propagation in the former case, whereas it did not in the latter case.
Although the da/dN-ΔK curves for $R = -1$ and $R = 0.1$ tend to converge as ΔK increases it seems worthwhile to pay adequate attention to the initial high-(er) crack growth rates at $R = -1$. This may have a substantial influence on fatigue life, as the major part of fatigue life coincides with the region of relatively low ΔK-values (crack propagation rates).

During tests in sea-water a stress ratio $R = 0.5$ suggested a slightly higher crack growth rate than at $R = 0.1$. This would be in accordance with results obtained by Johnson |3| and by Vosikovsky |11|. The trend observed is obscured to some extent by experimental scatter, especially at relatively low ΔK-values.

The observation that the crack growth rate in the weld metal and in the HAZ does not differ substantially from the crack growth rate in the base material agrees with the findings of Berge et. al. |8| and Benoit et. al. |12|.

For both specimens the results showed a decrease of the crack growth rate ending in a complete stop of any crack growth. In order to reinitiate the crack the load amplitude was raised in steps of 10% up to a level of 130% respectively 230% of the original load. Although specimen 48-3 was planned to be tested in sea-water it was decided to restart crack growth at a higher frequency in air. The crack surfaces are shown in fig. 2.4.20. In fig. 2.4.21 the crack growth is shown in relation to the load amplitude and the number of cycles.
For reasons of comparability the crack surface of a specimen without material defects is shown in figure 2.4.22. The testing of this specimen yielded valid results.

In specimens 50-1 and 50-2, which had a relatively large thickness, the crack front shape proved to be very irregular. For this reason the evaluation of the test results was considered doubtful and consequently omitted.

Finally it should be remarked that some sea-water tests had to be terminated in a premature stage because of a very poor visibility of the crack, or because of a complete crack stop.

2.4.7. Comparison with the results of other investigations on similar or related materials

In figure 2.4.23 the results of tests performed in air during the present investigation are compared with the results from some other investigations emerging from |2|; these investigations enclose extensive and thorough studies on fatigue crack growth in BS 4360 : 50D steel.
As the figure shows there is a good agreement with the results of Johnson et. al. |3|. The line taken from the work by Austen |4| is lying somewhat above the lines mentioned before. This line has to be considered as an upper boundary however. The results of the various separate tests reported by Austen are all somewhat below the line in question. Consequently it may be stated that the present results are in good agreement with the results by Austen as well. Furthermore there is an excellent agreement with the results of tests on an X-65 line-pipe steel as carried out by Vosikovsky |5|.

Mutual comparison of other results of tests on fatigue crack propagation in similar materials in air, as shown in figure 2.4.24, reveals that these results sometimes show large differences, especially in the region of low ΔK-values.

2.4.6.6. Separate discussion of the results of some tests

Specimen 48-2 was tested in sea-water at a stress ratio R = 0.1. After load shedding and applying a maximum value of the nominal bending stress of 37 N/mm^2 the specimen was subjected to alternating loading periods with loading frequencies of 0.2 and 10 Hz. The duration of each period was sufficiently long for the measurement of the crack growth rate. This procedure was chosen to set a limit to the duration of the experiment.
The results are shown in 2.4.18.
The crack growth rate at a frequency of 0.2 Hz is larger than at a frequency of 10 Hz. This is in agreement with the findings of other investigations which reveal a higher crack growth rate (increment of crack length per cycle) as the frequency is lower. At low values of ΔK the crack growth rate in sea-water at a frequency of 0.2 Hz is a factor 1.4 higher than in air. This is not at variance with the results discussed earlier in this report as these results were obtained in an interval of higher ΔK-values.

At higher ΔK-values the relation of Paris ($da/dN = C\ \Delta K^m$) does not seem to be obeyed anymore; relatively low values of $\frac{da}{dN}$ were obtained as emerges from figure 2.4.18. This was thought to be due to crack closure effects, caused by corrosion products in the crack. During this stage of the test the crack front shape was not quite regular (straight) as could be concluded from the inspection of the fracture surfaces, after termination of the test. It is not clear if this is due to (macro-) defects in the material. If so, they could very well have been responsible for the relatively low crack growth rate.

The results of the testing of specimens 49-1 and 49-2 were considered doubtful, as already stated before. Inspection of the fracture surfaces revealed the presence of defects which possibly have influenced the crack growth process. These material defects clearly emerge from the photographs of the fracture surfaces, as shown in figure 2.4.19.

As specimens 49-1 and 49-2 were tested in the far beginning of the programme some additional tests were carried out on specimens 49-3 and 48-3; both specimens were taken out of the same region of the ground plate. Unfortunately these specimens seemed to have the same kind of defects resulting in even more severe effects on crack growth and consuming much testing time.

Inspection of the crack surfaces after testing learned that the results of specimen 59-2 are non-valid or at least doubtful.
The different behaviour of this specimen may possibly be explained by the suppressing effect of material inhomogenities.

Influence of stress ratio in sea-water

Figure 2.4.16 presents the result of a test in sea-water at R = -1 and the results of tests at R = 0.1.
In accordance with the results in air (fig. 2.4.15), the initial crack growth rate at R = -1 is notably higher than at R = 0.1. It seems that the effect of the stress ratio upon the crack growth rate is not influenced by the corrosive sea-water environment.
Comparison with the results presented in fig. 2.4.14 suggests that at negative stress ratios again some time is needed before the influence of the sea-water environment becomes effective and perceptible.

2.4.6.5. Weld metal

The test results on weld metal are presented and compared with the results on base material in figure 2.4.17. Concerning the tests carried out in air the figure shows that for the lower values of ΔK the crack growth rate in the weld metal does not differ from the crack growth rate in the base metal. However, at larger values of ΔK the increase in crack growth rate is found to be less than in base metal. The reason for this difference is not easy to explain. Besides, there still remains the question if the different behaviour of only one specimen can be considered to be representative for the behaviour of the weld metal.

Regarding the tests in sea-water the results show a crack growth rate of about 2.5 to 3 times as large as in air. This is in full agreement with the results on base metal. However, contrary to the tests on the HAZ and on base metal the magnitude of the difference seems to be rather constant throughout the interval of ΔK that was covered. There is no tendency of convergence to the results in air at lower and higher ΔK values. It should be emphasized however that the test in sea-water was terminated at a lower value of ΔK than the tests in air on base metal.

At lower ΔK-values the crack growth rate in the HAZ appears to be somewhat larger than in base metal. However, with increasing ΔK-values (crack lengths) the difference disappears. Concerning these differences it should be considered that similar differences are found between the results of the tests in different laboratories carried out under the same testing conditions as shown in fig. 2.4.7. In this repect these differences are not considered to be really significant.

Influence of sea-water (HAZ)

In fig. 2.4.14 the results of three tests in sea-water are compared with the results in air. All tests were carried at a stress ratio R = 0.1. The results show a great similarity with the results presented in fig. 2.4.11. For the HAZ the crack growth rate in sea-water is found to be about 4 times as high as in air, which is even larger than was found for crack propagation in base metal.
More significantly than for the tests on base metal (fig. 2.4.11) the results in fig. 2.4.14 show that initially the crack growth rate in sea-water is hardly larger than in air. It seems that during this stage of the test the influence of the sea-water on the crack growth rate is relatively small. At high values of the crack growth rate the corrosive effect decreases, as was observed in the same way at the tests on base metal.

Influence of stress ratio in air (HAZ)

In fig. 2.4.15 the results are presented for one specimen tested at a stress ratio R = 0.1 and for two specimens tested at R = -1. As mentioned before the calculation of ΔK is based upon a stress range $\Delta\sigma$ only enclosing the tensile part of the load cycle, whereas the compressive part is neglected. Comparison of specimen 54-2 with 59-1 learns that the crack growth rate during loading at R = -1 is much higher than under loading at R = 0.1. Especially during the initial stage when the crack length is still small the difference in crack growth rate is very large. Compared with the results on base metal (fig. 2.4.10) the crack growth rate at R = -1 is much higher in the HAZ than in the base metal. The difference does not disappear at larger crack lengths. The only explanation seems to be the presence of residual stresses due to the welding procedure in spite of stress-relieving.

2.4.6.3. Base metal in sea-water

Influence of sea-water

In fig. 2.4.11 the results of the tests in sea-water are compared with the results of tests carried out in air.
The specimens had a crack orientation TS and were tested at a stress ratio R = 0.1. For the tests in sea-water small perspex boxes were installed around the specimens, surrounding the notched part of the specimen and the expected crack path.
Crack initiation was realised by applying a load shedding procedure under high frequency (6 Hz) in air. After crack initiation the tests were continued in sea-water at a frequency of 0.2 Hz.
Figure 2.4.11 shows a significant influence of the environment with a crack growth rate in sea-water up to three times as high as in air. This is in accordance with the results as mentioned in the conclusions of chapter 2.2. At larger crack growth rates the difference decreases and seems to disappear. It seems if the crack growth rate has an upper limit above which the influence of the corrosive sea-water environment on crack growth vanishes.
Concerning the results in the initial stage of crack propagation it is remarkable that the influence of the sea-water environment appears not immediately fully effective during this stage.

Influence of stress ratio (R > 0)

In fig. 2.4.12 the results of tests in sea-water are presented. The experiments were carried out at stress ratios R = 0.1 and R = 0.5. As is shown in fig. 2.4.12, only a slight influence of the stress ratio has been found. However, it should be noticed that all R-values are positive; consequently no compressive part is included in the stress cycles.
For the lower values of ΔK a wide scatter and variability in crack growth rate can be observed for one of the specimens. The reason for this behaviour is not clear.

2.4.6.4. Heat Affected Zone

Comparison of HAZ with base metal in air

In fig. 2.4.13 the results of tests on material from the heat affected zone are compared with tests on base metal.

For the time being it is not possible to explain these phenomena in a satisfactory way. They may be due to small changes in the residual stress distribution, the microstructure and crack closure effects, as these parameters and effects may significantly influence the crack growth rate at low values of ΔK and for small crack lengths.

Influence of stress ratio ($R = 0.1$ and $R = -1$)

The results of the tests with different R-values are given in fig. 2.4.10. Comparing these results it should be notified that the results of the experiments with a positive stress ratio ($R \geq 0$) are based upon a calculation of ΔK-values, using $\Delta\sigma = \sigma_{max} - \sigma_{min}$, being the double stress amplitude. However, for the results of the experiments with a negative stress ratio ($R < 0$), ΔK is calculated using $\Delta\sigma = \sigma_{max}$, being the tensile part of the double stress amplitude.
Comparing the results it is found that at small crack lengths the crack growth rate at a negative stress ratio ($R = -1$) is much higher than the crack growth rate at a positive stress ratio ($R = 0.1$). This difference disappears at further crack growth. In order to explain this apparent anomaly it is remembered that the fatigue crack originated at the root of a mechanical notch. At the root of such a notch there will be a stress singularity, not only during tensile loading but also during compressive loading. Consequently a certain degree of compressive plastic deformation at the notch root will occur during the compressive phase of the load cycle. When the fatigue crack is still very short the material surrounding the entire crack will undergo the last-mentioned compressive plastic deformation. Because of this deformation the crack may already open up after the moment the load has passed its minimum value so that the compressive phase - at least partly - contributes to crack growth. With increasing crack length the crack tip moves away from the notch root. As a consequence the effect of the mechanism described above (stress singurality at the notch root during compressive loading) will fade out as testing proceeds.
Although in fig. 2.4.10 also the results of the specimens 49-1 and 49-2 are given, their reliability is open to doubt. Obviously the rate of crack growth is notably smaller at larger ΔK values. This may - possibly - be due to a suppressing effect of material inhomogenities (inclusions). The results of these tests will be discussed separately.

Only in the region of low ΔK-values and crack growth rates small differences are found between the results from the different laboratories, which differences are not considered to be significant.

The results can be described in a quantitative way by the relation

$$\frac{da}{dN} = 6.1 \times 10^{-9} \times \Delta K^{3.0} \quad (\frac{da}{dN} \text{ in mm/c; } \Delta K \text{ in MPa}\sqrt{m})$$

As emerges from figure 2.3.7 the relation of Paris ($\frac{da}{dN} = C\ \Delta K^{m}$) gives a very satisfactory description of these crack growth data between $\Delta K \simeq 6$ and $\Delta K \simeq 80$ MPa$\sqrt{m}$. The line representing the relation $\frac{da}{dN} = 6.1 \times 10^{-9} \times \Delta K^{3.0}$ is also drawn in the subsequent $\frac{da}{dN}$ - ΔK plots.

Influence of crack orientation

The results of tests on specimens with crack orientations LS, TS and TL are presented in fig. 2.4.8.
The results do not show a significant difference due to the influence of the crack orientation.

Influence of stress relieving and saw-cutting

From the first experiments on crack propagation it was learned that the crack front shows a tendency of lagging behind at half thickness, especially at small crack lengths, i.e. during the first stage of the tests. This phenomenon was attributed to internal stresses due to oxygen cutting. To verify this assumption it was decided to test some specimens after stress relieving, whereas some other specimens were taken out of the plate by saw-cutting. Inspection of the crack surfaces after testing revealed however that the initial anomalous crack front shape was not eliminated by stress relieving or saw-cutting.
The results of these tests are compared in fig. 2.4.9. It seems evident that in the case of stress relieving and saw-cutting initially the crack growth rate is suppressed. However, for further crack growth no difference is found between a saw-cut specimen and an oxygen-cut specimen. The same result is found for one of the stress relieved specimens. The other stress relieved specimen shows an increased crack growth rate on further crack growth.

At TNO crack length values a were primarily calculated from the values of the electrical potential drop V over the notch opening using a theoretical solution for the relation between a and V |1|. These values were compared with the results of the optical crack length measurements. From this comparison a new set of crack length values was determined. Subsequently, a best fitting polynomial of the second degree was laid along seven consecutive points of the a vs N graph; the values of a and da/dN at the middle N value were calculated. This procedure was repeated for a number of points.

The value of the range of the stress intensity factor ΔK was calculated according to the formula (taken from |1|).

$$\Delta K = \Delta\sigma\sqrt{\pi a} \cdot F(a/b)$$

$$\text{with } F(a/b) = \sqrt{\frac{2b}{\pi a}\tan\frac{\pi a}{2b}}\ \frac{0.923 + 0.199\ (1 - \sin\frac{\pi a}{2b})^4}{\cos\frac{\pi a}{2b}}$$

In this formula $\Delta\sigma$ represents the double amplitude of the nominal bending stress, a the crack length and b the specimen height.

The results thus obtained were plotted in diagrams in which the crack growth rate was plotted - on a logarithmic scale - as a function of ΔK (also on a logarithmic scale), the range of the stress intensity factor.

2.4.6.2. Base metal in air

Base metal tested in three participating laboratories

The results of the tests on specimens of base metal were singled out as a primary base for comparison. The specimens had a crack orientation LS and were tested in air at a stress ratio R = 0.1.
In order to check the comparability of results obtained in different laboratories, the three laboratories carried out some tests on similar specimens under the same testing conditions.
The results of these tests are shown in fig. 2.4.7, and prove to be in good accordance, especially when emerging from experiments carried out in the same laboratory.

load shedding procedure. This technique was applied to facilitate crack initiation and to produce a straight crack front.

Experiments in sea-water were carried out by surrounding the notched part of the specimen by a small perspex box. Synthetic sea-water which was aerated continuously was circulated through this box. The composition was in accordance with the ASTM specification D1141-52, however without addition of stock solution no. 3. More detailed information about the sea-water composition has been supplied in chapter 2.2. The sea-water temperature (18-21^{o}C) and the p_H (8,0-8,2) were monitored continuously. The composition of the sea-water was controlled periodically and adjusted when necessary; regularly a fresh mixture of sea-water was supplied. All parameters were kept in agreement with table 2.2-5.

During all experiments in sea-water the loading frequency was 0.2 Hz. During all experiments in air a much higher frequency was applied (20 Hz ultimately). During a number of tests the frequency was periodically decreased to a lower value (e.g. 1 Hz) and increased to the original value afterwards in order to produce beach marks or to minimise the amount of crack growth during the absence of the responsible operator.

No uniform values for the minor and the major span were used. The minor span was at least twice the specimen height however. During the experiments in sea-water the minor span generally had a larger value because of the presence of the perspex box.

Experiments were terminated when the ratio crack length/specimen height had reached a value of about 0.6.

2.4.6. Discussion of results

2.4.6.1. Evaluation and presentation

The results of the experiments carried out at the University of Technology in Delft and at the University of Technology in Eindhoven were evaluated by plotting - for each experiment - crack length (a) versus number of load cycles (N). The value of da/dN at various crack lengths was calculated from the a versus N graph of the specimen in question.

It was set in operation automatically after a preset, sufficiently large increase of the electrical potential drop across the notch. The increase in crack length between two consecutive recordings of the video-equipment was chosen to be about 0.3 mm.
Parallel lines (perpendicular to the crack; spacing 1 mm) were grooved into both sides of the specimens so that the position of the crack tip could be localised rather accurately.
The accuracy of these recordings was $\pm$ 0.1 mm.

2.4.5. Programme

Main parameters; number of tests

The programme carried out is listed in table 2.3-I

Details about test conditions

The experiments were carried out under constant amplitude loading (sine wave form). At the beginning of most tests a load shedding procedure had to be applied to realise crack initiation at the notch root within an acceptable time. Frequently this was accomplished by starting the test at a value between 130 and 180% of the intended range of the cyclic load. This value was subsequently lowered in steps of about 10% after penetration of the crack through the corresponding crack tip plastic zone. On the whole the stress ratio R was kept constant during the load shedding procedure, although in some tests with a stress ratio R = 0.1 the lower value of the load was kept constant. The entire load shedding procedure which has always been carried out in air at room temperature, took about 2-3 mm crack growth. Therefore only measurements from a crack length of 9-10 mm on are considered to be valid; results obtained at a lower crack length value are considered to be influenced by the load shedding procedure and are consequently rejected.

During the experiments performed at the University of Technology in Eindhoven and during several experiments performed at the Metal Research Institute the specimen was initially inserted into the test machine in a reversed position (notch region loaded in compression). In this position it was subjected to some ten-thousands of load cycles with the same maximum load value as at the start of the load shedding procedure. Subsequently the specimen was reversed and subjected to the described

In specimens for experiments on crack growth in the HAZ the centre of the initial notch was located at a distance of 1 mm from the fusion boundary, in the HAZ. In specimens for experiments on crack growth in the weld metal the initial notch was in the weld metal, a few mm from the fusion boundary. This is illustrated in figure 2.4.5. In welded specimens only experiments on crack growth in the short transverse direction were performed.

All welded specimens were post weld heat treated before testing. Two specimens made from base material were post weld heat treated before testing as well, viz 48-4 and 53-3.

2.4.4. Equipment

2.4.4.1. Loading equipment

At the University of Technology in Delft three loading machines with capacities of 50, 100 and 350 kN were used simultaneously; the latter was used for experiments in a sea-water environment.
At the University of Technology in Eindhoven a 120 kN loading machine was used, whereas at the Metal Research Institute a 350 kN machine was used. In all loading machines a double acting hydraulic actuator was operating under precision servovalve control in a closed loop system. Figure 2.4.6a shows a general view of one of the testing facilities whereas a detail of another testing equipment is shown in figure 2.4.6b.
All test fixtures were designed to allow the support pins to rotate and move apart slightly, thus maintaining rolling contact throughout the test.

2.4.4.2. Measuring equipment

At the Universities of Technology in Delft and Eindhoven the crack length was measured periodically at both sides of the specimens by means of microscopes. In order to facilitate accurate measurements of the crack length a grid was printed on both specimen sides in the vicinity of the crack path. The accuracy of the measurements was $\pm$ 0.05 mm in air and $\pm$ 0.1 mm in sea-water.

At the Metal Research Institute crack growth was recorded in two ways, viz. by video-recording at both specimen sides and by continuous recording of the electrical potential drop across the notch opening (PD-technique using DC). The video-recording equipment was not operating continuously but in an intermitting way.

2.4.3. Specimens

Crack growth studies have been performed using single edge notched specimens loaded in four point bending.

The orientation of the specimens has been characterised according to the ASTM-system. In this system L is used for the indication of the longitudinal direction (direction of rolling), T(transverse) for the transverse direction, and S(short transverse) for the thickness direction. A combination of two letters is used to specify the orientation; the first letter refers to the direction of loading (tensile direction), the second letter refers to the direction of crack growth. This is shown in fig. 2.4.1. Figure 2.4.2 shows the pattern according to which the specimens from series 47 through 61 were taken out of the plate.

Generally the specimens were taken out of the plates by oxygen cutting. Two specimens however, were taken out by saw cutting (71-1 and 71-3).

For the majority of the specimens (orientations LS and TS) the values of the nominal thickness and the nominal width were 35 mm and 70 mm respectively. Two specimens with the orientation TL had a square nominal section (70 X 70 mm), whereas two additional specimens with the orientation LS had a thickness of 130 mm and a width of 70 mm.

The majority of the specimens was notched by making a 1 mm wide and 5 mm deep saw cut; in the root a finer saw cut was made with a width of 0.3 mm and a depth of 2 mm as shown in figure 2.4.3a. The specimens tested at the University of Technology in Eindhoven were notched in a different way leading to a slight chevron-like notch; this is shown in figure 2.4.3b.

Specimens for experiments with respect to crack growth in the weld metal and in the heat affected zone (HAZ) were taken from the plates obtained by welding plate parts as indicated in figure 2.4.2 in the vertical up position (3G). The geometry of the weld and the build-up sequence is shown in figure 2.4.4. The welding procedure was the same as described in chapter 2.1.

2.4.1. Introduction

Complementary to the endurance tests crack propagation studies have been carried out in order to generate diagrams in which the crack growth rate is plotted as a function of the range of the stress intensity factor. Such plots will reveal the influence of the material condition (base metal; heat affected zone; weld metal), as well as the influence of the orientation. Moreover, it was envisaged to check if the influence of the environment observed during the testing of welded joints would be confirmed by crack growth studies based on a fracture mechanics approach. Another important parameter to be varied was R, the stress ratio being the ratio of the minimum and the maximum nominal stress during fatigue loading. Finally crack propagation data would supply a basis for the calculation of fatigue life of welded joints. For such joints the period of crack initiation is often assumed to be relatively short. Neglecting this initiation period the fatigue life of the joint in question may be obtained by integration of a suitable crack propagation law.

The above mentioned crack growth studies were performed at the University of Technology in Delft (Ship Structures Laboratory), the University of Technology in Eindhoven (Laboratory of Structural Fatigue) and the Metal Research Institute TNO in Apeldoorn.

2.4.2. Material; welding consumables

The specimens have been taken from a normalised carbon manganese steel in accordance with Euronorm 113-72 Grade Fe E355 KT requirements. The material thickness was 70 mm. The chemical composition and the mechanical properties have been listed in chapter 2.1, table 2.1-1 and table 2.1-2.

Some series of specimens have been taken from welded plates. These plates were manufactured by manual metal arc welding using basic coated low hydrogen electrodes, AWS class E7016. Welding details have been tabulated in chapter 2.1, table 2.1-4.

* Metal Research Institute TNO
Apeldoorn

** Delft University of Technology
Ship Structures Laboratory

2.4 FATIGUE CRACK PROPAGATION TESTS

Apeldoorn/Delft, April 1981

* ir. H.Wildschut and

** ir. H.G.Scholte

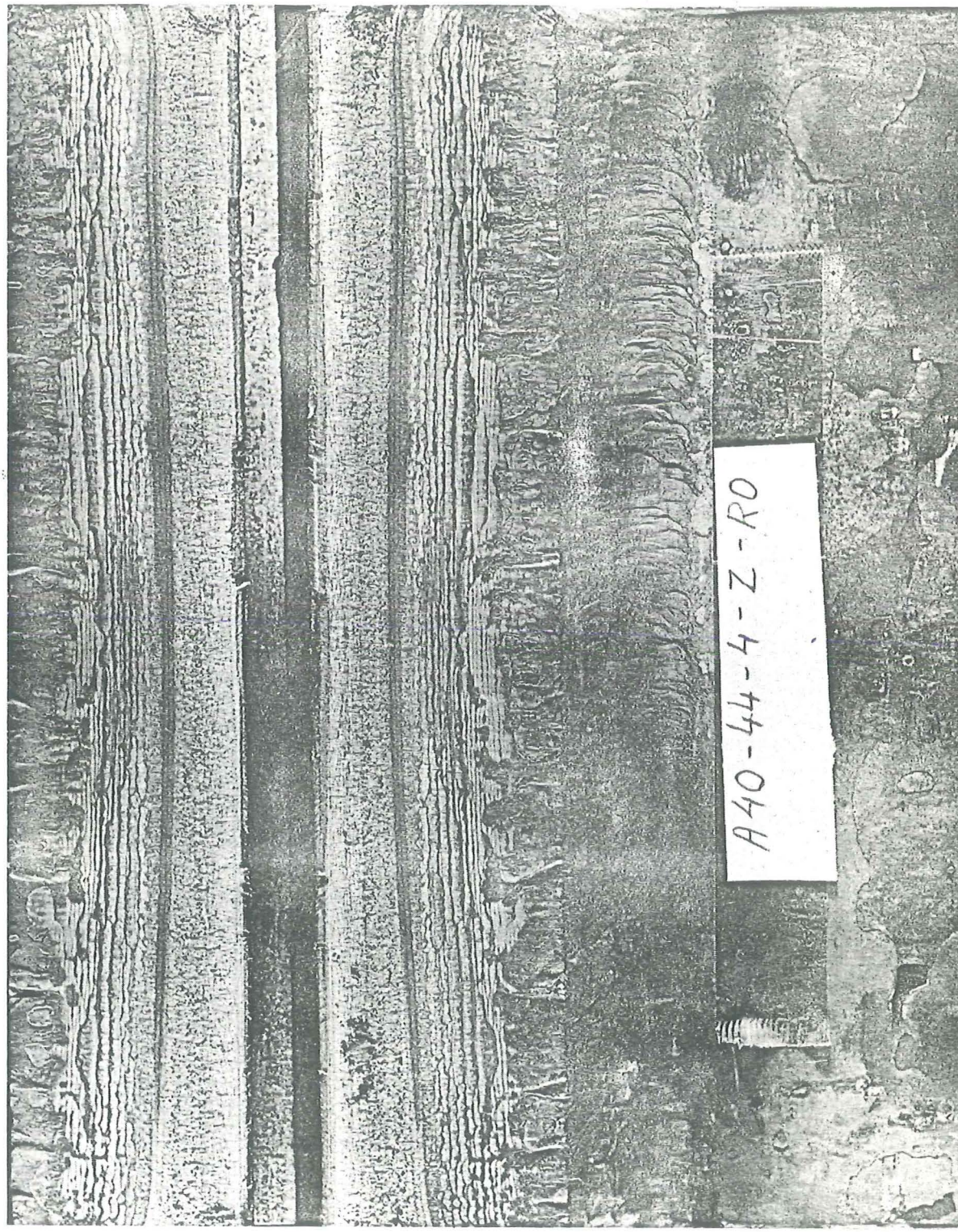

Fig. 2.3.10 Fracture surface, test in seawater

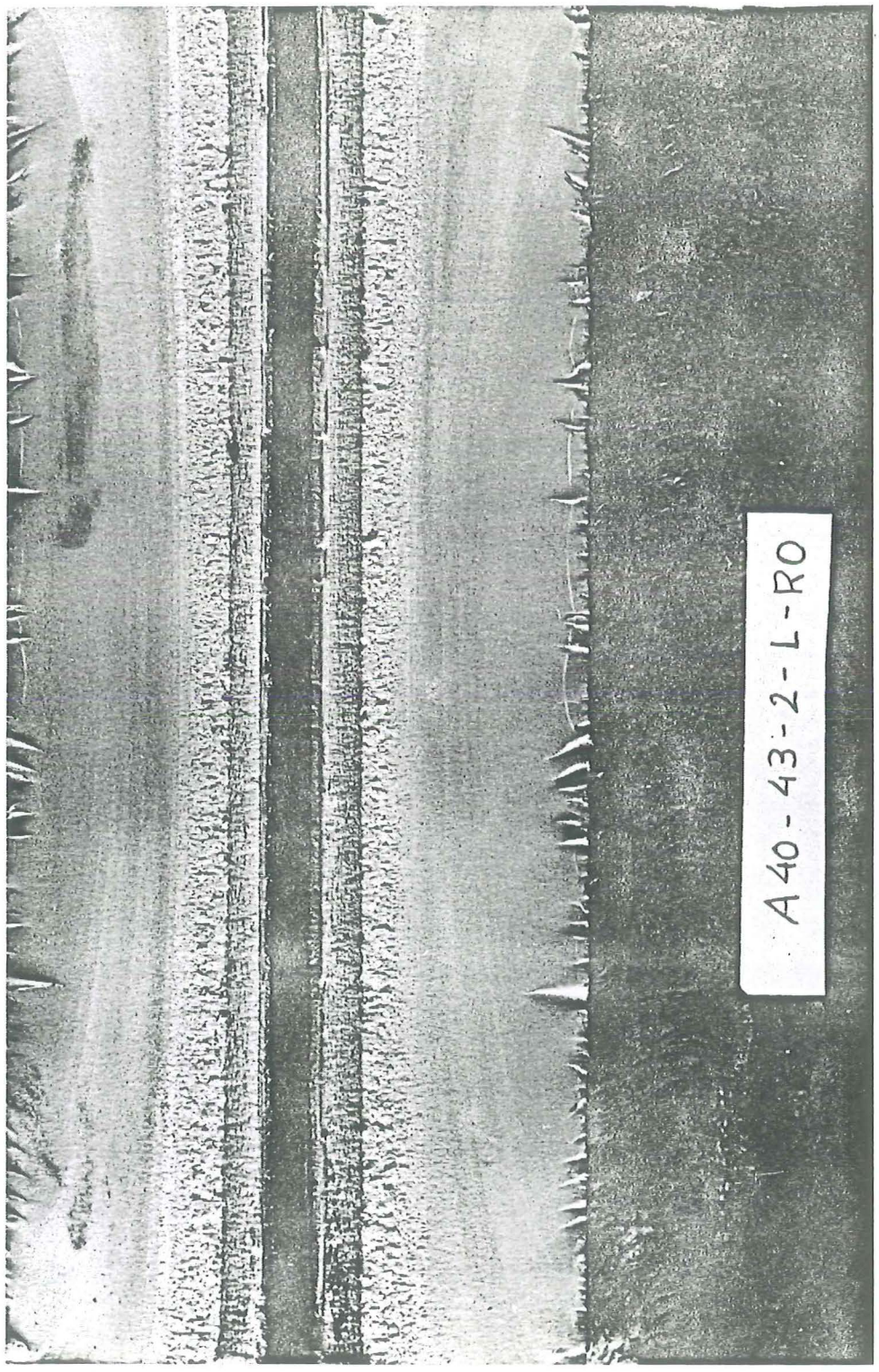

Fig. 2.3.9 Fracture surface, test in air

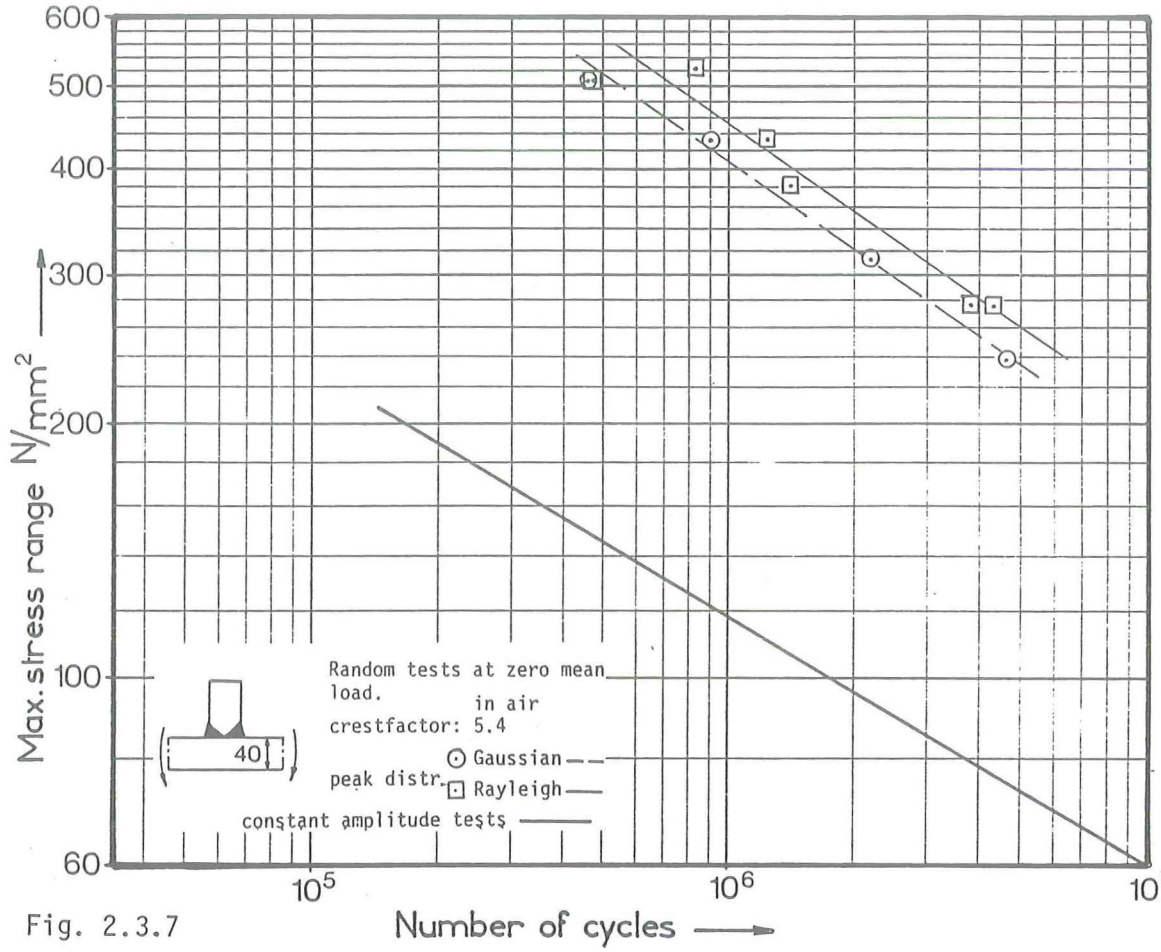

Fig. 2.3.7

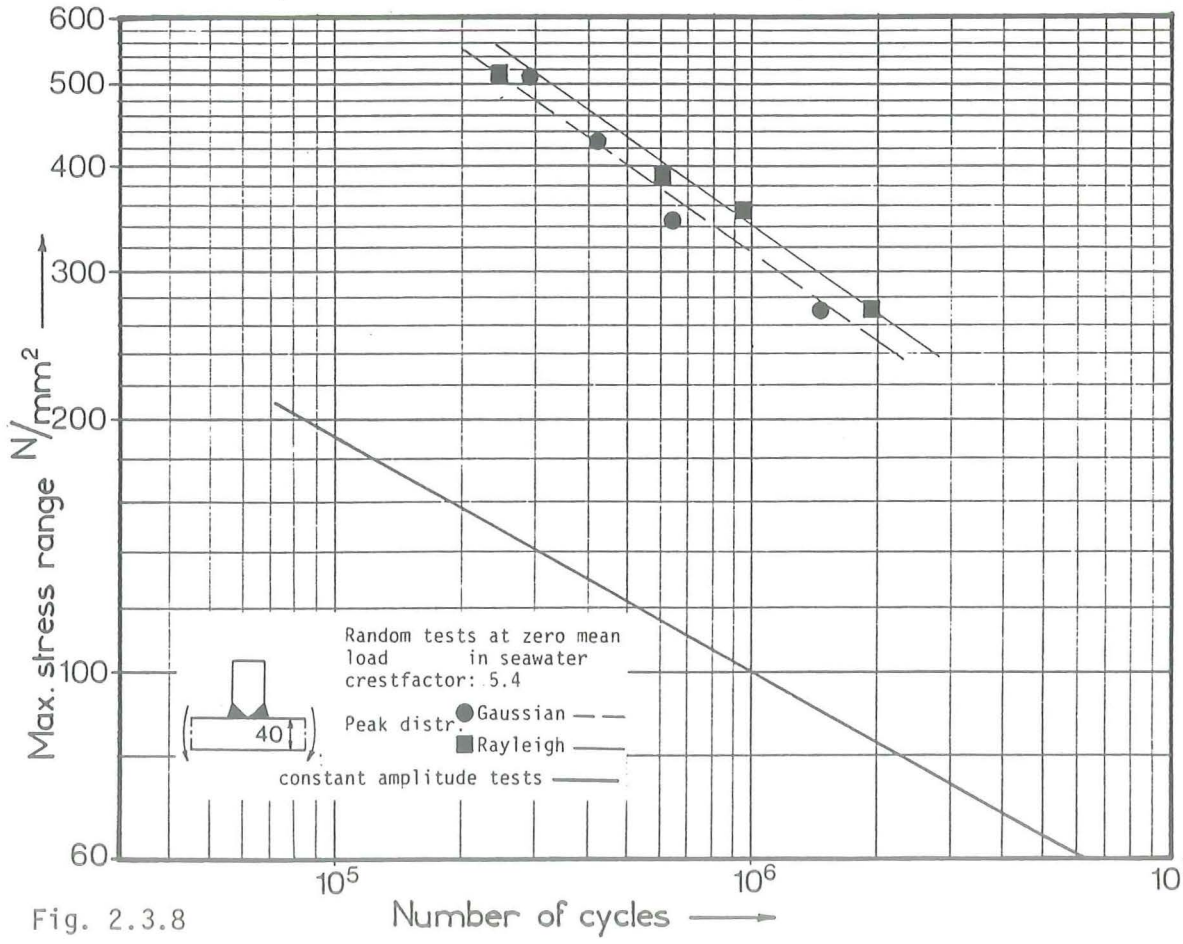

Fig. 2.3.8

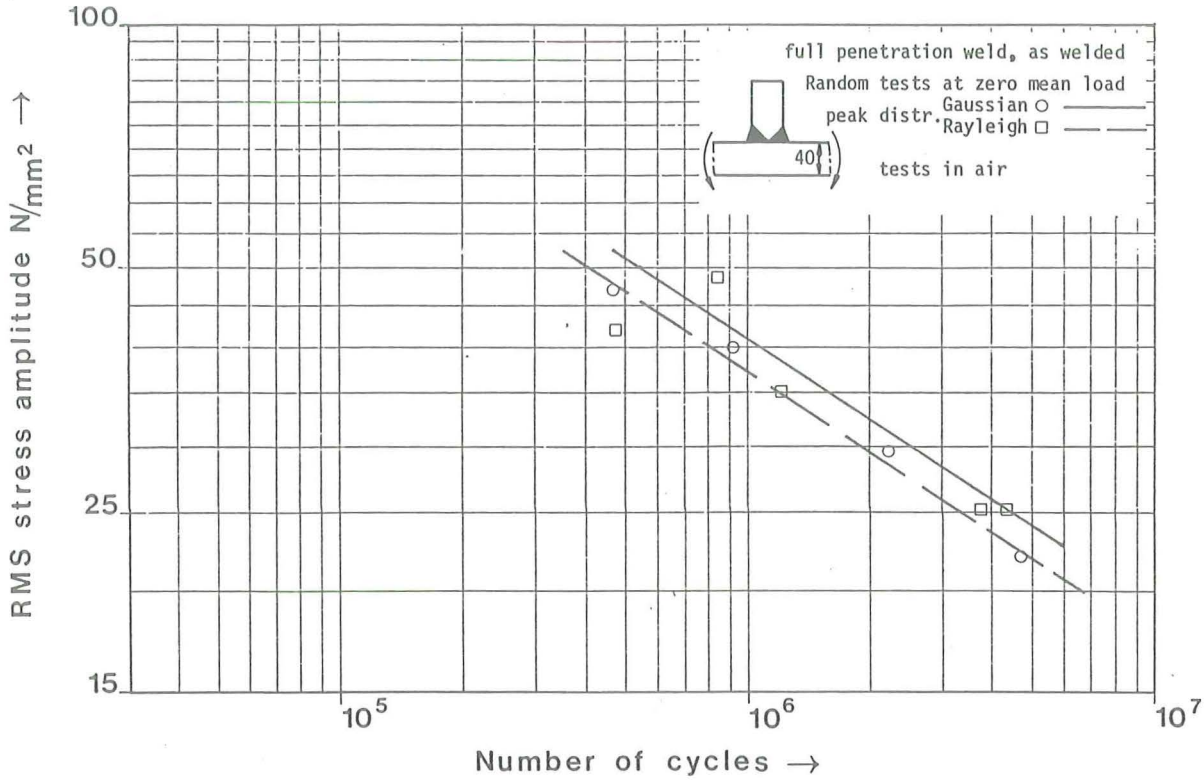

Fig. 2.3.5. Comparison of tests on 40 mm specimens under variable amplitude loading with Gaussian and Rayleigh peak. distributions in air.

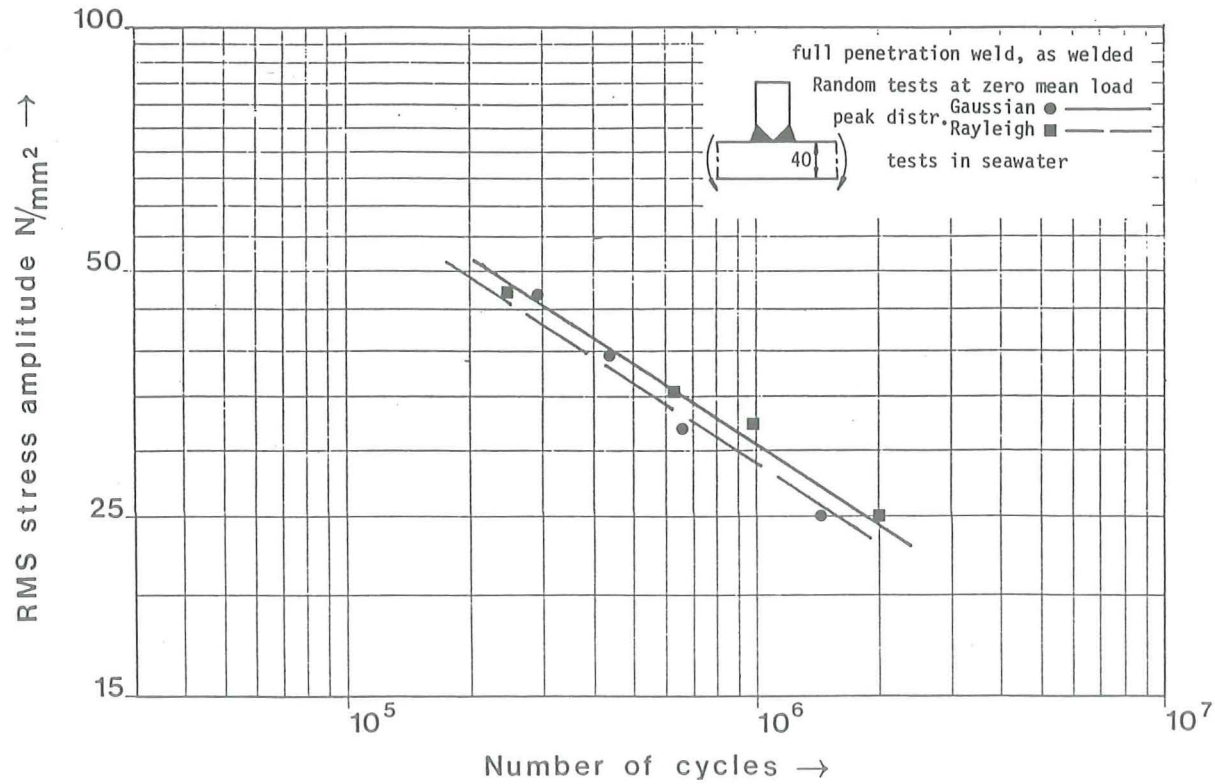

Fig. 2.3.6 Comparison of tests on 40 mm specimens under variable amplitude loading with Gaussian and Rayleigh peak distributions in seawater.

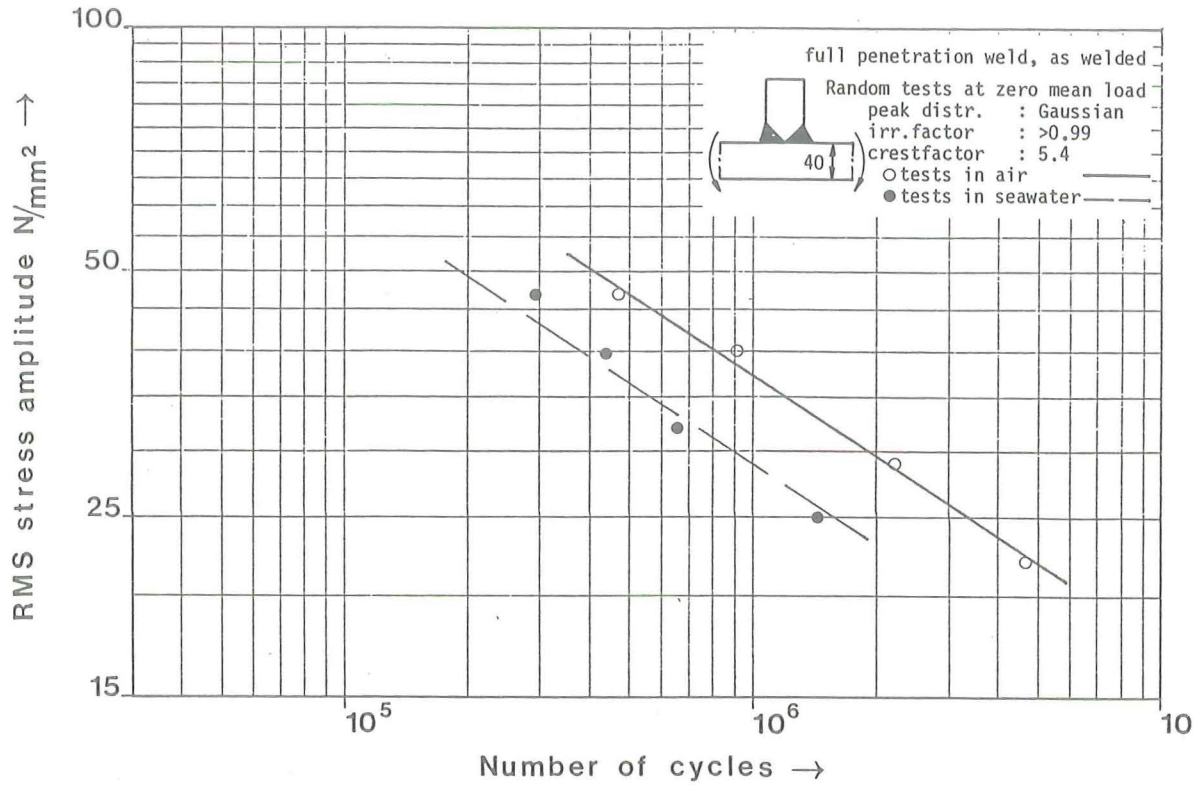

Fig. 2.3.3 Fatigue behaviour of 40 mm specimens under narrow band variable amplitude loading with a Gaussian peak distribution in air and seawater.

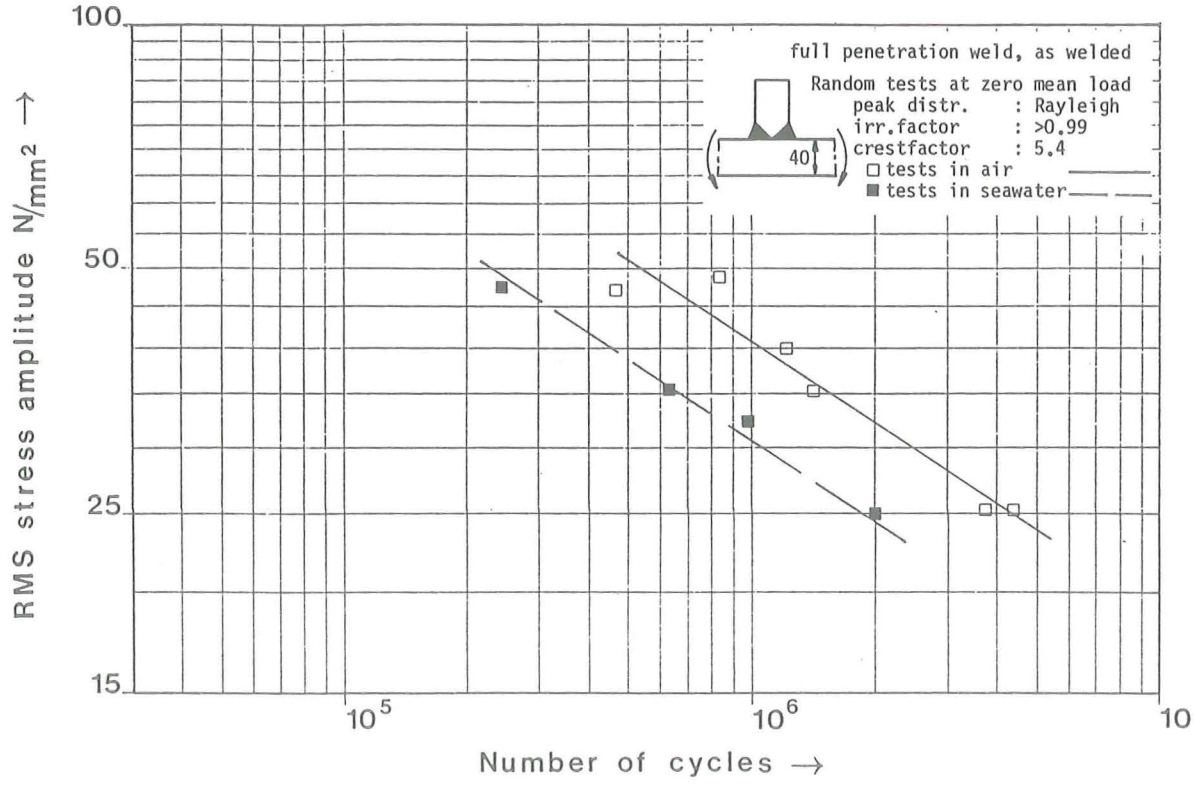

Fig. 2.3.4 Fatigue behaviour of 40 mm specimens under narrow band variable amplitude loading with a Rayleigh peak distribution in air and seawater.

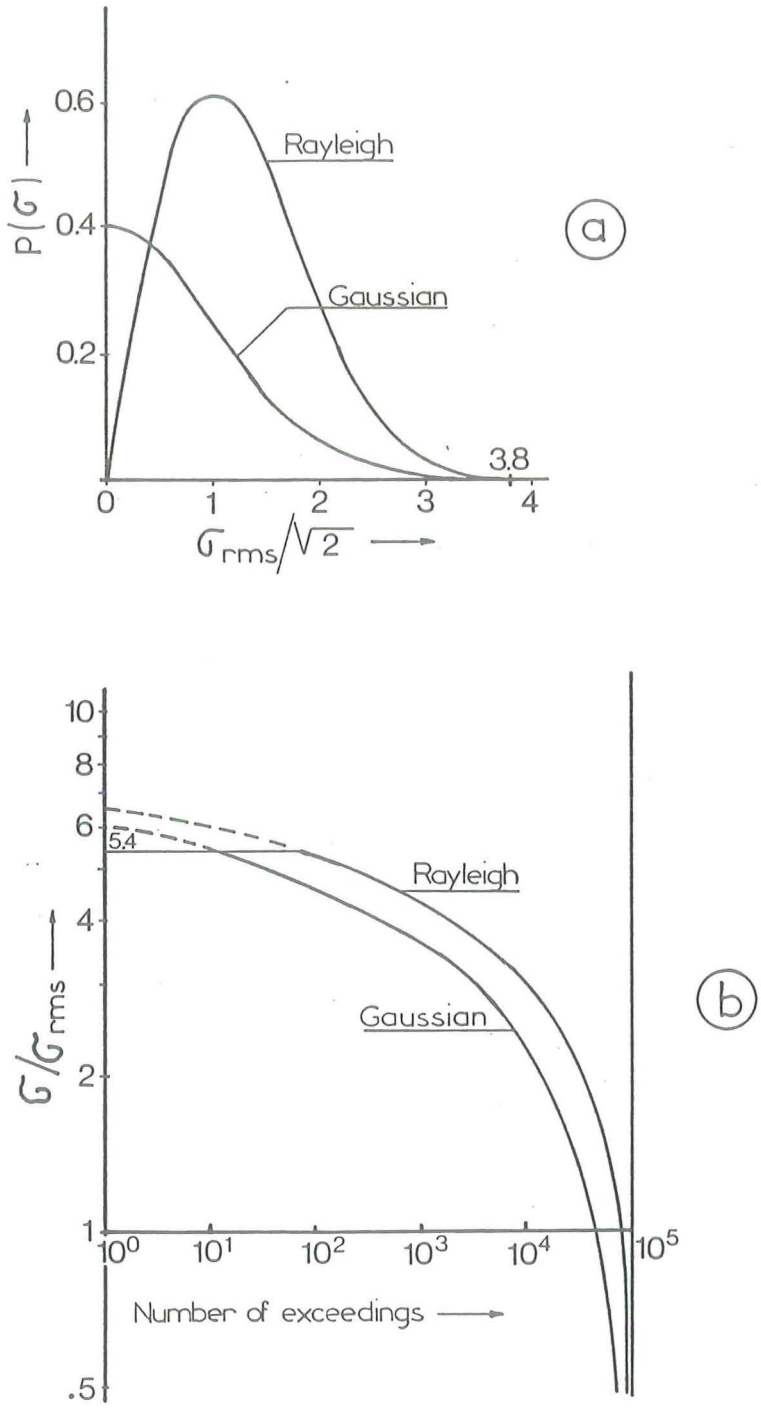

Fig. 2.3.2 Distributions (a) and corresponding Load Spectra (b)

2.3.11. Figures

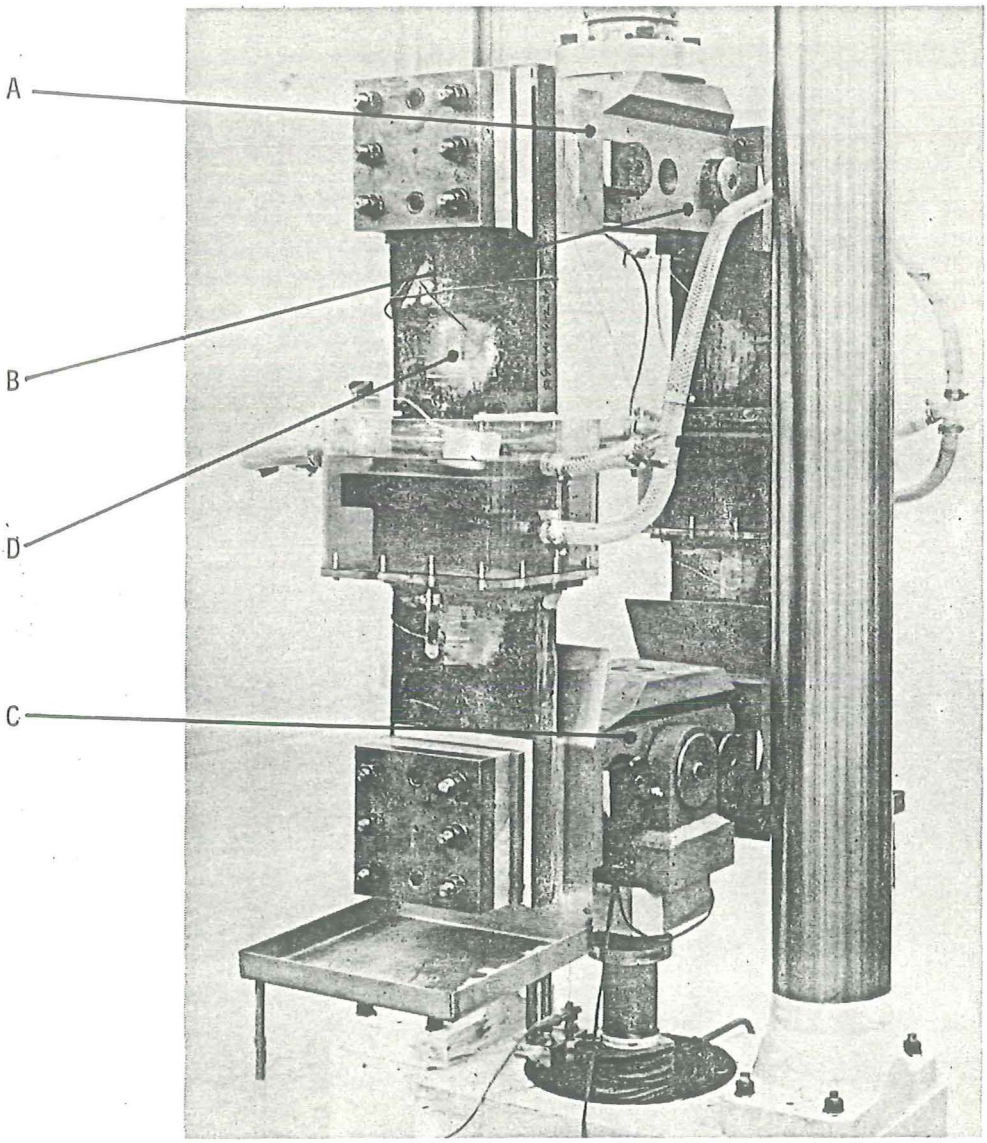

Fig. 2.3.1. 250 kN twin loading machine

2.3.10. Tables

Table 2.3.1. Summary of test conditions

Loading	: pseudo random
Irregularity factor	: narrow band process, J > 0.99
Block length	: 100.000 cycles
Peak (range) distribution	: Gaussian and Rayleigh
Crest factor	: 5.4 (both distributions)
Frequency band	: 2.29 $\pm$ 0.15 Hz in air 0.229 $\pm$ 0.015 Hz in seawater
Environment	: air and synthetic seawater
Specimen condition	: as-welded

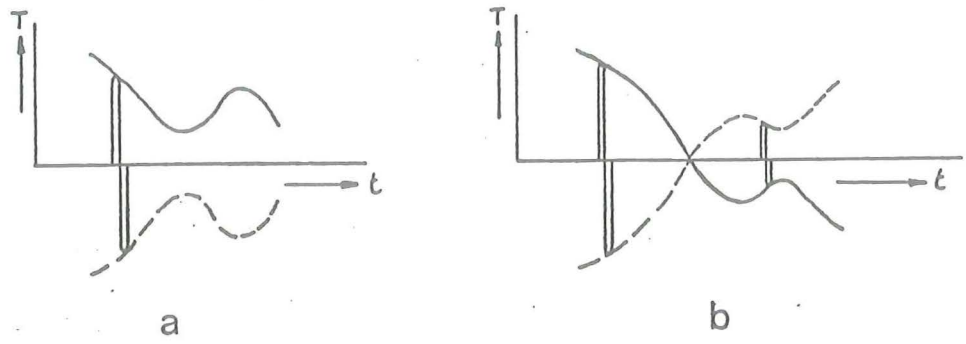

Fig. 2.3.A1 The envelope T as a function of time
a. T follows a Rayleigh distribution
b. T follows a Gaussian distribution

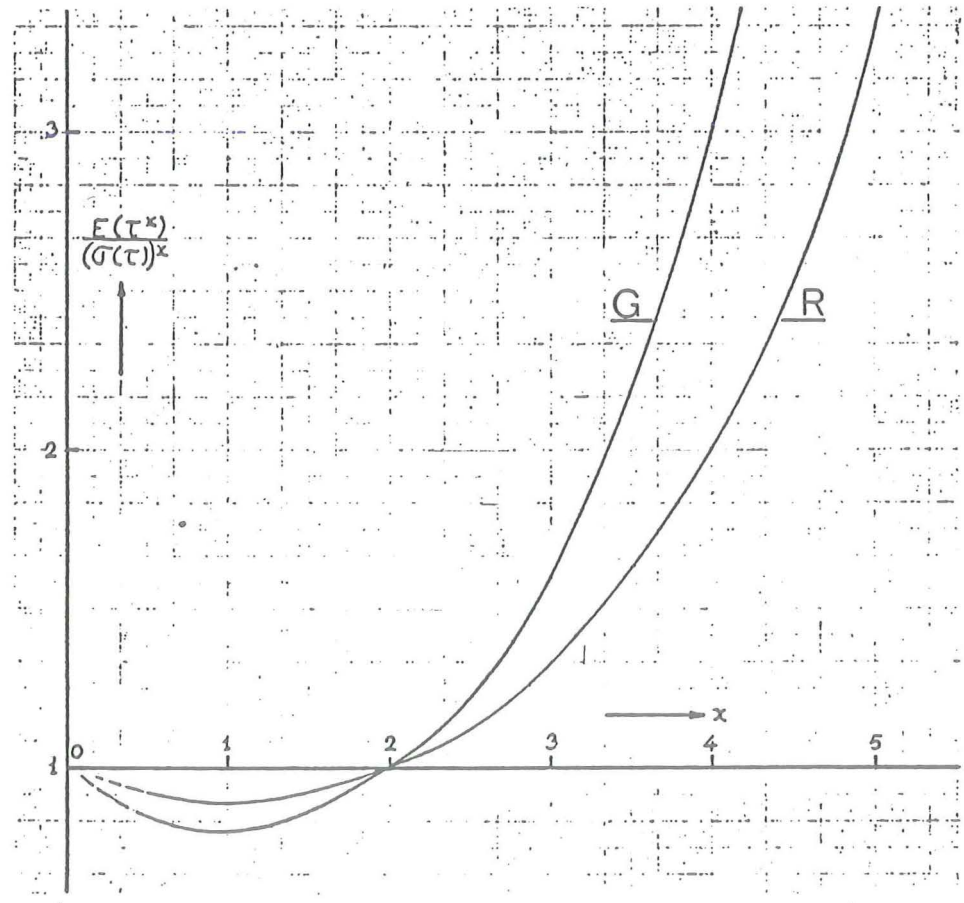

Fig. 2.3.A2 Expectancy of τ^x as a function of x

$p(\tau)$ \ x	0	1	2	3	4	5
$\frac{2\tau}{\sigma^2} \exp\left(-\frac{\tau 2}{\sigma^2}\right)$ (Rayleigh)	1	$\frac{\sigma}{2}\sqrt{\pi}$	σ^2	$\frac{3\sigma^3}{4}\sqrt{\pi}$	$2\sigma^4$	$\frac{15}{8}\sigma^5\sqrt{\pi}$
$\frac{1}{\sigma\sqrt{2\pi}} \exp\left(-\frac{\tau^2}{2\sigma^2}\right)$ (Gaussian)	1	$\sigma\sqrt{\frac{2}{\pi}}$	σ^2	$2\sigma^3\sqrt{\frac{2}{\pi}}$	$3\sigma^4$	$8\sigma^5\sqrt{\frac{2}{\pi}}$

When x is not an integer, as is usual when x is derived from experimental results, $E(\tau^x)$ can be interpolated or read from a graph of

$\frac{E(\tau^x)}{(\sigma(\tau))^x}$ as a function of x as is given in fig. 2.3.A2.

(so when $J \to 1$), $F(t)$ can be written as

$$F(t) = T(t) \sin 2\pi ft$$

The envelope $T(t)$ of the load signal contains *) all the peaks τ. These peaks occur at constant time intervals $\frac{1}{f}$ and therefore

$$p(T) = p(\tau)$$

and also

$$\sigma(T) = \sigma(\tau)$$

Note however that

$$F_{rms} = \tfrac{1}{2}\sqrt{2} \cdot \sigma(\tau) \qquad \text{(B3)}$$

as the area under the envelope is only partially filled by the sinusoidal signal (see fig. 2.3.A1).

Gaussian:

For the Gaussian distribution the envelope can be regarded as "double rectified" so that

$$E(\tau^X) = 2 \int_0^\infty \tau^X \, p(\tau) d\tau$$

Rayleigh:

As the Rayleigh distribution is defined for $\tau \geq 0$ the expectation of τ^X can be calculated

$$E(\tau^X) = \int_0^\infty \tau^X \, p(\tau) \, d\tau$$

Values of $E(\tau^X)$ when $p(\tau)$ has a Rayleigh c.q. a Gaussian probability density are given in the following table.

*) this is correct when the bandwidth of $T(t)$ is very small compared to f. For small bandwidths it is a good approximation.

2.3.9. Appendix 2.3.-I

Expected life according to Miners rule for narrow-band random loading.

To compare the variable amplitude tests, here the expected life is given according to Miners rule:

$$\sum_i \frac{n_i}{N_i} = 1$$

where n_i = number of cycles at level τ_i

N_i = number of cycles to failure at level τ_i

The expected number of cycles n_i at level τ_i within the life $\bar{n}$ is :

$$\bar{n}\, p(\tau_i)d\tau$$

$$\sum \frac{n_i}{N_i} = 1 \rightarrow \bar{n} \int_{\tau_{min}}^{\tau_{max}} \frac{p(\tau)d\tau}{N(\tau)} = 1$$

When the τ-N curve for constant amplitude loading is given by $\tau^X N = C$, it follows that (neglecting a fatigue limit):

$$\frac{\bar{n}}{c} \int_{\tau_{min}}^{\tau_{max}} \tau^X\, p(\tau)d\tau = 1$$

Now the integral is the expectation of τ^X and can be calculated, so

$$\bar{n} = \frac{C}{E(\tau^X)}$$

and

$$E(\tau^X) = \int_{-\infty}^{\infty} \tau^X\, p(\tau)\, d\tau$$

the expectancy of τ^X

When a random load, F(t), is operating within a narrow frequency band

2.3.8. References to chapter 2.3.

1. J.L. Overbeeke: The fatigue behaviour of heavy-duty spot welded lap joints under random loading conditions. Welding Research International 7 (1977), 3, 254 - 276.

2. W.T. Kirkby and P.R. Edwards: Constant amplitude or variable amplitude tests as a basis for design studies. Fatigue Design Procedures, Pergamon 1969, 253 - 290.

3. E. Gassner and W. Schütz: Assesment of the allowable design stresses and the corresponding fatigue life. Fatigue Design Procedures, Pergamon 1969, 291 - 307

4. J. Strating: Fatigue and stochastic loadings. Diss. Delft Univ. of Techn. 1973

5. J. Lewszuk and D.J. White: Effect of mean stress and cumulative damage in bending fatigue of fillet-welded mild steel plate subjected to narrow band loading. Proc. on the Conf. on Fatigue of Welded Structures. The Welding Institute 1971, 296 - 311

6. G.P. Tilly and D.E. Nunn: Variable amplitude fatigue in relation to highway bridges. Proc. Inst. Mech. Eng., 194 (1980) 259.

processes difficulties arise in the defining amplitudes.

- Statistical distributions are described by their statistical moments. For the common statistical distributions the second statistical moment, and so the rms-value, is a good measure of their intensity. For a one-parameter distribution the rms-value (and any other parameter) fully describes the distribution.
- Sometimes the maximum stress range in the spectrum is used to plot fatigue test results. Although the maximum stress range is very useful for design purposes, it is inadequate to charaterize test results, because the influence of (very)high ranges on the endurance is not solved.
  In narrow band testing the influence of the crest factor seems to be very low [1] , while in wide band testing its influence can be large [6] but is not clear.

So the charm of using σ_{rms} in fatigue is that it is an important statistical parameter and that it is not biased by fatigue.

2.3.7. Conclusions

From the here reported narrow band random fatigue tests on welded specimens in air and synthetic seawater environment the following conclusions can be drawn:

1. On the base of the rms-value of the stresses or the ranges, there is little difference in endurance between 2 spectra that are quite different in low amplitude content.
2. The measured endurance is a factor 1.0 - 1.3 larger than the expected life as calculated through Miners rule.
3. The ratio of the endurance for the 2 load spectra is $N_R/N_G = 1.25$ and almost equal to the ratio of their Miners summations.
4. The endurance in seawater is a factor 2.2 shorter than the endurance in air. This result compares well with the results for constant amplitude tests reported in chapter 2.2.

The ratio between the average random endurance N and the expected life $\bar{n}$ at σ_{rms} = 30 N/mm^2 is then as follows:

	Gaussian	Rayleigh
air :	$\frac{N}{\bar{n}} = 1.3$	1.2
seawater :	$\frac{N}{\bar{n}} = 1.2$	1.0

In view of experimental scatter and analytic approximations (a.o. no fatigue limit) one can say that Miners rule yields good results. Furthermore, for a cubic relationship between S and N, the ratio $\bar{n}_R/\bar{n}_G = 1.20$ while the experimental determined ratio is $N_R/N_G = 1.25$ in air as well as in seawater. The difference between the calculated and the experimental determined ratio is very low indeed in view of the differences in spectra as explained in the previous paragraph. Similar results were reported in [1] and proposals to use Miners rule for synthesizing spectra have been done before [2,3].

2.3.6.3. The use of σ_{rms}

In the preceding paragraphs the random loading is characterized by the root mean square value of the stress $\sigma(t)$ and some arguments are forwarded to clarify its use.

- The term σ_{rms} is incorrect. What is meant is the standard deviation. Only when R = -1, these two items are equal. However, as the term is already widely in use it will be difficult to change it.
- σ_{rms} bears no relationship to the fatigue process. It is defined in the time domain and the definition of fatigue as repeated plastic deformation excludes time effects. However, on the basis of σ_{rms} endurances tend to amalgamate [1,4,5].
- The same holds for the (power)spectral density as frequency effects are low in "laboratory air" environment and are excluded in plasticity.
- It may be argued that the rms-value of the stress amplitude is more meaningful. For narrow band excitation the amplitudes are well defined, and $(rms)_{ampl} = (rms)_{stress} \cdot \sqrt{2}$. However, for wide-band

2.3.6. Discussion of results

2.3.6.1. Load spectra

As can be seen from figure 2.3.2a, the major differences between the two different types of random loading are as follows:
The Gaussian distribution contains large amounts of cycles with low to very low amplitudes, while the Rayleigh one contains only small amounts of these.
On the other hand the Rayleigh distribution contains more high amplitudes.
The corresponding load spectra, plotted as dimensionless stress versus number of exceedings on a double logarithmic scale, are shown in fig. 2.3.2b.

2.3.6.2. Cumulative damage

The influence of the shape of load spectra is usually expressed through a fatigue damage calculation based on Miners rule. This rule, originally stated as $\sum_i n_i/N_i = 1$ in relation to blocks of different constant amplitude, can also be expressed in the parameters of a statistically defined load spectrum. The derivation of the expected endurance $\bar{n}$ is given in Appendix I.
Cumulative damage calculations based on this appendix yields the following results:

I $S^{3.0}N = C_1 : 1.60\ \bar{n}_G = 1.33\ \bar{n}_R = N_{c.a.}$

II $S^{3.3}N = C_2 : 1.97\ \bar{n}_G = 1.51\ \bar{n}_R = N_{c.a.}$

III $S^{3.5}N = C_3 : 2.17\ \bar{n}_G = 1.61\ \bar{n}_R = N_{c.a.}$

I is the adopted - and well fitting - relationship for the random tests

II holds for constant amplitude tests in air at R = 0.1 (table 2.2.7)

III holds for c.a. tests in seawater at R = 0.1 (table 2.2.7).

No results at c.a. and R = -1 are available. However, as the specimens were tested in the as-welded condition, the difference between R-ratios of 0.1 and -1 will be small. So the expected life calculations were based on table 2.2.7.

Tests were terminated (= endurance N) when the crack depth at the sides of the specimens had grown to at least half the plate thickness. As can be seen from fig. 2.3.9 and 2.3.10, the remaining uncracked area was then less than 40% of the cross section.

2.3.5.2. Test results

Test results are given in table 2.3.2 and plotted in fig. 2.3.3 through 2.3.6 on the base of σ_{rms}.
Fig. 2.3.3 and 2.3.4 show the results in air versus those in seawater. Fig. 2.3.5 and 2.3.6 show the influence of peakdistribution. Furthermore, these test results are also plotted as a function of the maximum stress range in fig. 2.3.7 and 2.3.8 (see also fig. 2.3.2b).

As the number of test results is too low to calculate a reliable S-N curve, an S-N curve of the type $S^3N = C$ was adopted and plotted in fig. 2.3.3 through 2.3.8.

The constant C as calculated by linear regression is then:

distribution	environment	$\sigma^3_{rms}\ N = C$
Gaussian	air	5.22×10^{10}
Gaussian	seawater	2.52×10^{10}
Rayleigh	air	6.94×10^{10}
Rayleigh	seawater	2.95×10^{10}

From the above it follows that:
The endurance in seawater is reduced by a factor 2.2 with regard to the endurance in air.

$$\frac{N_{air}}{N_{seawater}} = 2.2 \quad \text{(Gauss and Rayleigh)}$$

The endurance for a Rayleigh distribution of load ranges is 1.25 times the endurance for a Gaussian one

$$\frac{N_{Rayleigh}}{N_{Gauss}} = 1.25 \quad \text{(air and seawater)}$$

is equal to ($^{\text{amplitude}}/\sqrt{2}$), the rms value of the modulated carrier is the rms of x(t) divided by $\sqrt{2}$, and the crestfactor becomes $3.80\sqrt{2} = 5.4$. Fig. 2.3.2 shows a graph of the distribution.

Rayleigh distribution of peaks (ranges)

The Rayleigh distribution was produced by shaping the noise generator output by means of non-linear amplification before feeding it into the VCA-oscillator.
Details and accuracy of this shaping are given in Appendix A of [1].
Fig. 2.3.2 shows a graph of this distribution.

2.3.5. Test conditions and results

2.3.5.1. Test conditions

Testing conditions were restricted by the following:

- In view of the testing time involved at a frequency of 0.2 Hz in seawater, the number of cycles to failure had to be restricted to roughly 2 million cycles.
- The maximum bending stress was restricted to $^{2}/3\ R_{0.2}$ in view of plasticity effects and usual maximum design stresses.
  At $R_{0.2} = 400\ ^{N}/mm^{2}$ this means a max. stress of $\sigma = 270\ ^{N}/mm^{2}$, and, together with a crestfactor of 5.4, a maximum $\sigma_{rms} = 50\ ^{N}/mm^{2}$.
  For this reason the Rayleigh distribution was clipped to equal the crestfactor (5.4) of the Gaussian distribution, and furthermore alternating loading, that is R = -1, was applied throughout.
- As the lower numbers of cycles to failure were of the order of 300.000, the applied blocklength was set at 100.000 cycles.

A summary of the testconditions is given in table 2.3.2.
During all tests the specimens were regularly inspected for cracks with the help of a magnifying glass. The number of cycles to initiation, as given in table 2.3.2 corresponds to the first observed crack of 10 - 30 mm in length. This length depended upon inspection interval and visibility, the latter of which is poor in seawater. Multiple crack initiation was often observed, especially for weld toes with a more smooth appearance.

For this purpose, arms A were bolted to the ends of the specimens. These arms were connected through knuckle joints to the fixed machine head B and to the symmetrical swivelarm C, mounted on the actuator rod. So both specimens are loaded by the same normal load, but as the length of arms A can be chosen, the bending moment in the two specimens can be quite different.
The ratio normal stress/max. bending stress was less than 2%.
Although the friction in the joints caused some hysteresis, the peak (range) distribution was not affected by friction as proven by dynamic straingage measurements.
Furthermore the stresses in the specimens were periodically monitored by dynamic straingage readings from the straingages D on the specimens.

2.3.4.2. Machine input signal

For controlling the fatigue machines, pseudo-random generators of the type Hewlett-Packard 3722A were used throughout. These generators deliver a digital generated, repeatable output signal x(t) with an almost Gaussian probability together with a constant power spectral density within the bandwidth.
The selected bandwidth was 0 - 0.15 (0.015) Hz at a blocklength of 43690 (436900) seconds.
The corresponding crestfactor ($^{\text{max.peak}}/_{\text{rms}}$) was 3.80.
The output of this noise generator was fed into a VCA-oscillator in order to modulate a sinusoidal carrier signal of 2.29 (0.229) Hz.
In this way a sinusoidal signal with random varying amplitude and an irregularity factor $J \rightarrow 1$ was produced with a blocklength of 43690 times 2.29 = 100.000 cycles.
The peak or range distribution of this signal is now equal to the probability density (time domain) of x(t), while its frequencyband is within a narrow band of magnitude 2.29 ± 0.15 (0.229 ± 0.015 Hz).

Gaussian distribution of peaks (ranges)

As the pseudo-random generator delivers an output signal x(t) with a Gaussian probability density, the modulated carrier has a Gaussian distribution of peaks or ranges. Fig. 2.3.2 shows the dimensionless "load" spectrum. However, as the rms value of a sinusoidal signal

Air

Experiments were carried out under normal laboratory conditions.
Monitors have indicated:
a temperature range of 17 - 26 ^{o}C
a relative humidity range of 45 - 60 %.
All specimens were thoroughly degreased by organic solvents before testing.
Testing frequency was 2.29 cps.

Seawater

Experiments in seawater were carried out by inserting the fatigue critical part in an open perspex box (see fig. 2.3.1). Synthetic seawater, which was aerated continuously, was circulated through this box. The composition of the seawater was in accordance with ASTM D 1141-52, except for omitting stock solution 3. Further details are given in chapter 2.2.5.
Seawater temperature (20 $\pm$ 1 ^{o}C) and p_H (8.0 - 8.2) were monitored continuously. The composition of the seawater was controlled regularly and adjusted when necessary. Periodically a fresh mixture of seawater was supplied. All parameters were kept in agreement with tabel 2.2.5. Testing frequency was 0.229 cps, which is slightly higher than the test frequency (0.20 cps) used for the constant amplitude tests reported in chapter 2.2 and 2.4.
This deviation in frequency was necessary in order to generate a random block of 100.000 cycles.

2.3.4. Equipment

2.3.4.1. Testing machines

Tests were carried out on 2 fatigue machines with capacity 250 kN and 120 kN respectively. Both machines are equiped with servo-controlled hydraulic actuators. Load feedback was used throughout.
In order to double the testing capacity, two specimens were tested together in specially built rigs. Fig. 2.3.1 shows the set-up.
The specimens were loaded in bending by a highly excentric load.

2.3.1. Introduction

Additional to the endurance tests under constant amplitude loading, tests were carried out under random loading. The reason to do these tests is an obvious one: off-shore structures are loaded by random varying magnitudes of wind and waterforces.
The loading spectra chosen are:
- a Rayleigh distribution of ranges
- a Gaussian distribution of ranges.

The first spectrum corresponds to a sea-state (storm) as adopted in the English part of this E.C. program.
The second spectrum corresponds to a sea-state (storm) as adopted in the German part of the E.C. program.

Tests were carried out using air as well as seawater as an environment.

2.3.2. Material and specimens

The steel used to fabricate the specimens is a normalised carbon-manganese steel. It complies with Grade Fe E355 KT according to Euro-norm 113-72.
The chemical composition and mechanical properties are given in table 2.1.1 and table 2.1.2.
Plate thickness was 40 mm.
The specimens were T-shaped, (type A, fig. 2.2.1) and consisted of strips L x W = 1000 x 218 mm to which a gusset plate, 80 mm high, was welded in the traverse direction by a full penetration, K-type weld.
Consumables used were basic coated low hydrogen electrodes AWS class E7016.
The specimens were tested in the as welded condition.

Further details about materials, consumables and welding procedure are given in par. 2.2.3.

2.3.3. Environment and test frequency

During the endurance tests the following environments were used:

Eindhoven University of Technology
Laboratory for Structural Fatigue

2.3 Random-load tests on plate specimens

Eindhoven, April 1981.

ir. M.H.J.M. Zwaans
P.A.M. Jonkers
ir. J.L. Overbeeke

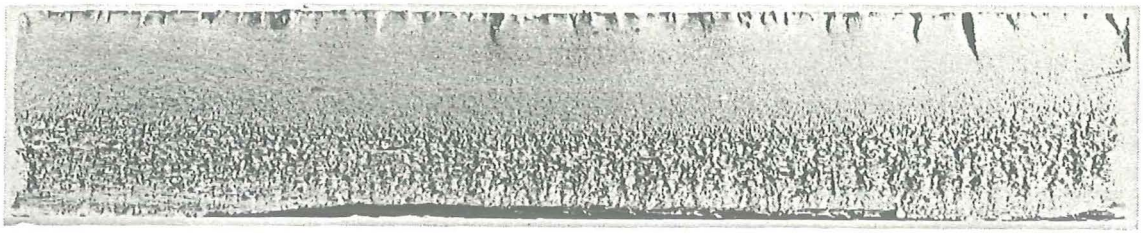

As welded (A40-1-3)

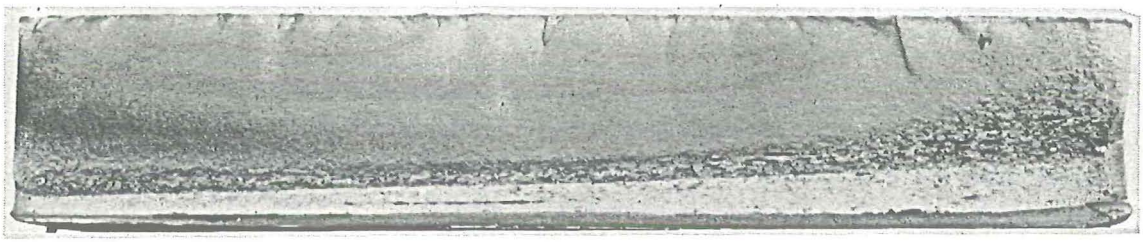

TIG-dressed (A40-22-3)

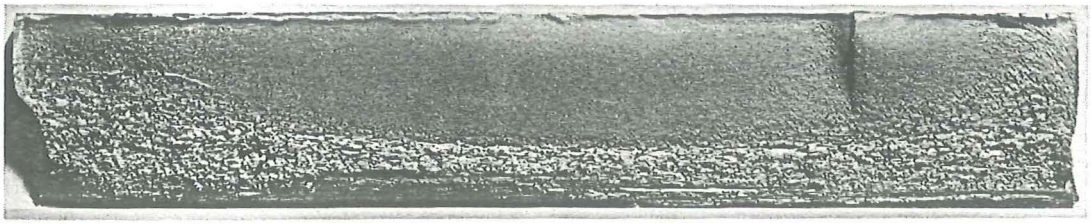

Grinding (A40-20-3)

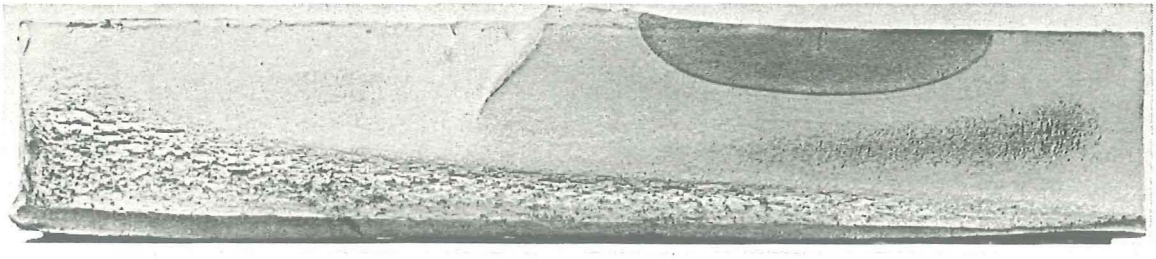

Grinding (A40-20-5)

Fig. 2.2.75 Effect of finishing the weld toe on the decreasing of the formation of multiple crack initiation

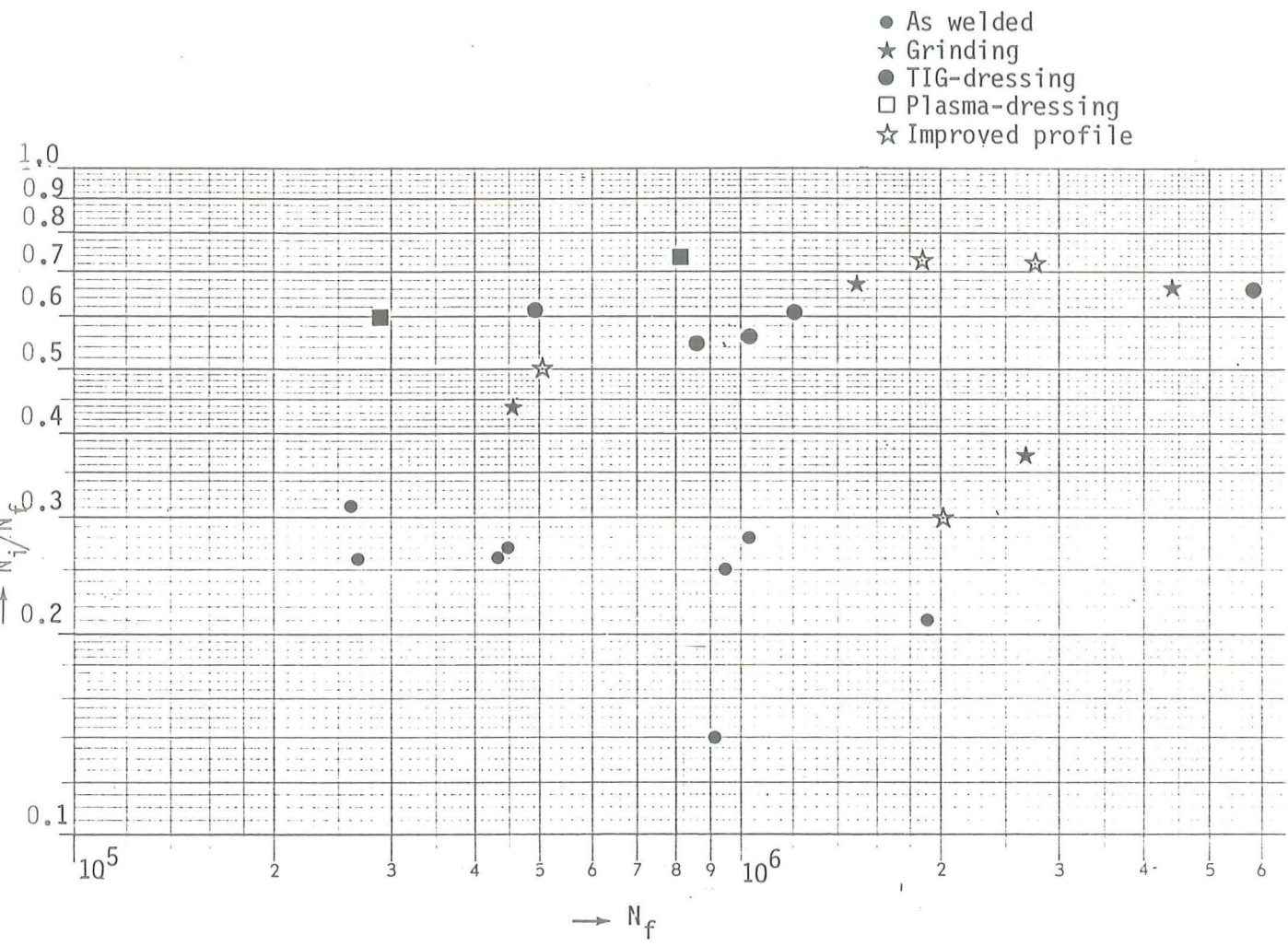

Fig. 2.2.74 Influence of weld toe finishing on crack initiation.

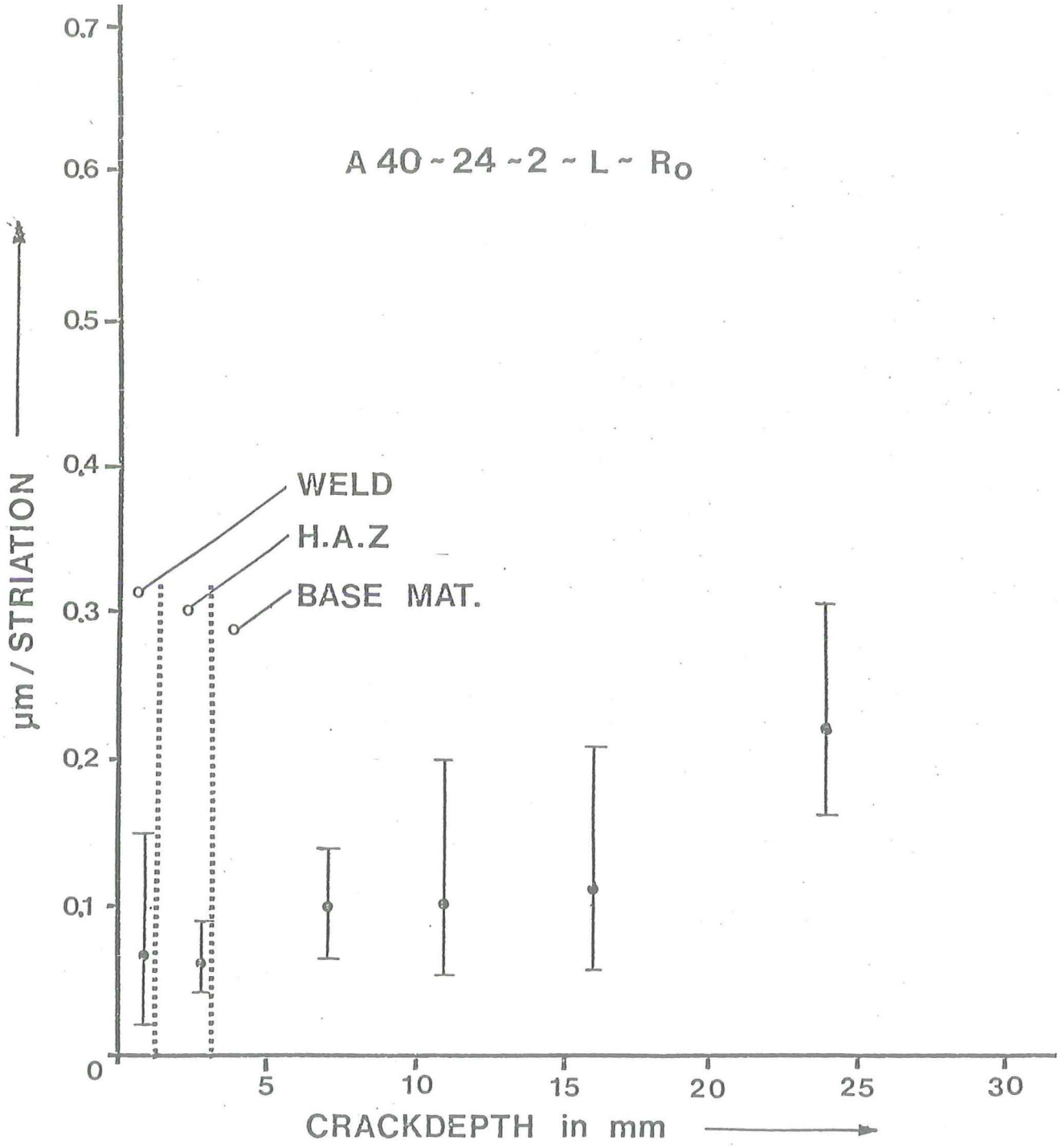

Fig. 2.2.73 Striation spacing as a function of crack depth from specimen A40-24-2-L-RO.

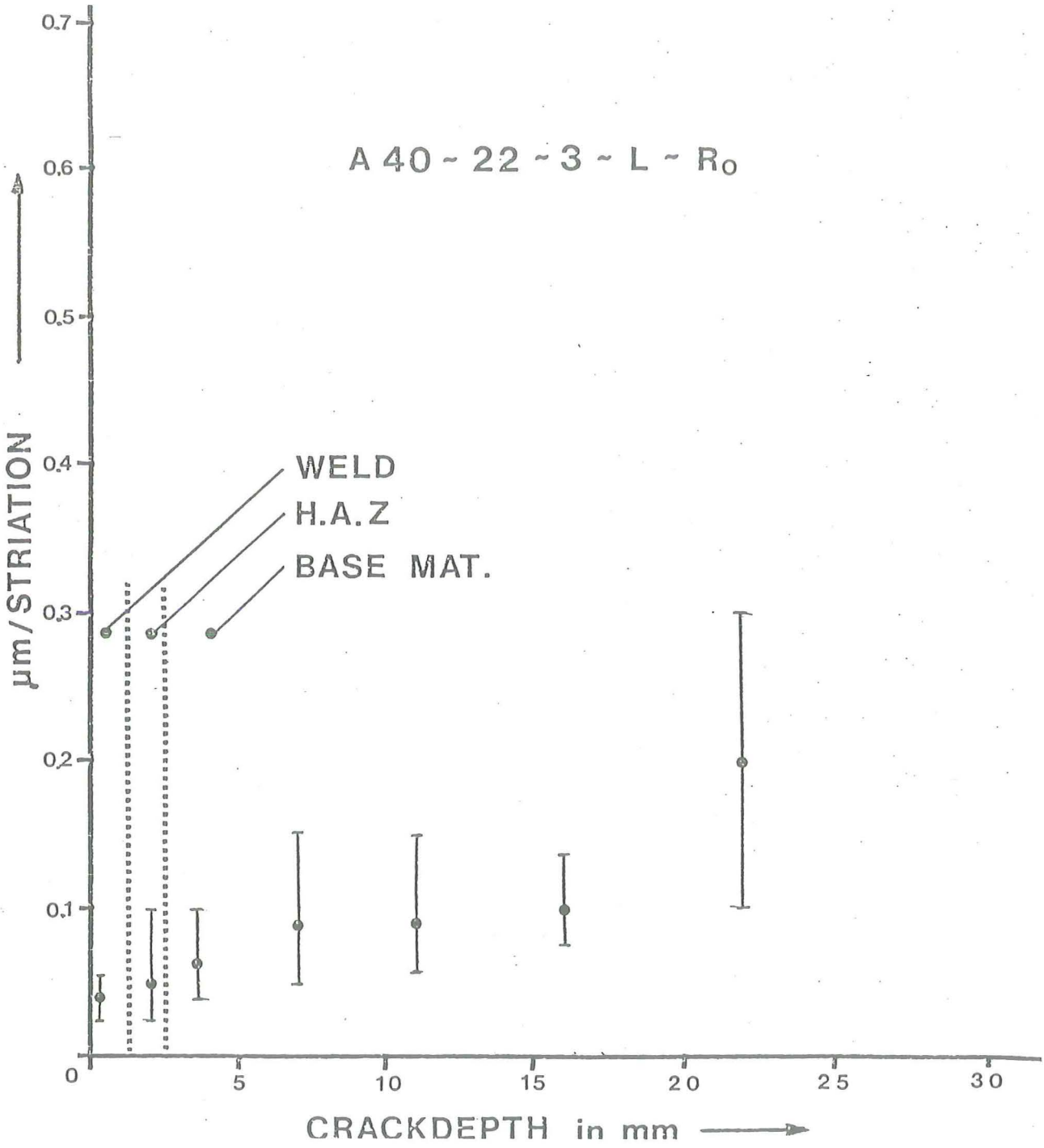

Fig. 2.2.72 Striation spacing as a function of crack depth from specimen A40-22-3-L-RO

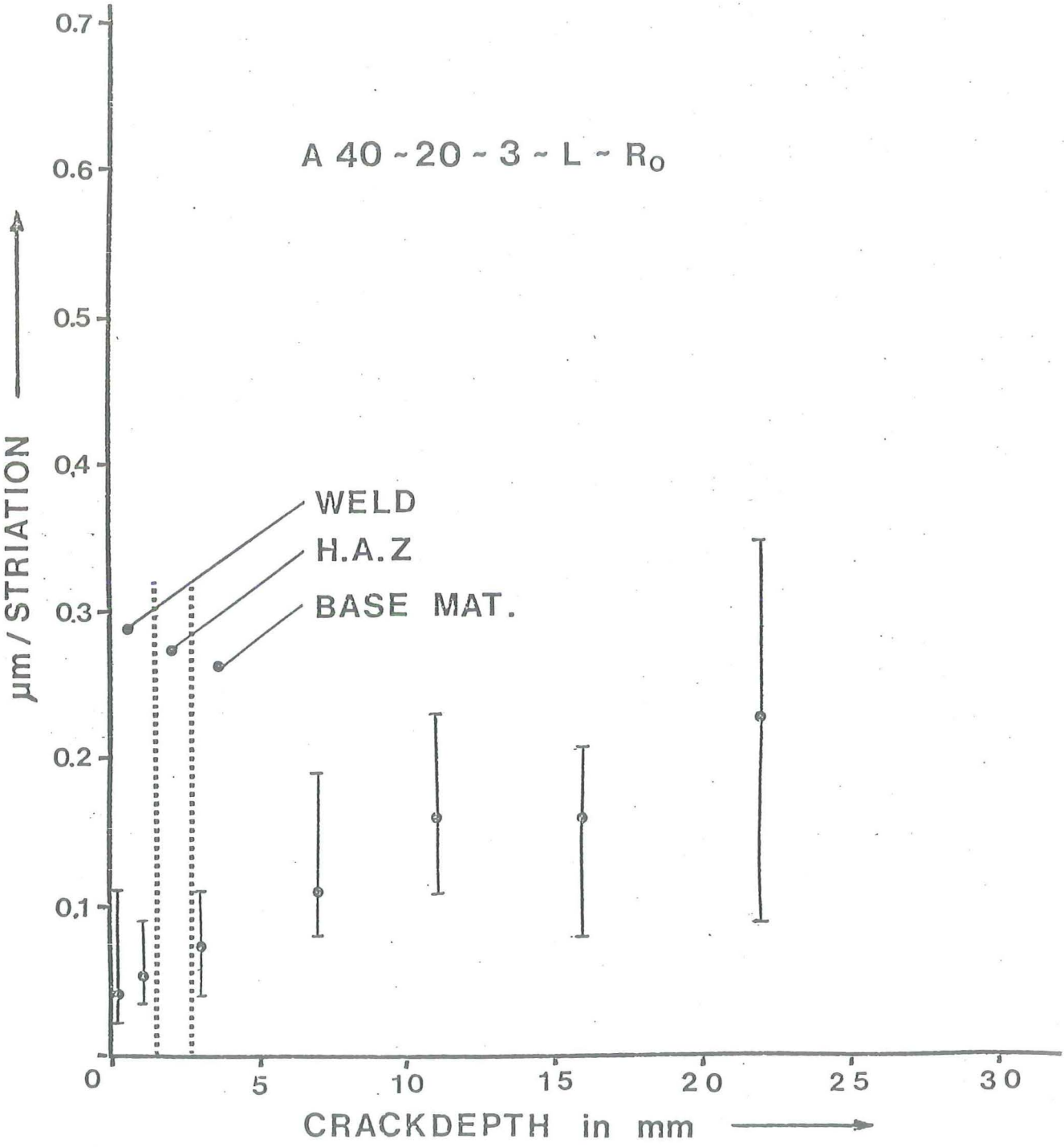

Fig. 2.2.71 Striation spacing as a function of crack depth from specimen A40-20-3-L-R0

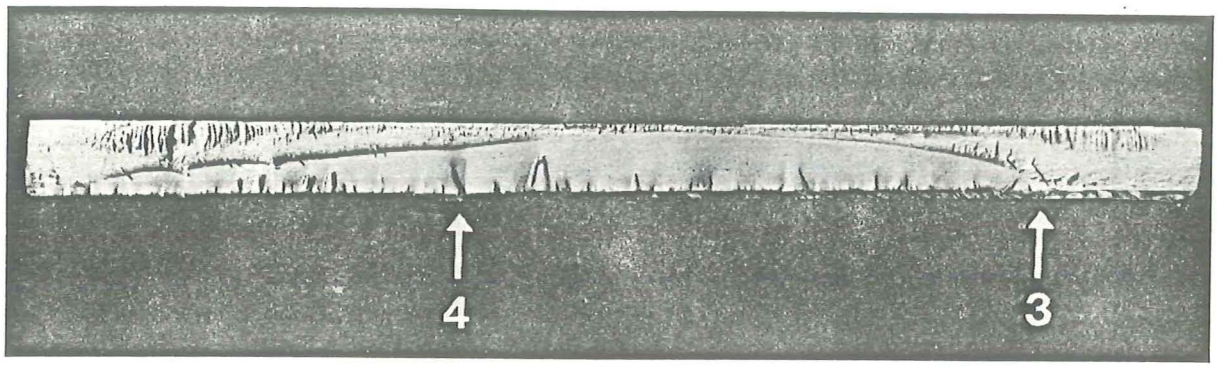

Fig. 2.2.69 magn. 0.8x

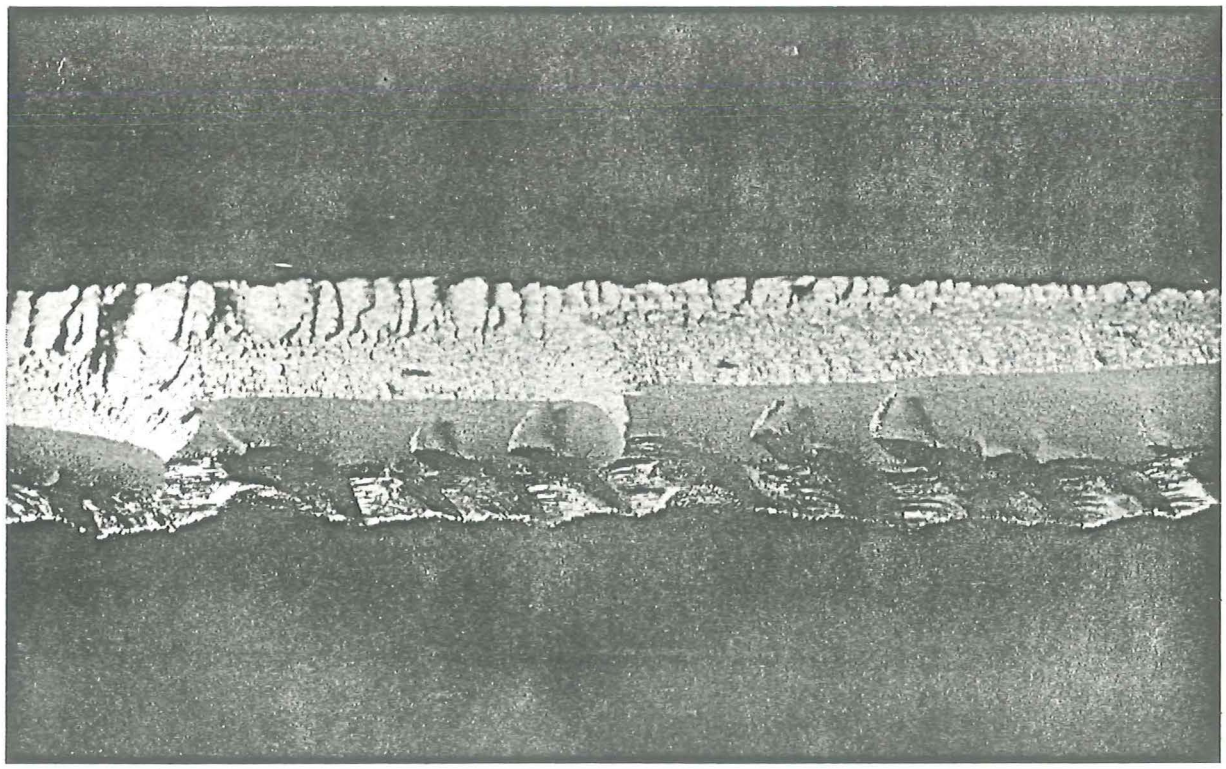

Fig. 2.2.70 magn. 4x

Figs. 2.2.69 and 2.2.70 are macrographs of cracks developed at the side of the gusset opposite the main crack. Fig. 2.2.70 is a detail of fig. 2.2.69 (left).

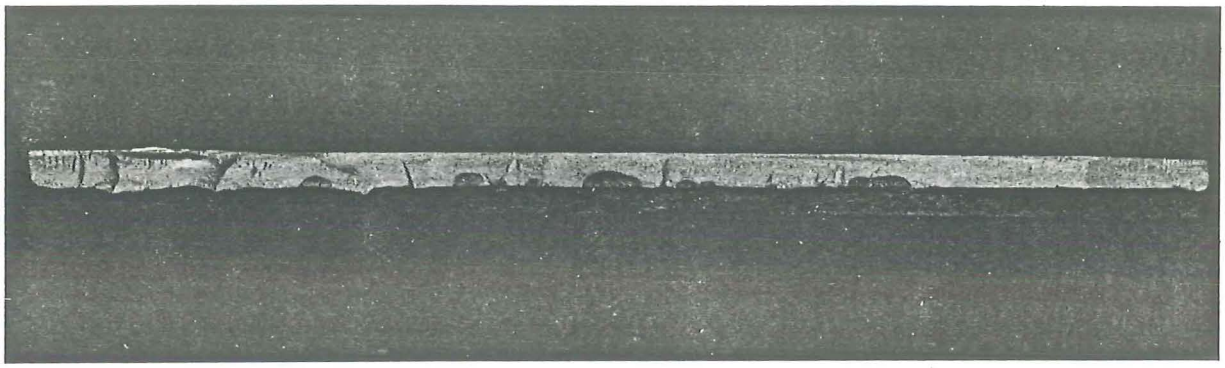

Fig. 2.2.68 magn. 0.8x

Macrograph of secondary cracks developed near the weld at the side of the gusset opposite the main crack.

Fig. 2.2.67A magn. 9000x

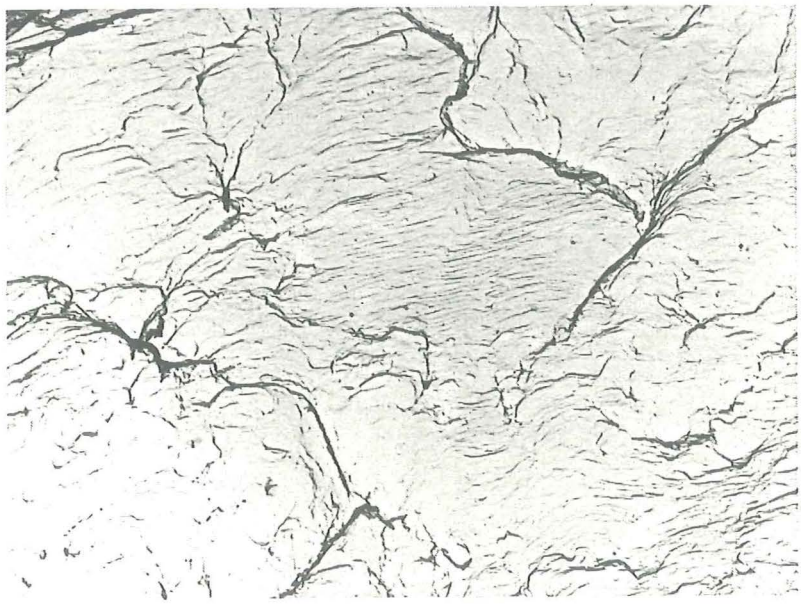

Fig. 2.2.67B magn. 9,000x

Figs. 2.2.67A and 2.2.67B are TEM-micrographs of the fracture surface of specimen A40-1-5-L-RO. Each micrograph shows differences in spacing at the same depth (18 mm).

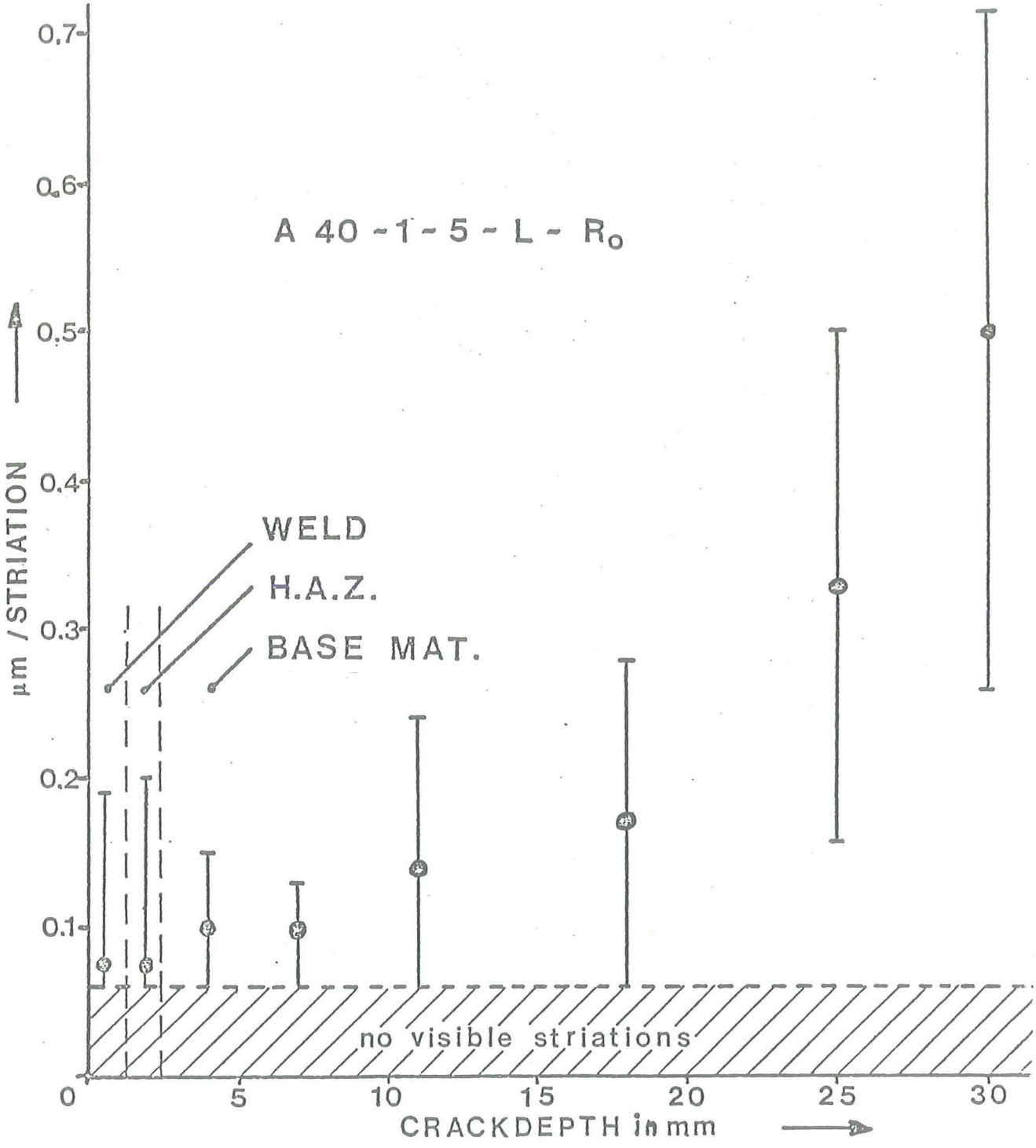

Fig. 2.2.66 Striation spacing as a function of crack depth from specimen A40-1-5-L-RO.

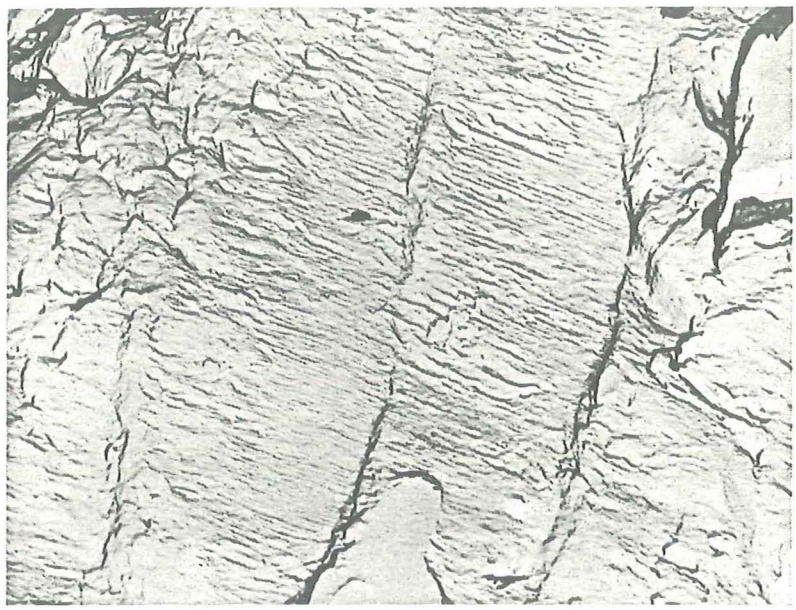

Fig. 2.2.65A magn. 12,000x

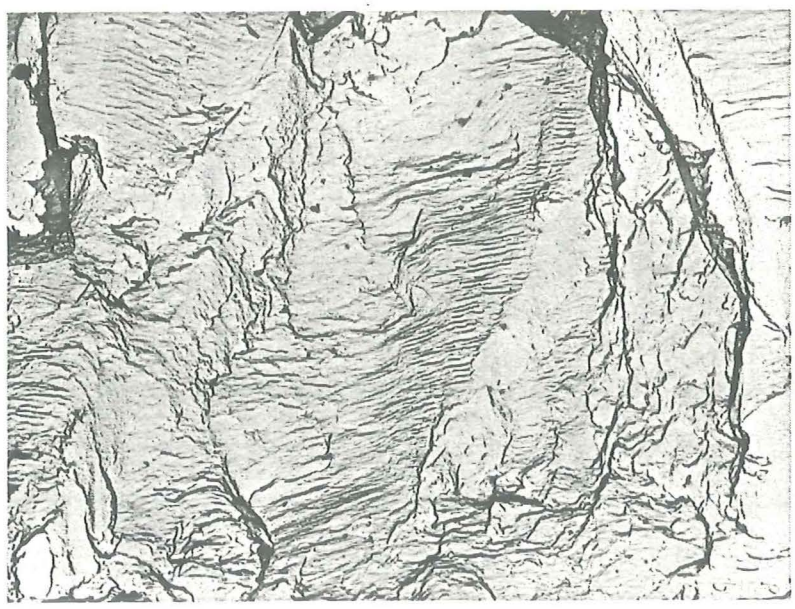

Fig. 2.2.65B magn. 12,000x

TEM-micrographs of the fracture surface of specimen A40-1-5-L-RO
Fracture appearances at 1 mm (Fig. 2.2.65A) and 3 mm (Fig. 2.2.65B) from crack origin.

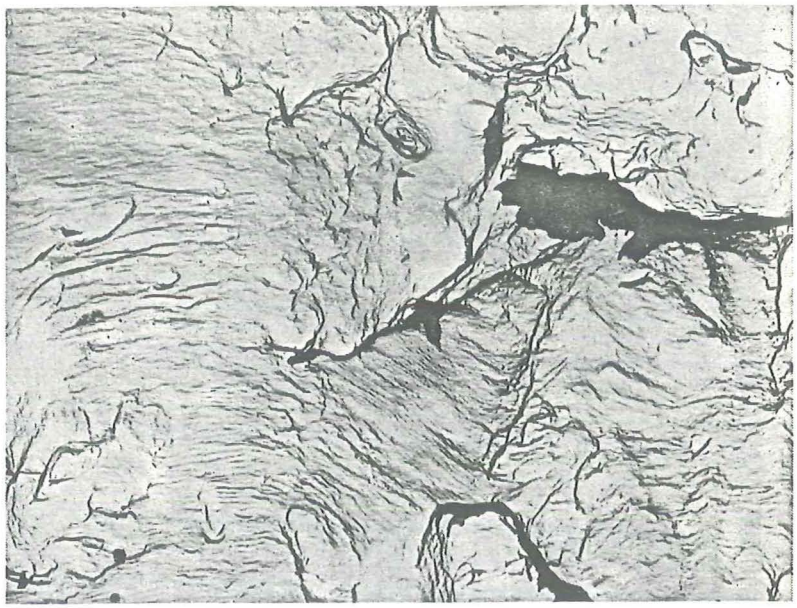

Fig. 2.2.64A magn. 12,000x

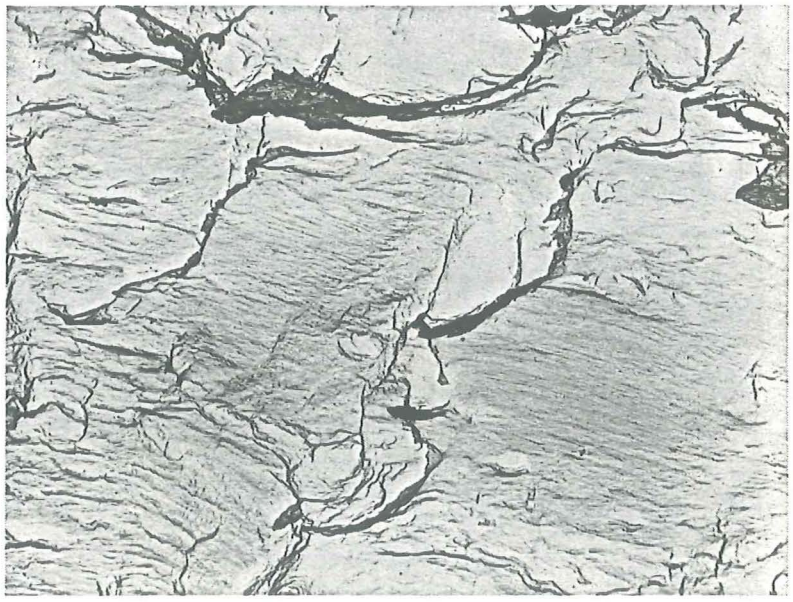

Fig. 2.2.64B magn. 12,000x

Figs. 2.2.64A and 2.2.64B are TEM-micrographs of the fracture surface of specimen A40-1-5-L-RO. Fracture appearance at 0.4 mm from crack origin. Mean striation spacing is 0.04 μm.

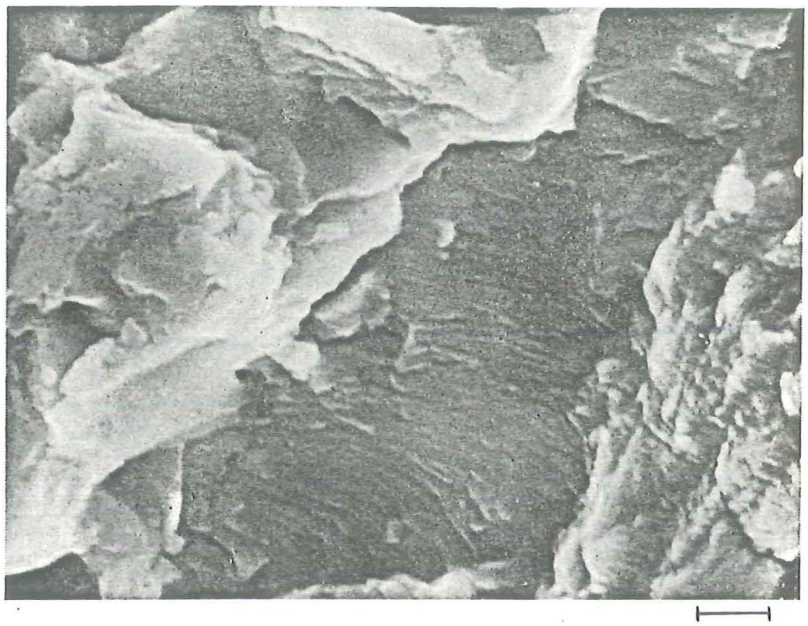

1.6 μm

Fig. 2.2.63A

2.3 μm

Fig. 2.2.63B

Figs. 2.2.63A and 2.2.63B are SEM-micrographs of the fracture surface of specimen A40-1-5-L-RO. Crack growth direction is from bottom left to top right in both photographs. Striation spacing is 0.3 μm

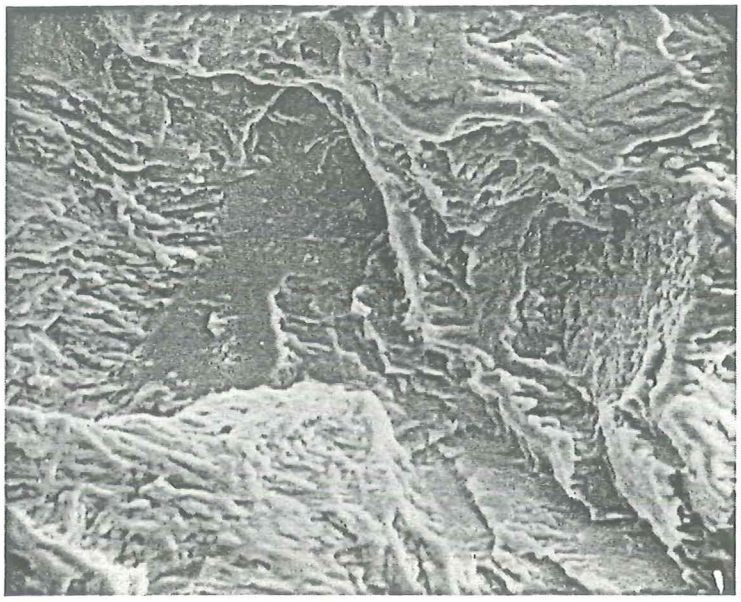

Fig. 2.2.61 magn. 600x

Detail of an area broken by cleavage (see black arrow, Fig. 2.2.60)

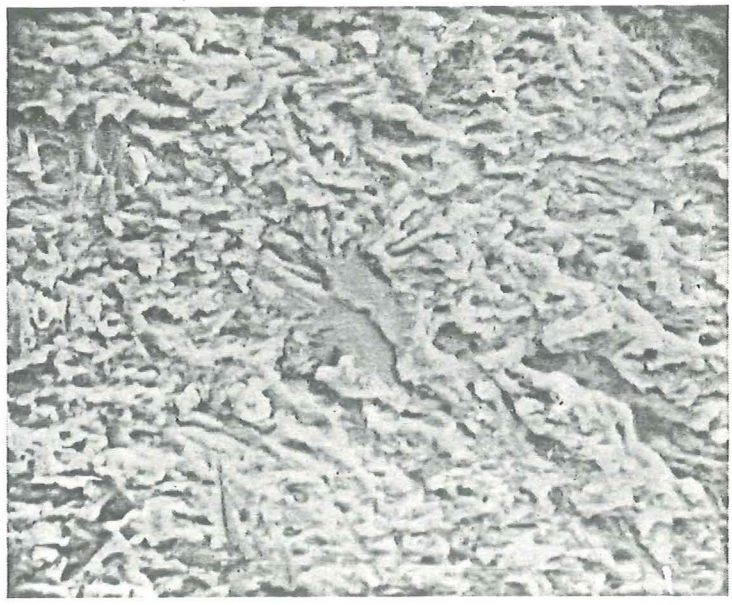

Fig. 2.2.62 magn. 1,000x

Appearance of the fatigue fracture in the weld material.
The centre of the micrograph shows a facet of cleavage.

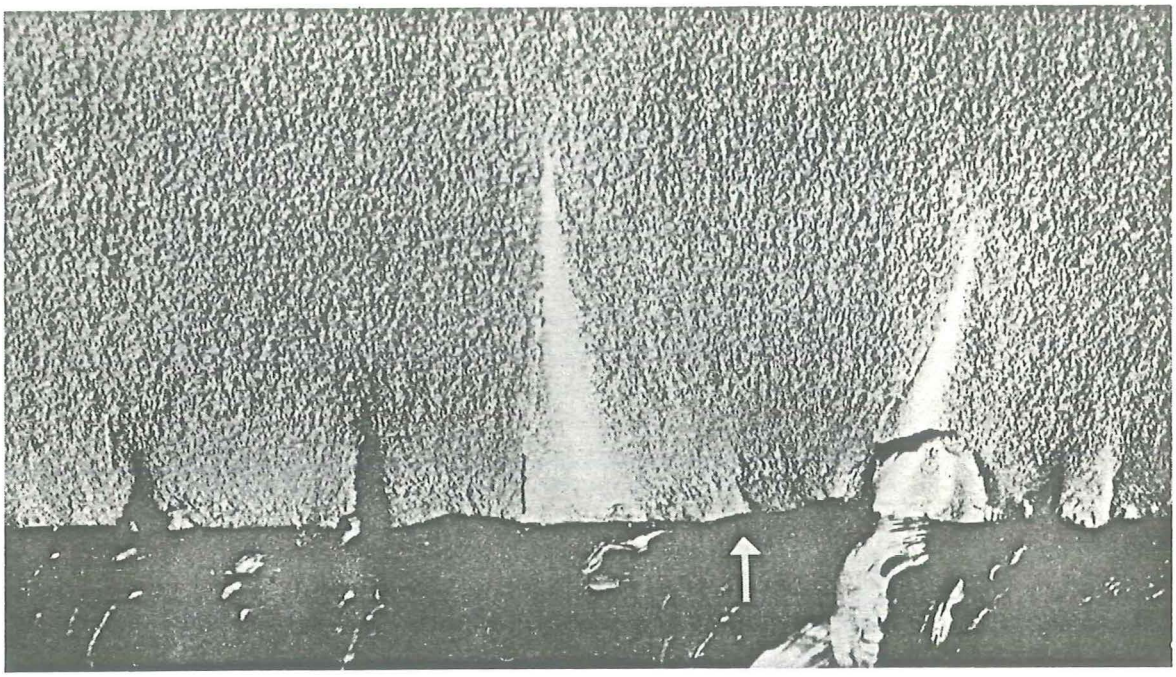

Fig. 2.2.59 magn. 6x

Detail of the fracture surface shown in Fig. 2.2.57. The arrow indicates an area where a crack has been initiated. Note the coarse structure at the crack's origin, corresponding with the coarse structure in the upper part of the specimen shown in Fig. 2.2.58

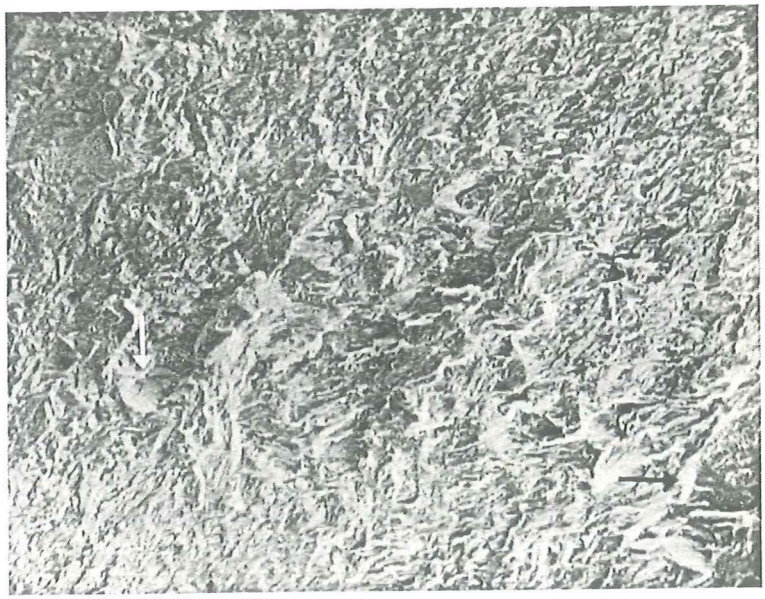

Fig. 2.2.60 magn. 130x

SEM-micrograph of the coarse structure indicated by the arrow in Fig. 2.2.59. Crack growth direction is from bottom left to top right in this photograph. The arrows indicate areas broken by cleavage.

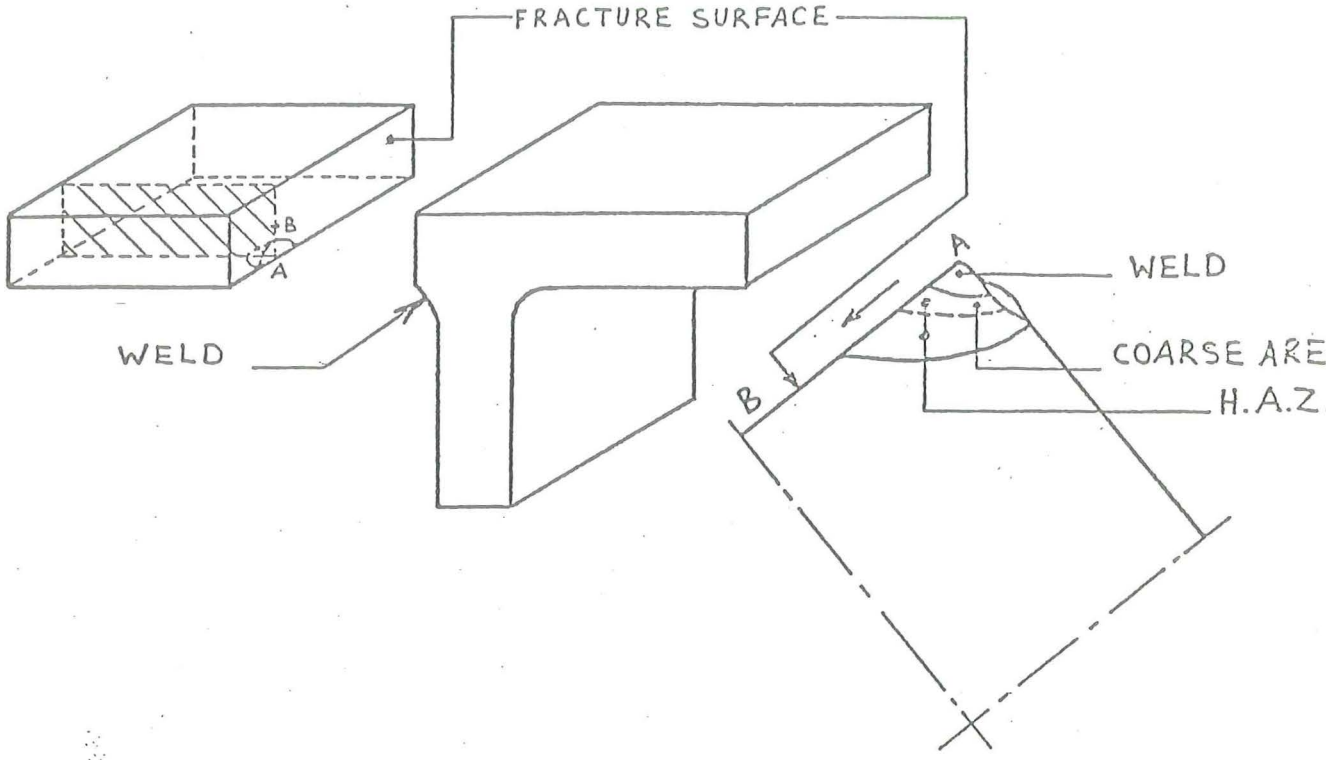

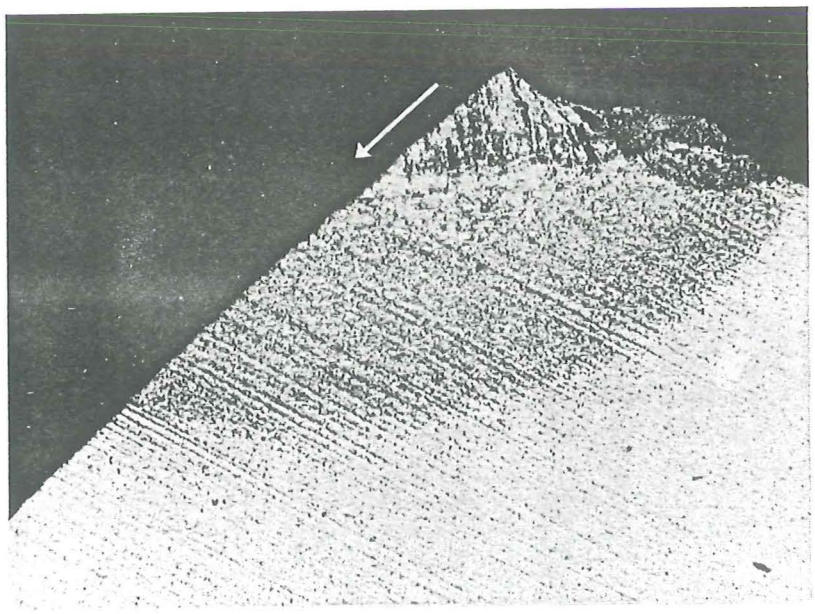

Fig. 2.2.58 magn. 25x

Cross-section at the fatigue fracture surface opposite of the surface shown in Fig. 2.2.57. The arrow indicates the direction of crack growth. The sketch above shows how the specimen has been prepared.

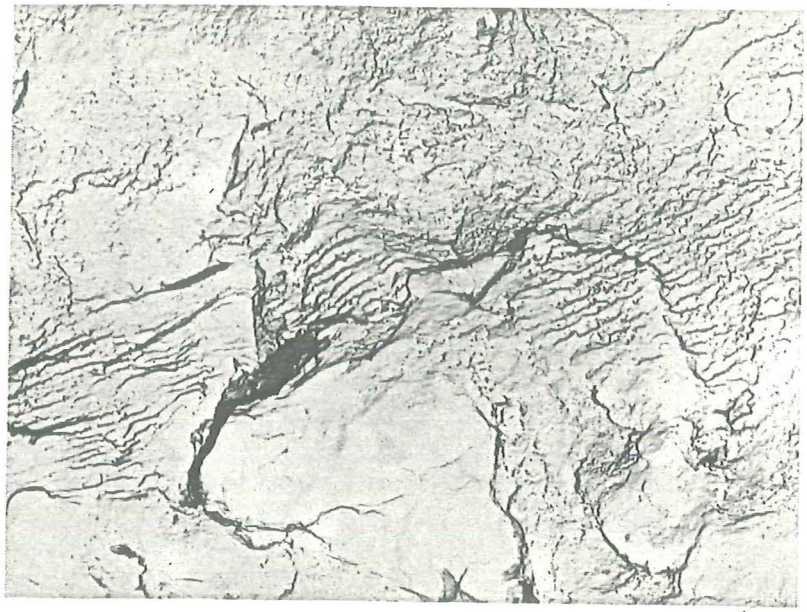

1.1 μm

Fig. 2.2.56

Striations on a fracture surface which during the endurance test had been exposed to seawater. The fracture surfuce was found to be heavily attacked.

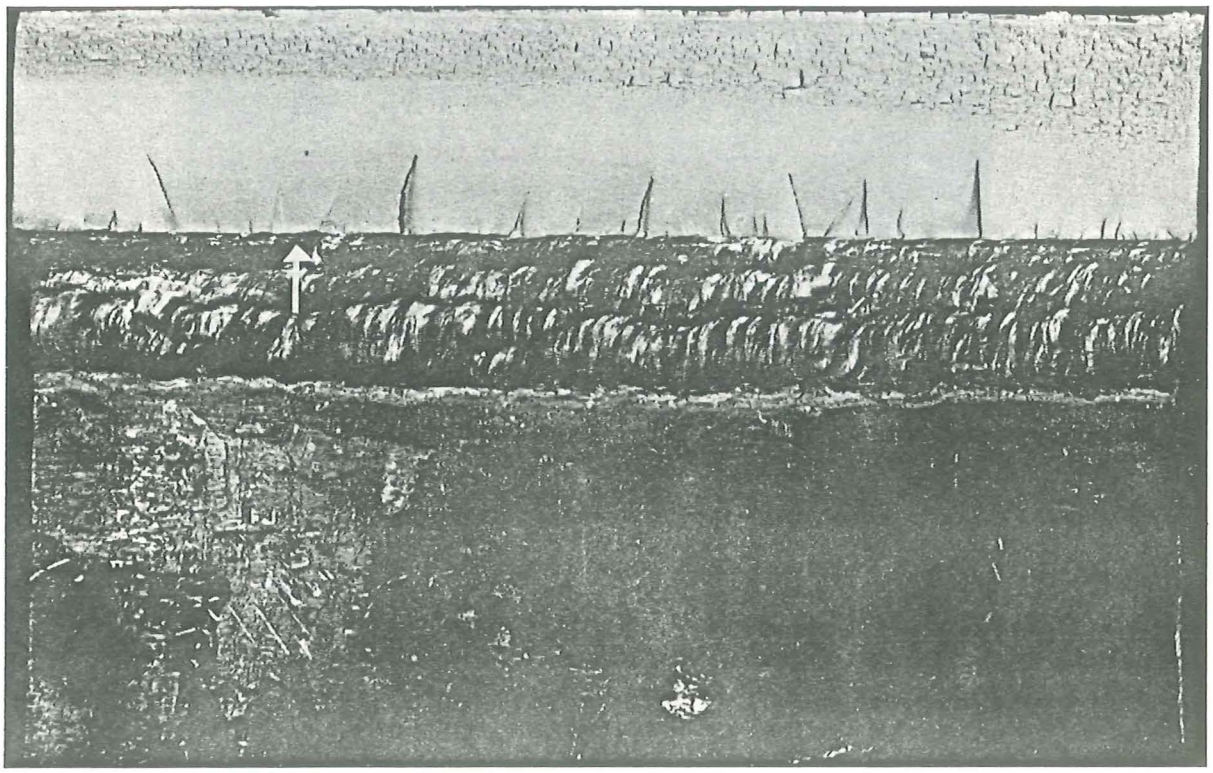

Fig. 2.2.57

mag. 0.8x

Fracture surface of specimen A40-1-5-L-RO. The arrow indicates where, on the counterpart of this fracture surface, a metallographic specimen was prepared. (See Fig. 2.2.58)

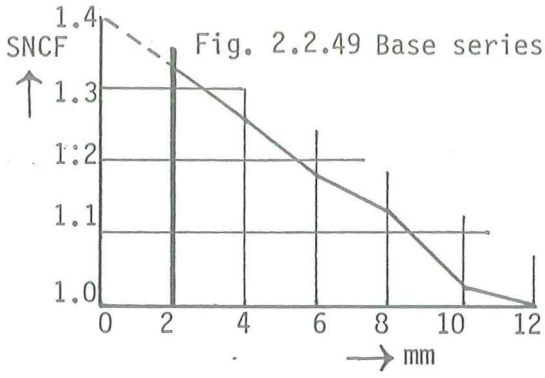

Fig. 2.2.49 Base series a.w.

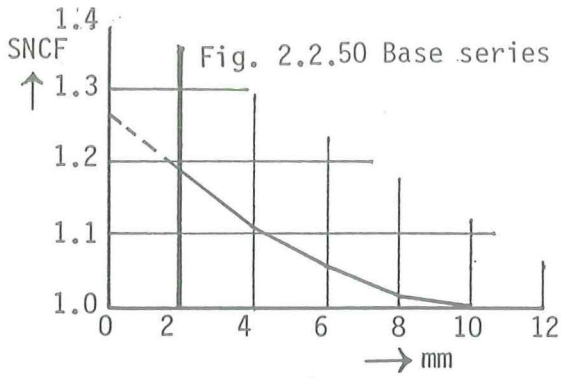

Fig. 2.2.50 Base series PWHT

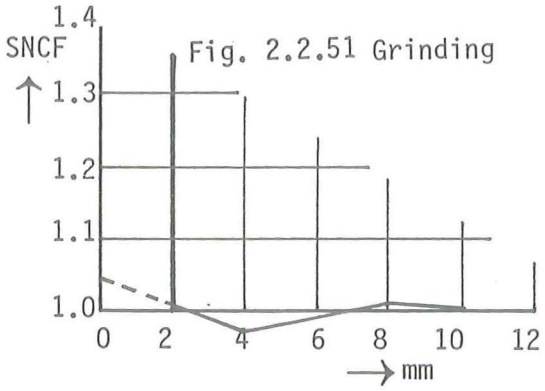

Fig. 2.2.51 Grinding

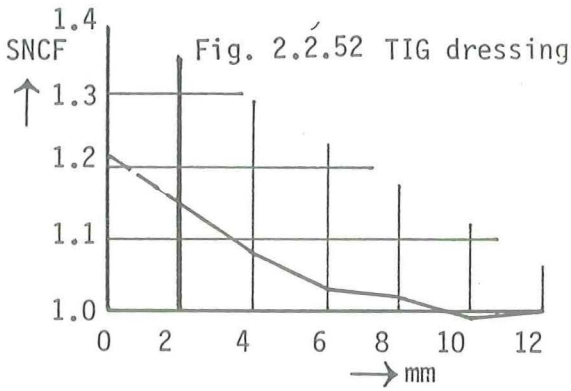

Fig. 2.2.52 TIG dressing

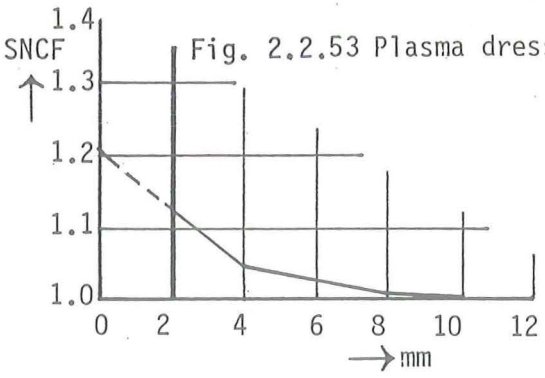

Fig. 2.2.53 Plasma dressing

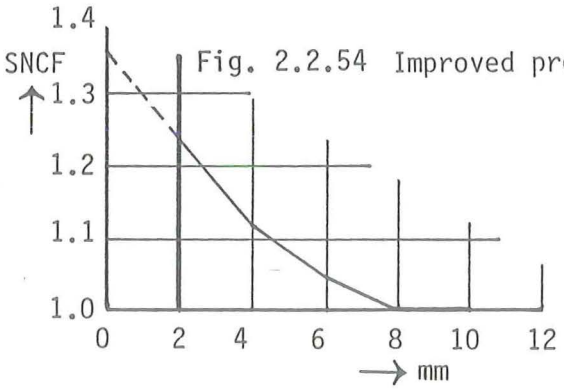

Fig. 2.2.54 Improved profile

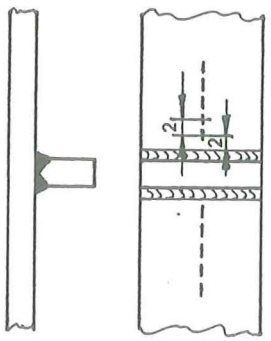

Fig. 2.2.21 Location of straingauges

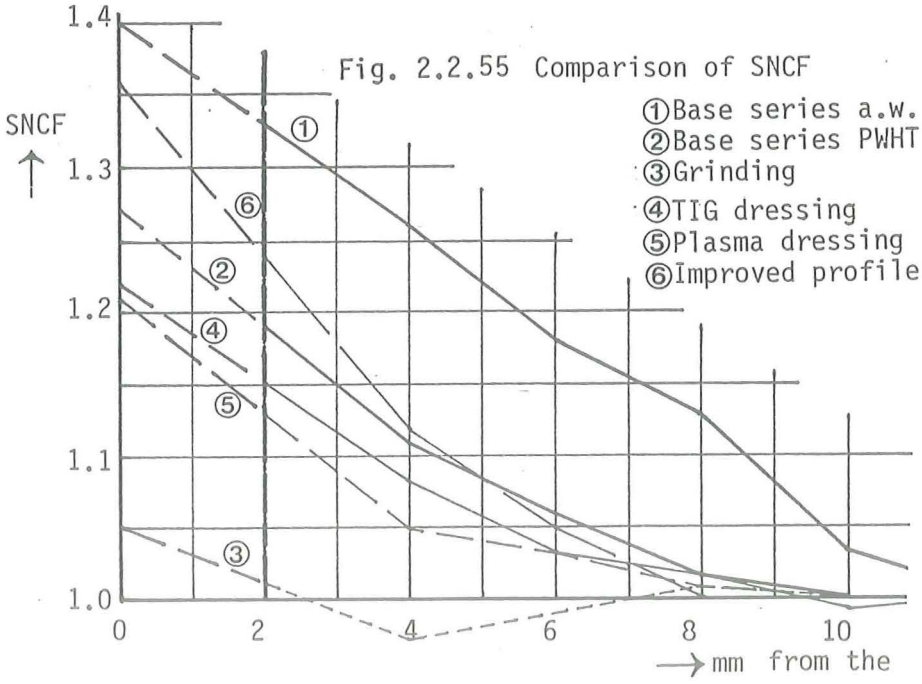

Fig. 2.2.55 Comparison of SNCF

①Base series a.w.
②Base series PWHT
③Grinding
④TIG dressing
⑤Plasma dressing
⑥Improved profile

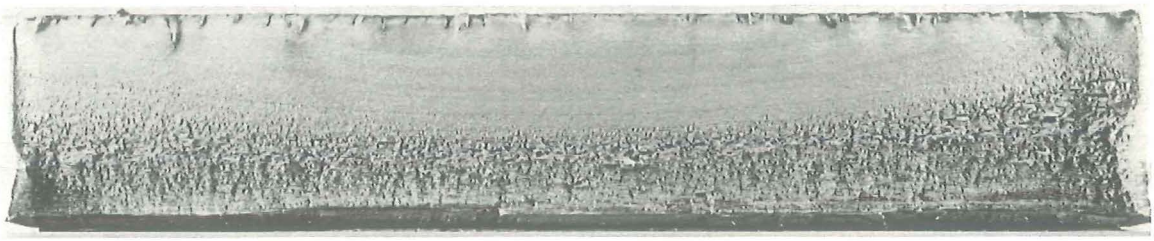

Fig. 2.2.48 Crack front markings generated during testing of a 40mm specimen.

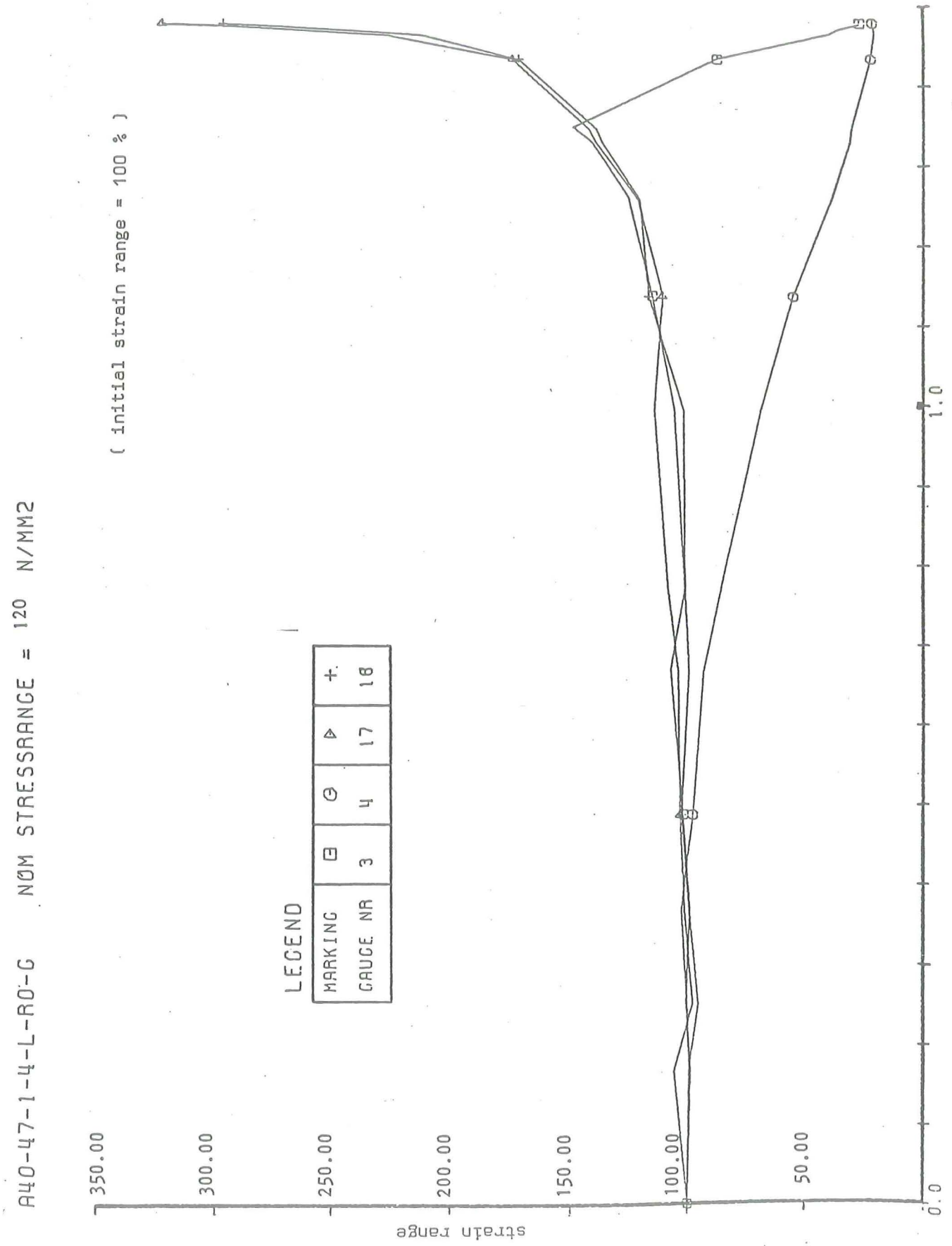

Fig. 2.2.47 Variation of strains at the back face (opposite the weld) during testing of a 40 mm I-shape specimen.

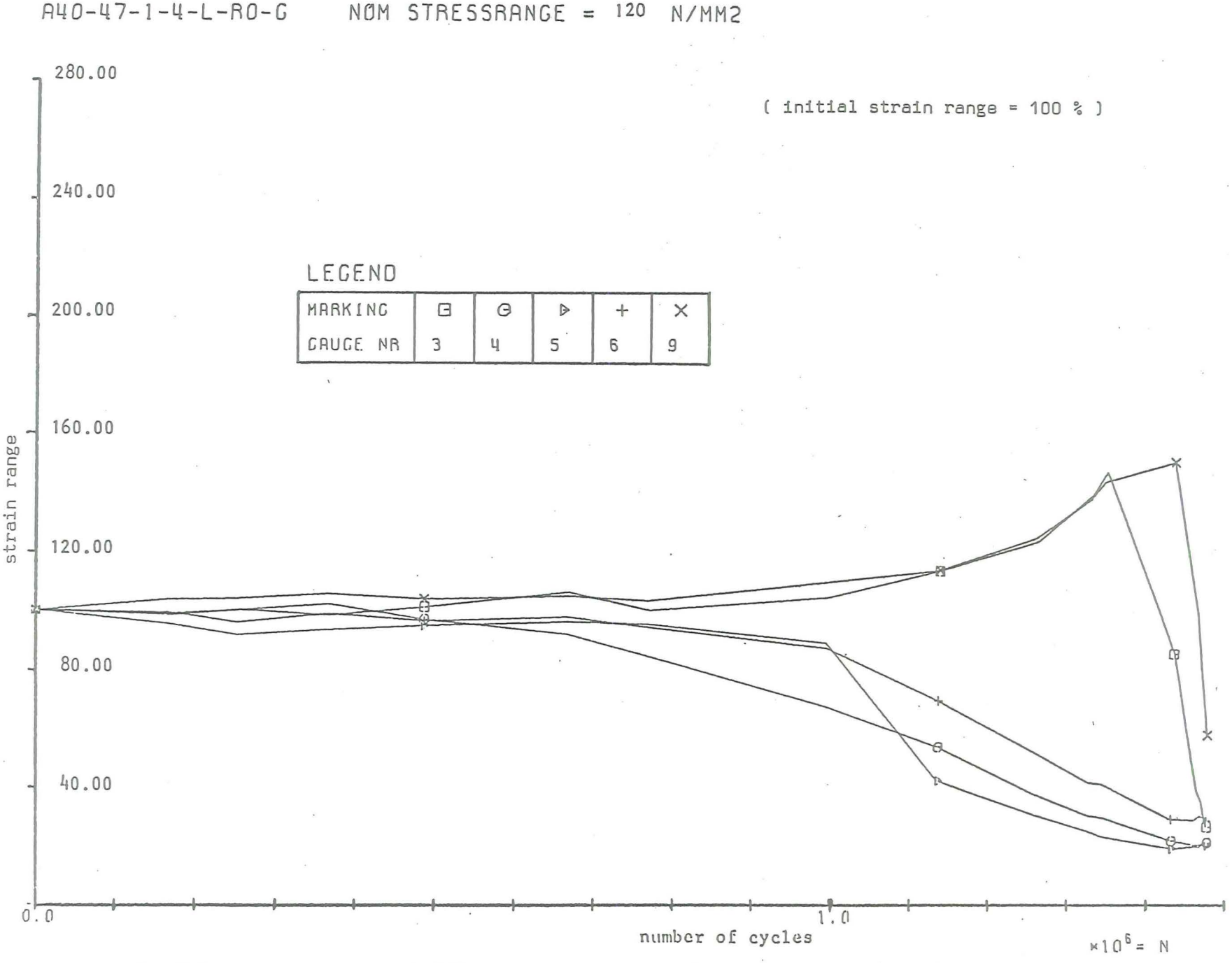

Fig. 2.2.46 Variation of strain near the weld toe during testing of a 40 mm T-shape specimen.

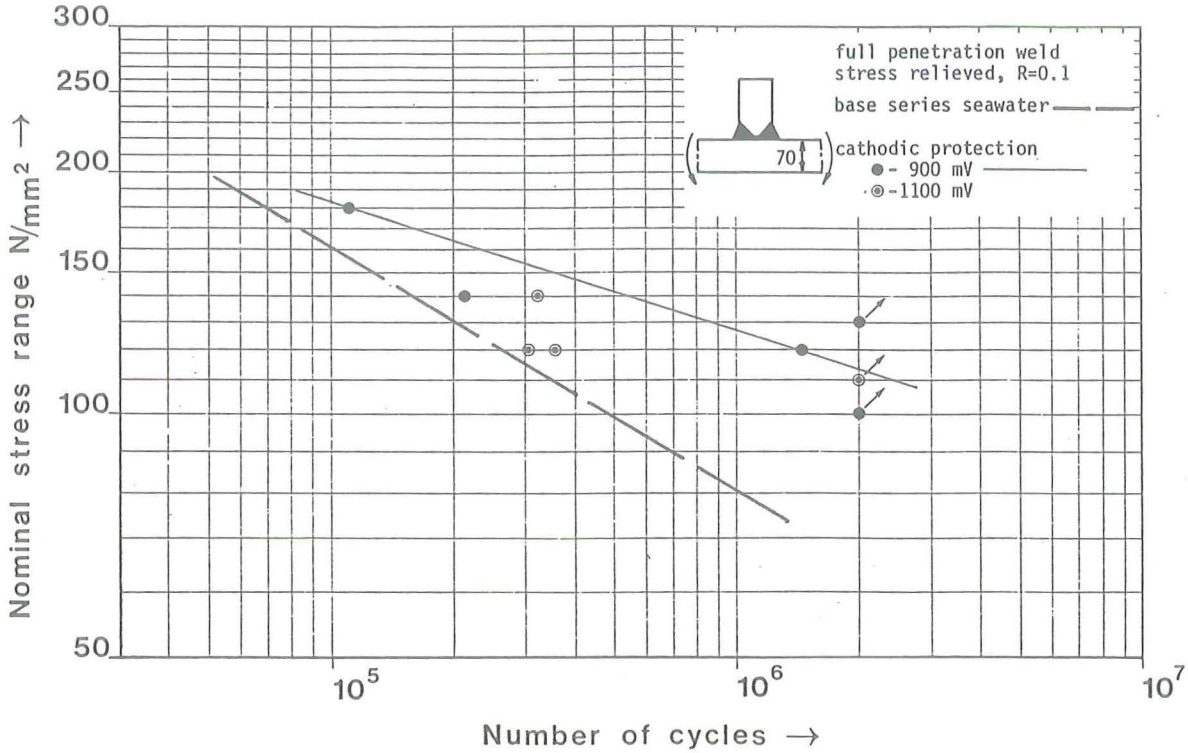

Fig. 2.2.45 Fatigue behaviour of cathodically protected and over-protected 70 mm specimens in seawater at a stress ratio R = 0.1.

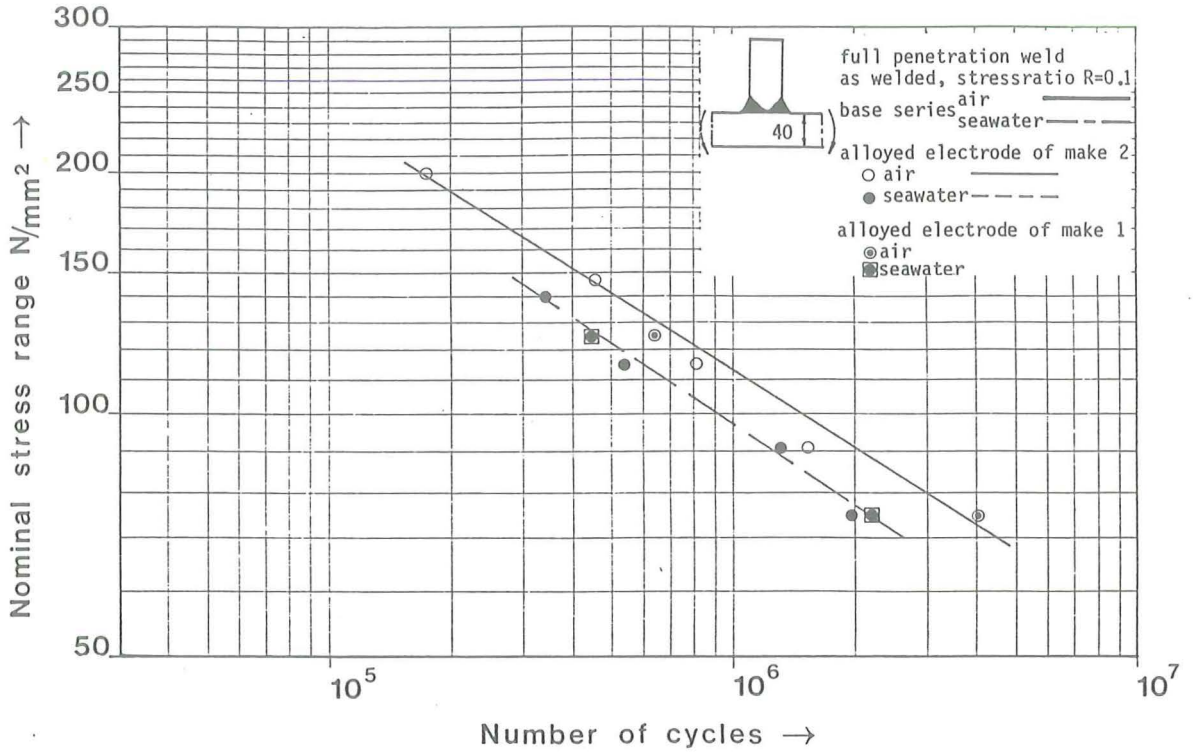

Fig. 2.2.43 Fatigue behaviour of 40 mm , with 2.5% Ni-alloyed electrodes welded specimens in air and seawater at a stress ratio R = 0.1.

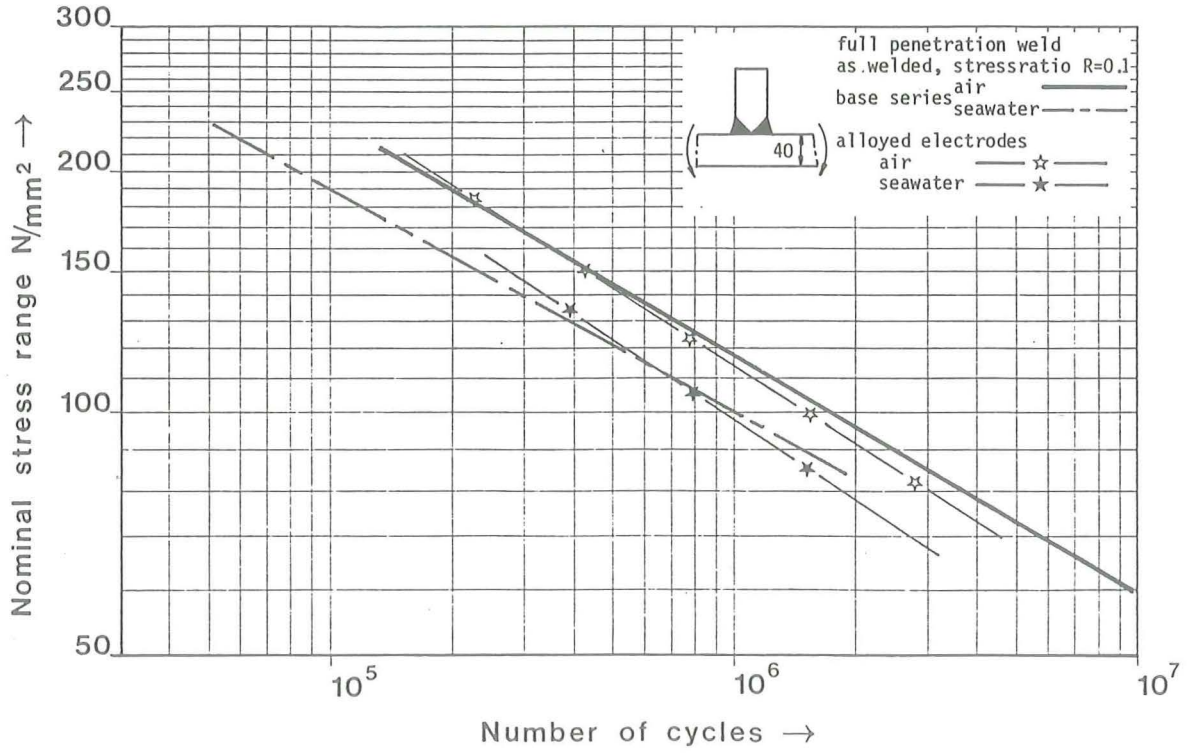

Fig. 2.2.44 Comparison of the tests of the 40 mm, with alloyed electrodes welded specimens and the basic tests.

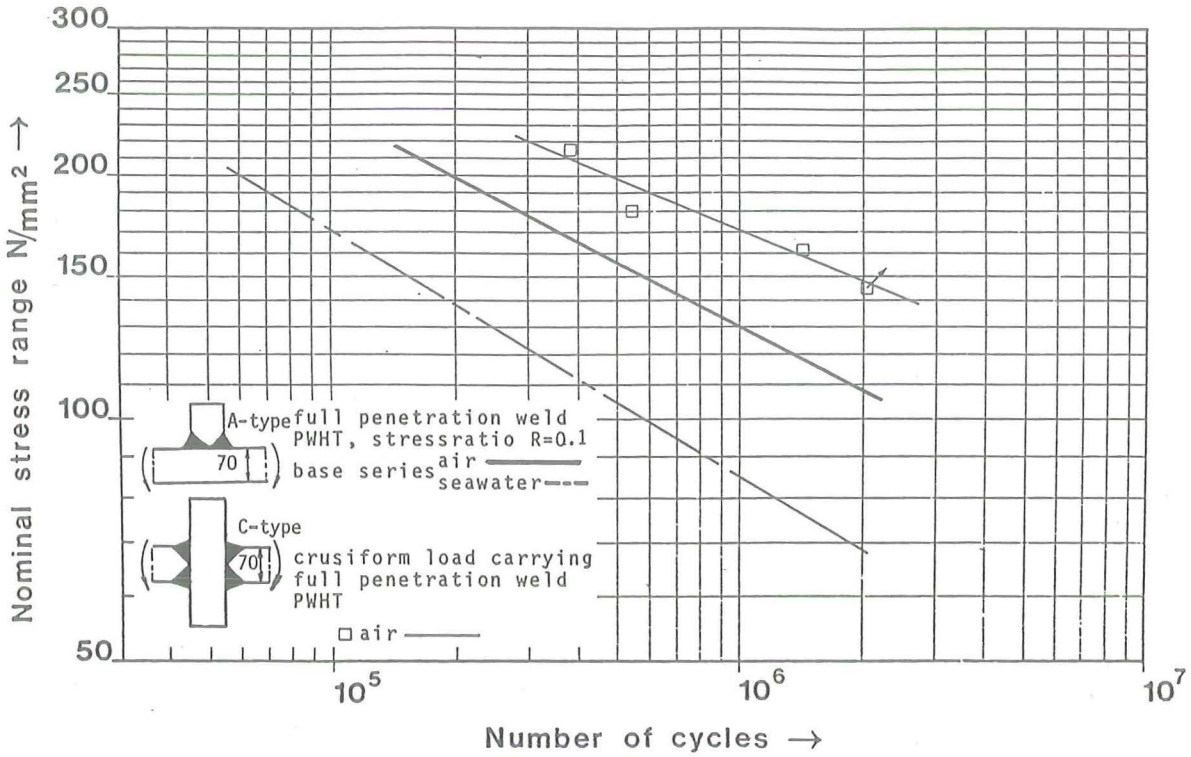

Fig. 2.2.41 Fatigue behaviour of 70 mm C-type specimens in air at a stress ratio R = 0.1.

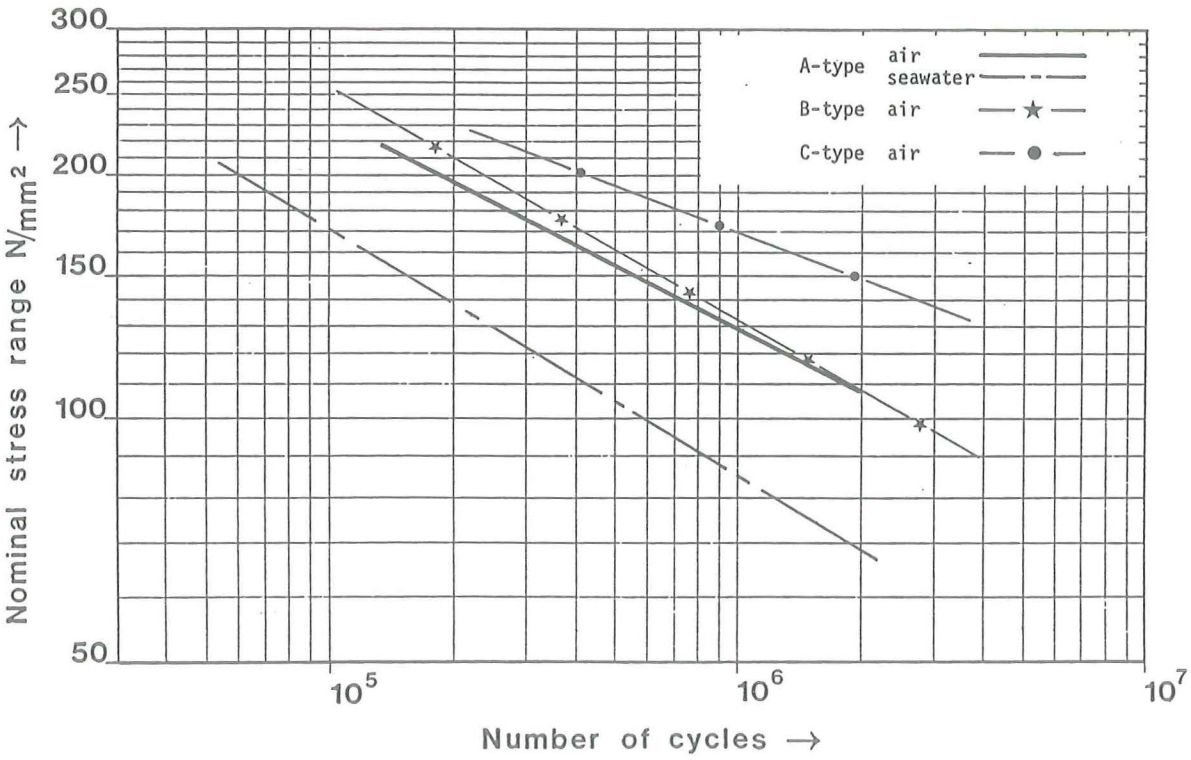

Fig. 2.2.42 Comparison of the tests on the A-type, B-type and C-type 70 mm specimens.

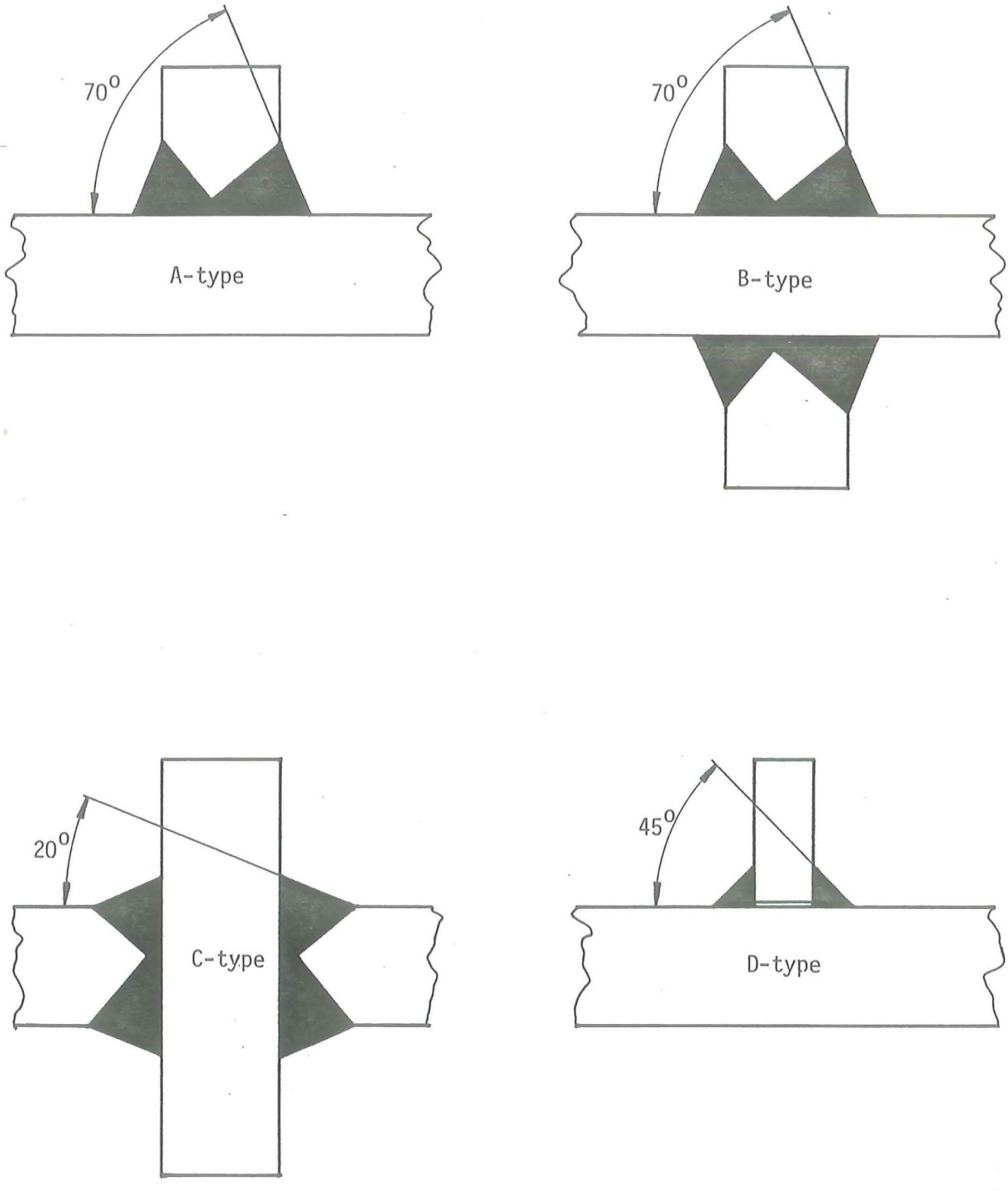

Fig. 2.2.40 Angle of transition between the weld and the main plate of the four different specimen types.

Contents

ECSC CONVENTION 7210-KB/6/602 (J.7. 1 f/76)
FINAL REPORT

FATIGUE AND CORROSION FATIGUE BEHAVIOUR OF OFFSHORE STEEL STRUCTURES

By: J. de Back' and
G.H.G. Vaessen" et al.

Delft/Apeldoorn, April 1981

Investigation with financial aid of the
European Community of Steel and Coal.

' Delft University of Technology
Stevin Laboratory
Department of Civil Engineering

" Metal Research Institute TNO
Apeldoorn